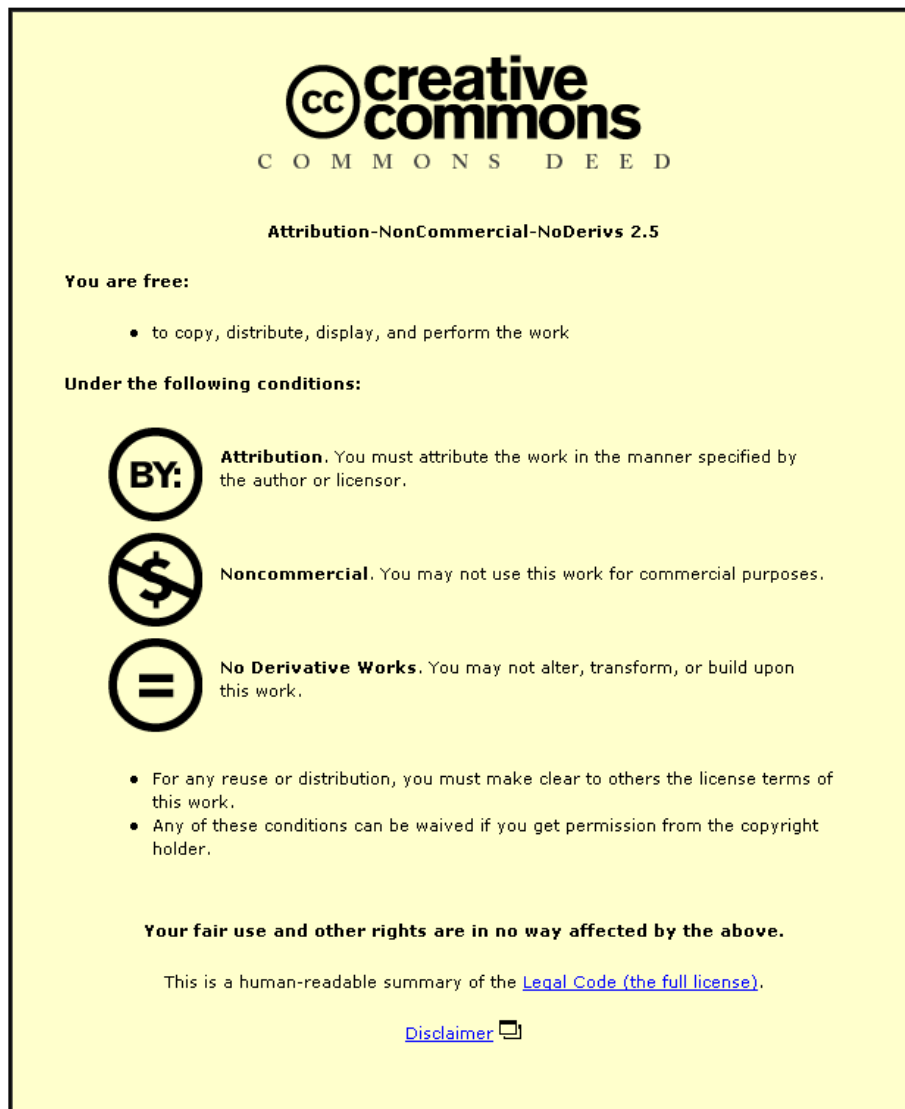


This item was submitted to Loughborough's Institutional Repository (<https://dspace.lboro.ac.uk/>) by the author and is made available under the following Creative Commons Licence conditions.



For the full text of this licence, please go to:
<http://creativecommons.org/licenses/by-nc-nd/2.5/>

**Miniaturized DGS and EBG Structures for Decoupling
Multiple Antennas on Compact Wireless Terminals**

By
Qian Li

A Doctoral Thesis

Submitted in partial fulfilment
of the requirements for the award of

Doctor of Philosophy
of
Loughborough University

28 May 2012

TO MY FAMILY

Certificate of Originality

This is to certify that I am responsible for the work submitted in this thesis, that the original work is my own except as specified in the acknowledgements or in footnotes, and that neither the thesis nor the original work contained therein has been submitted to this or any other institution for a higher degree.

..... (Signed)

..... (Date)

Acknowledgements

Over the past three years, I have been a PhD student in the Department of Electronic, Electrical and Systems Engineering at Loughborough University. In recognition of my time there, I would like to thank my supervisor, Dr Alexandros Feresidis, for his encouragement, guidance and inspiration throughout my PhD study. More importantly, his impact on my professionalism and personality will last a lifetime.

Special thanks go to my second supervisor Mr Robert D Seager for his guidance and for helping my final viva. My gratitude also goes to Dr Alford Chauraya, who gave invaluable input at the beginning of my research, and great support on my measurement works which were conducted in the Antenna Measurement Laboratory at Loughborough University. Although we were working on completely different research fields, he provided lots of suggestions and support for the design of MIMO antennas. I would like to acknowledge Dr Xiaoyu Li for her valuable suggestions and encouragement during the course of my PhD study.

Additionally, I would like to thank to my good friend Dr Xiaoming Wang for our many useful discussions on the study process and for sharing the ups and downs of PhD life.

Last but certainly not least, I would like to thank my parents, for their support, patience and encouragement. Without their motivation and understanding, it would have been impossible for me to complete this work.

ABSTRACT

MIMO (Multiple Input Multiple Output) technology has been presented to significantly increase the wireless channel capacity and reliability without requiring additional radio spectrum or power. In MIMO systems, multiple antennas are mounted at both the transmitter and the receiver. When this technology is employed for a compact wireless terminal, one of the most challenging tasks is to reduce the high mutual coupling between closely placed antenna array elements. The high mutual coupling produces high correlation between antenna elements and affects the channel capacity of MIMO system. The objectives of this thesis are to design practical miniaturized structures to reduce high mutual coupling for small wireless terminals. The research is conducted in the following areas.

Initially, a PIFA design and two-element PIFA array are proposed and optimized to operate at 1.9GHz. A pair of two coupled quarter-wavelength linear slits is inserted in a compact ground plane, resulting in significant reduction of the mutual coupling across antenna operating frequency band. In order to take up less space on the ground plane, instead of the linear slits, miniaturized convoluted slits are implemented between the two closely placed PIFAs. Although the convoluted slits have small area and are positioned close to the edges of the ground plane, the miniaturized convoluted slit structures achieve a reduction of mutual coupling between antenna elements and succeed in reducing the effect of the human body (head and hand) to the antennas.

In order to further reduce the size of the slits etched on the compact ground plane, a novel double-layer slit-patch EBG structure is proposed. It consists of a two-layer

structure including conducting patches and aperture slits placed on either side of a very thin dielectric layer. They are placed in very close proximity to each other (55 μm). A two-element printed CPW-fed monopole array operating around 2.46GHz and a two-element UWB planar monopole array operating from 3GHz to 6GHz have been employed to investigate the proposed slit-patch EBG structures. The optimised double-layer slit-patch EBG structure yields a significant reduction of the mutual coupling and produces the maximum miniaturization of antenna array. Another novel convoluted slit-patch EBG structure has been presented to reduce the mutual coupling between two PIFAs operating at 1.9GHz. These results demonstrate that the slit-patch EBG structure is a feasible technology to reduce the mutual coupling between multiple antennas for compact wireless terminals.

List of Publications

- [1] Alexandros P. Feresidis, Qian Li, Isolation Enhancement of Monopole Antennas and PIFAs on a Compact Ground Plane, *Loughborough Antennas & Propagation Conference*, 2009, UK.
- [2] Qian Li, Alexandros P. Feresidis, Mutual coupling reduction between PIFAs on handheld devices, *Antennas and Propagation Society International Symposium*, 2010, Canada.
- [3] Qian Li, Alexandros P. Feresidis, Reduction of Mutual Coupling between Compact MIMO Antennas Arrays, *Loughborough Antennas & Propagation Conference*, 2010, UK.
- [4] Qian Li, Alexandros P. Feresidis, Mutual coupling reduction between closely-packed MIMO PIFA arrays, *European Conference on Antennas and Propagation*, 2011, Italy.
- [5] Qian Li, Alexandros P. Feresidis, Miniaturised Slit-Patch EBG Structures For Decoupling PIFAs on Handheld Devices, *Loughborough Antennas & Propagation Conference*, 2011, UK
- [6] Alexandros P. Feresidis, and Qian Li, Miniaturised Slits for Decoupling PIFA Array Elements on MIMO Handheld Devices, *Electronics Letters*, vol. 48, no. 310-312, March, 2012
- [7] Qian Li, Alexandros P. Feresidis, Miniaturised Slit-Patch EBG Structures For dual-element UWB planar monopole array, *IEEE Trans. on Antennas and Propagation*, 2012 (Submitting)

Table of Contents

Acknowledgements.....	I
ABSTRACT.....	II
LIST OF PUBLICATIONS.....	IV
Table of Contents	V
List of Figures	VIII
List of Abbreviations.....	XVI
Chapter 1 Introduction	1
1.1 Background	1
1.1.1 Mobile and Wireless Communications Systems.....	2
1.1.2 MIMO System	3
1.2 Motivation.....	4
1.3 Contribution Highlights	5
1.4 Chapter Outlines	7
References.....	8
Chapter 2 MIMO Systems on Compact Wireless Terminals.....	12
2.1 Introduction.....	12
2.2 Wireless Channel and Capacity	13
2.3 Compact Mobile and Wireless Terminal Antennas.....	15
2.3.1 Planar Inverted-F Antenna	17
2.3.2 Printed CPW-fed Monopole	20
2.3.3 UWB Monopole Antenna	21

2.4 Mutual Coupling and Correlation	23
2.5 EBG Structures	26
2.6 Defected Ground Structure	30
2.7 CST Microwave Studio.....	31
2.8 Summary	33
References.....	34
Chapter 3 Linear and Convolted Slits on Ground Plane.....	44
3.1 Introduction.....	44
3.2 Planar Inverted – F Antenna Design and Simulation.....	45
3.2.1 Antenna Geometry Design.....	46
3.2.2 Single Modified PIFA Design.....	48
3.2.3 Dual-element PIFA Array Design	49
3.3 Linear Slits on Ground Plane	52
3.3.1 Linear Slit Etched on Ground Plane	53
3.3.2 Fabrication and Measurement.....	59
3.4 Convolted Slits on Ground Plane.....	61
3.4.1 Single Convolted Slit on Ground Plane	62
3.4.2 Dual Convolted Slits on Ground Plane.....	66
3.4.3 Fabrication and Measurement.....	72
3.4.4 Effect of Human Body on Radiation Properties of PIFAs	75
3.5 Single Convolted Slit between Closely-Packed PIFAs.....	82
3.5.1 A single Slit on Ground Plane.....	82
3.5.2 Fabrication and Measurement.....	88
3.5 Summary	89

References.....	91
Chapter 4 Slit-Patch EBG Structures on compact wireless terminals	93
4.1 Introduction.....	93
4.2 Theory and Geometry	95
4.3 Microstrip Line Excitation.....	97
4.4 Printed CPW Monopoles with Slit-Patch Structure.....	101
4.5 UWB Planar Monopole with Slit-Patch Structure.....	116
4.6 Summary.....	130
References.....	131
Chapter 5 Convoluted Slit and Conducting Patch on Mobile Terminals.....	134
5.1 Introduction.....	134
5.2 Double Layer Convoluted Slit-Patch Design.....	136
5.3 Decoupling PIFAs on Compact Ground Plane	140
5.4 Summary.....	147
References.....	147
Chapter 6 Conclusions and Future Work	149
6.1 Conclusions.....	149
6.2 Future Work	152
Appendix Wheeler-Cap Method for measuring antenna efficiency	154

List of Figures

Figure 1.1 The growth of the wireless and mobile communication systems	3
Figure 2.1 Multiple channels of a 2x2 MIMO system	14
Figure 2.2 MIMO channel capacity for different number of antenna elements [8]	15
Figure 2.3 Radiation patterns of one dipole in a dual-element antenna array for different separations (d) [18]	16
Figure 2.4 The evolution process from monopole to PIFA [19]	17
Figure 2.5 Configuration of a Planar Inverted-F Antenna	18
Figure 2.6 (a) The geometry and (b) Return Loss of the dual-band PIFA with a U-shape slot patch	19
Figure 2.7 Geometry of a CPW-fed printed monopole [30]	20
Figure 2.8 The relation between UWB and other wireless communication systems	21
Figure 2.9 Different UWB Planar monopoles [39]	22
Figure 2.10 Electromagnetic coupling between antenna elements on a compact ground plane	23
Figure 2.11 (a) The configuration of PIFAs on 200mm×100mm ground plane and (b) Simulated S21 with various separations(D) between PIFA elements	24
Figure 2.12 Correlation coefficient between two IFAs over different separations	26
Figure 2.13 The characteristic of an EBG structure	27
Figure 2.14 Three EBG structures: (a) one microstrip line with periodic holes ground plane [64] (b) a mushroom-like surface structure [65] (c) a woodpile structure consisting of square dielectric bars [66]	28
Figure 2.15 Schematic of proposed Complementary Dipole array	29
Figure 2.16 Two monopoles antennas on the proposed ground plane [80]	30
Figure 2.17 The Simulated surface current distribution of a dual-element PIFA array at 2.35 GHz [80]	31

Figure 2.18 CST Microwave studio overview [81]	32
Figure 2.19 Grid approximation of rounded boundaries (a) standard (b) Perfect Boundary Approximation [83]	33
Figure 3.1 The five different PIFA configurations: (a) simple PIFA, (b) simple PIFA With the shorting pins on the top edge, (c) U-slotted PIFA, (d) L-slitted PIFA, (e) PIFA with 3 slits	46
Figure 3.2 Return loss results (S11) of PIFAs corresponding to different PIFA configurations shown in Figure 3.1	47
Figure 3.3 Geometry of the PIFA radiating patch	48
Figure 3.4 Geometry of the antenna system	48
Figure 3.5 Simulated return loss (S11) of the modified PIFA	49
Figure 3.6 Current distribution of a PIFA on ground plane at 1.9GHz	49
Figure 3.7 Four different configurations for the position of two antennas on a ground plane	50
Figure 3.8 (a) S11 and (b) S21 of the antenna system for four different configurations of the two array shown in Figure 3.7	51
Figure 3.9 Surface current induced by the PIFAs at 1.9GHz	52
Figure 3.10 Four configurations of slits on a ground plane	53
Figure 3.11 Simulated mutual coupling results (S21) of four configurations	53
Figure 3.12 Current distributions for the four configurations at 1.9GHz	54
Figure 3.13 Two slits inserted at two edges of the ground plane	55
Figure 3.14 S21 of antenna array for different slit lengths	55
Figure 3.15 S21 of antenna array for different distance between two slits	56
Figure 3.16 S-parameter of proposed slit on the ground plane	57
Figure 3.17 Simulated S21 with and without the two linear slits	57
Figure 3.18 (a) Current flow (b) Electric field on the ground plane (c) Magnetic loop between two linear slits at resonant frequency	58

Figure 3.19 Simulated radiation patterns of (a) the original array configuration when PIFA1 (the left element) is excited and (b) the decoupled array in the presence of the slits, when the same element is excited	59
Figure 3.20 Prototype system using the proposed slitted ground plane	60
Figure 3.21 Simulated and measured S-parameters for the prototype with the conventional ground plane	61
Figure 3.22 Simulated and measured S-parameters the prototype with the proposed linear slits	61
Figure 3.23 Single miniaturised slit inserted in the ground plane	62
Figure 3.24 Mutual coupling of antenna array for different slit length	63
Figure 3.25 Mutual coupling of antenna array for different slit width	63
Figure 3.26 S-parameters of antenna array with a convoluted slit on top edge of ground plane	64
Figure 3.27 (a) Current distribution and (b) Current flow on the ground plane when a single slit etched close to top edge of ground plane	64
Figure 3.28 S-parameters of antenna array with a convoluted slit on bottom edge of ground plane	65
Figure 3.29 (a) Current distribution and (b) Current flow on the ground plane when the slit is etched close to bottom edge of ground plane	65
Figure 3.30 Proposed miniaturised convoluted slits	66
Figure 3.31 Mutual coupling(S21) of antenna array for different slit lengths	67
Figure 3.32 Return Loss (S11) of antenna 1 for different slit lengths	67
Figure 3.33 Slits shift along the x-axis in (a) opposite direction, (b) same direction	68
Figure 3.34 Mutual coupling (S21) of antenna array when slits shifted along the X-axis in (a) the opposite direction, (b) the same direction	69
Figure 3.35 S-parameters of the PIFA array with the convoluted slits	70
Figure 3.36 Simulated surface current flow on the ground plane in the presence of the resonating slits at 1.92GHz	71

Figure 3.37 The magnetic field distribution in the plane normal to the ground and through the centres of the two slits. Maximum magnetic field of opposite direction flows through the two slits	71
Figure 3.38 Simulated total efficiency of antennas	72
Figure 3.39 Prototype of antenna system using the proposed slitted ground plane	73
Figure 3.40 Measured S-parameters for a PIFA array (a)without slit and(b)with slit	73
Figure 3.41 PIFA array within a wheeler cap [14]	74
Figure 3.42 Measured total efficiency of antennas with and without slits	74
Figure 3.43 Simulated model of a hand on the ground plane with two PIFAs	76
Figure 3.44 (a) Reflection coefficient (S11) of antenna 1 (b) Mutual coupling (S21) of the antenna system with a conventional ground plane in the presence of the hand at different distances S from the antenna	77
Figure 3.45 (a) Reflection coefficient (S11) of antenna 1 (b) Mutual coupling (S21) of the antenna system with the convoluted slit in the presence of the hand at different distances S from the antenna	78
Figure 3.46 Simulated model of hand and head with two PIFAs in the presence of the proposed convoluted slits	79
Figure 3.47 (a) Return loss (S11) of antenna 1 (b) Mutual coupling (S21) of the antenna system with a conventional ground plane in the presence of the head at different distances S from the ground plane	80
Figure 3.48 (a) Return loss of antenna 1 (b) Mutual coupling of the antenna system with two convoluted slits in the presence of the head at different distances S from the ground plane	81
Figure 3.49 Array of closely-packed PIFAs positioned on a 100x40mm ground plane (a) PIFA geometry (b) Array without slit (c) Array with proposed optimised convoluted slit	83
Figure 3.50 Simulated S-parameters of the two-element PIFA array with (a) no slits (b) S21 with slit of different total length, (c) S21 with slit of different width , (d) optimised slit inserted on a ground plane	85

Figure 3.51 Current flow and distribution and current on ground plane	86
Figure 3.52 Correlation coefficient between two PIFAs on different ground planes	86
Figure 3.53 Simulated radiation patterns of a) the original array configuration when PIFA1 is excited and b) the array with the slits, when PIFA1 is excited, c) the array with the slits, when PIFA2 is excited	87
Figure 3.54 Prototype system using the proposed slitted ground plane	88
Figure 3.55 Measured S-parameters for the two-element PIFA array (a) without slit (b) with optimised slit	89
Figure 4.1 (a) The slit-patch EBG structure, (b) Complementary dipoles schematic and (c) Equivalent circuit of slit-patch EBG structure	97
Figure 4.2 Geometry of one slit-patch EBG structure excited by microstrip line	98
Figure 4.3 S21 of slit-patch EBG with and without the conducting patch	99
Figure 4.4 S21 of slit-patch EBG with different width of conducting patch	100
Figure 4.5 Multiple double-layer slit-patch structures with periodicity ($D=5\text{mm}$)	100
Figure 4.6 S21 of multiple double-layer slit-patch structures	101
Figure 4.7 Geometry of a U-shape slot printed monopole	102
Figure 4.8 Simulated S11 of proposed printed monopole	103
Figure 4.9 (a) The configuration and (b) Experimental model of dual element printed monopole antenna array	103
Figure 4.10 Simulated and measured S-parameters of dual-elements antenna array with a conventional ground plane	104
Figure 4.11 Current flow and distribution on ground plane induced at 2.44GHz	105
Figure 4.12 (a) The configuration and (b) Experiment model of the dual element antenna array with one slit-patch structure	106
Figure 4.13 Simulated and measured S-parameters of the dual-element antenna array with one slit-patch EBG structure	106
Figure 4.14 Current flow and distribution on the ground plane with one slit-patch EBG structure	107
Figure 4.15 Simulated radiation patterns of (a) the original array configuration	

when printed monopole 1 (the left element) is excited at 2.45GHz and (b) the antenna array in the presence of one slit-patch structure, when the same element is excited	108
Figure 4.16 (a) The configuration and (b) Experimental model of the dual element antenna array with two slit-patch structure	109
Figure 4.17 Simulated and measured S-parameters of printed monopole array with two slit-patch structure	110
Figure 4.18 (a) Correlation coefficient between the two antennas (b) Total efficiency of the whole antenna system in the presence of multiple slit- patch structures	111
Figure 4.19 The variable interelement distance (D) between two monopoles	112
Figure 4.20 (a) S11 and (b) S21 of the antenna system for different separation (D) between two monopoles	113
Figure 4.21 (a) The configuration and (b) Experiment model of the dual element antenna array with two slit-patch structure when D is 8mm	114
Figure 4.22 Simulated and measured S-parameters of printed monopole array with two slit-patch structure when D is 8mm	114
Figure 4.23 (a) Prototype and (b) Simulated and measured S-parameters of the dual element antenna array with a conventional ground plane when D is 8mm	115
Figure 4.24 One UWB monopole planar geometry	117
Figure 4.25 Simulated S11 of the UWB planar monopole	118
Figure 4.26 (a) The configuration and (b) Experimental model of the dual element antenna array	118
Figure 4.27 Simulated and measured S-parameters of the dual-elements antenna array	119
Figure 4.28 (a) The configuration and (b) Experiment model of dual element antenna array and with one slit-patch structure	120
Figure 4.29 Simulated and measured S-parameters of the UWB planar monopole	

array with one slit-patch structure	121
Figure 4.30 (a) The configuration and (b) Experimental model of the dual element antenna array with two slit-patch structure	122
Figure 4.31 Simulated and measured S-parameters of UWB planar monopole array with two slit-patch structure	123
Figure 4.32 (a) The configuration and (b) Experiment model of the dual element antenna array with three slit-patch structure	123
Figure 4.33 Simulated and measured S-parameters of UWB planar monopole array with three slit-patch structure	124
Figure 4.34 Current flow and distribution on the ground plane with three slit-patch structure at 3.5GHz	125
Figure 4.35 (a) S11 and (b) S21 of the antenna array for different positions	126
Figure 4.36 (a) The configuration and (b) Experimental model of the dual-element antenna array with three slit-patch structure when D is 1mm	127
Figure 4.37 The simulated and measured S-parameters of the dual-element antenna array with three slit-patch structure when D is 1mm	127
Figure 4.38 Current flow and distribution on the ground with three slit-patch structure when D is 1mm	128
Figure 4.39 The total efficiency of the whole antenna system in the presence of multiple slit-patch structures	129
Figure 5.1 Configuration of the slit-patch EBG structure	136
Figure 5.2 Single convoluted slit excited by a microstrip line	137
Figure 5.3 Geometry of one convoluted slit-patch EBG structure	137
Figure 5.4 Simulated S21 with and without a conducting patch	138
Figure 5.5 Simulated S21 with different width of conducting patch	139
Figure 5.6 Two identical slit-patch EBG structures on the ground plane	139
Figure 5.7 Simulated S21 with multiple double-layer slit-patch structures	140
Figure 5.8 Two-element PIFA array with (a) Two convoluted slits, (b) Two convoluted slit-patch structures	141

Figure 5.9 Simulated S-parameters of the PIFA array with two convoluted slits on ground plane	141
Figure 5.10 Simulated (a) S11 and (b) S21 of the PIFA array with the different width of slit-patch	142
Figure 5.11 Simulated S-parameters of the PIFA array with the slit-patch on the ground plane	143
Figure 5.12 Two-element PIFA array with four convoluted slit-patch structures	143
Figure 5.13 Simulated S-parameters of PIFA array with four slit-patch structures	144
Figure 5.14 Correlation coefficient for two and four Slit-patch EBG structures	144
Figure 5.15 Photograph of the PIFA array with(a) two slit-patch structures (b) four slit-patch structures on the ground plane	145
Figure 5.16 Measured S-parameters for the PIFA array (a) with two slit-patch structures and (b) with four slit-patch structures	146
Figure A.1 The Wheeler-Cap method and the equivalent circuit	155

List of Abbreviations

1-D	One-dimensional
1G	First Generation
2-D	Two-dimensional
2G	Second Generation
3-D	Three-dimensional
3G	Third Generation
4G	Fourth Generation
AWGN	Additive White Gaussian Noise
BLAST	Bell labs Layered Space –Time
CPW	Coplanar Waveguide
CST	Computer Simulation Technology
DGS	Defected Ground Structures
EBG	Electromagnetic Band Gap
EM	Electromagnetic
FDTD	Finite Difference Time Domain
FE	Finite Element
FIT	Finite Integral Technique
GSM	Global System for Mobile Communications
IFA	Inverted-F Antenna
ILA	Inverted-L Antenna
LAN	Local Area Network
MC	Mutual Coupling
MEG	Mean Effective Gain
MIMO	Multi-Input Multi-Output
MoM	Method of Moments

PBA	Perfect Boundary Approximation
PBG	Photonic Band Gap
PCS	Personal Communication Service
PDA	Personal Digital Assistant
PIFA	Planar Inverted-F Antenna
SAR	Specific Absorption Rate
SISO	Single-Input Single-Output
SIMO	Single-Input Multiple-Output
UWB	Ultra WideBand
UMTS	Universal Mobile Telecommunications System
VoIP	Voice over Internet Protocol
WAN	Wide Area Network
WiFi	Wireless Fidelity
WIMAX	Worldwide Interoperability for Microwave Access
WLAN	Wireless Local Area Network

Chapter 1

Introduction

1.1 Background

With the development of new wireless communication technologies, wireless communication services have had an enormous impact throughout the whole world in the last few decades. In 2011, the wireless and mobile communication service subscribers were about 87% of the world's population. However, this proportion of the population was just 34.4% in 2005 [1]. Recently, wireless communication has gone into a faster growth period due to some technologies such as cellular networks, PCS (Personal Communications Service) and Internet access. After the Internet access was widely deployed, wireless communication systems connected consumers all over the world. People are now dependent on the wireless and mobile communication services for everyday activities in all walks of life, including entertainment, business, and industry. Improving the performance of wireless communication systems by increasing the data rate, making the systems more reliable, ensuring they are power efficient and selling them more cheaply, are all critical factors in meeting the tremendous growth of consumers' demand.

1.1.1 Mobile and Wireless Communications Systems

From 1990's, mobile communication technologies have experienced significant growth from first-generation (1G) analogue voice-only communication to the fourth-generation (4G) mobile telephone technology, as illustrated in Figure 1.1. The 2G digital communication technologies have been widely deployed including GSM (Global System for Mobile Communications) in Europe, PAS (Personal Access System) in China, D-AMPS (Digital AMPS) in United States and Canada. Now, the third generation mobile communication technology provides users with some new services: Voice over Internet Protocol (VoIP), High speed Internet access, unparalleled network capacity and "always-on" access [2]. In the near future, based on all-IP network, fourth generation mobile technology will provide ultra-speed access services, IP telephony, gaming services, high definition TV, and other streaming multimedia[3].

After WLAN (wireless local area network) obtained its license-free spectrum bands, WLAN has become a very important part of the wireless communication market. The WLAN system, also called as Wi-Fi based on the IEEE 802.11 specifications, provides a high speed Internet access to personal wireless terminal within limited coverage. Large cities have built enormous wireless networks made up of Wi-Fi access points (Hot-Spots) due to its cheap price, high data rate and reliability. Both mobile communication and WLAN technologies need higher data rate to meet consumer's demands [4]. The channel capacity of a Single Input Single Output (SISO) system is depended on channel bandwidth and signal-to-noise ratio (SNR). However, the radio spectrum has been occupied by various wireless communication systems. Therefore, the study of increasing spectrum efficiency is an important research topic.

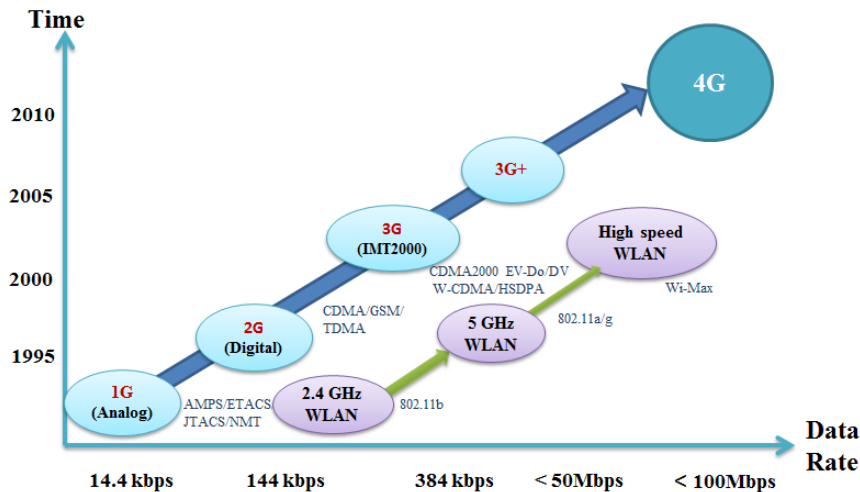


Figure 1.1 The growth of the wireless and mobile communication systems [4]

1.1.2 MIMO System

Initially, mobile phones were designed for voice communication services only. After the growth of wireless and mobile communication services in the last decade, huge numbers of mobile terminal devices went onto the market. With the requirement for data transmission increasing, there is a big challenge concerning how to obtain the expected data rate. The appearance of the Multiple Input Multiple Output (MIMO) system breaks through this technical limitation. In 1987, Winters proposed multiple antennas employed at both receiver and transmitter to increase the channel capacity with a fixed bandwidth [5]. In the late 1990s, the MIMO system was shown to be a viable method of developing the potential of the channel capacity [6, 7, 8]. From 2001, Lucent Technology (Bell Labs Innovations) and Stanford University have conducted measurements of the performance of MIMO systems in different environments [9-12]. The measurement results demonstrated that the capacity of the MIMO system had a significant improvement compared to the Single Input Single Output (SISO) system. Since then, research in MIMO systems has significantly increased, as the feasibility of MIMO technology has received overwhelming acceptance [8].

1.2 Motivation

When a MIMO system is employed for a compact wireless or mobile terminal, high electromagnetic coupling appears between antenna elements. The electromagnetic coupling is also called as mutual coupling. It disturbs the radiation pattern and the input impedance of every element [13]. Recent studies have shown that the high mutual coupling increase the correlation coefficient between MIMO antenna elements and significantly reduce the channel capacity of MIMO system [14-17]. The separation between antenna array elements (the distance of the feed points) is one important constraint in the design of MIMO systems for compact wireless terminal. Minimal mutual coupling could be obtained by placing the antenna elements more than a half wavelength apart in theory [13]. This is the reason why the MIMO systems had been mainly employed for the base stations and wireless routers which allow enough space to deploy an antenna array. It is a challenging task to place one MIMO antenna array into a compact wireless terminal with low mutual coupling. Therefore, the practical and realistic MIMO antenna system designs which are appropriate for compact wireless terminal devices must be carefully designed and optimized to reduce the mutual coupling between antenna elements.

Several methods have been presented to reduce the mutual coupling between antenna array elements. Novel antenna designs were proposed to achieve a high isolation for compact mobile terminals [18-20]. Electromagnetic Band-Gap structures were studied as a method to increase the isolation between array antennas [21-23]. Single [24] or multiple [25] defects (slots or slits) on the ground plane have also attracted significant interest due to the ease of fabrication and the applicability for different antenna types. By suppressing surface current flowing on ground plane between antenna elements, these methods succeed in reducing mutual coupling between antennas. Recently, an optimised pair of slits etched on the ground plane has been presented to significantly

reduce the mutual coupling between two Planar Inverted F Antennas (PIFAs) on a compact ground plane [26]. For an ideal MIMO antenna array, the antenna system should have a transmission zero between antenna elements [27]. For a dual-elements antenna array, the mutual coupling between antenna array elements should be less than -20dB [27].

1.3 Contribution Highlights

Methods for the reduction of the mutual coupling between closely spaced antennas include those using Electromagnetic Band-Gap structures (EBGs) or Deflected Ground Structure (DGS) to suppress the surface current on the ground plane [25, 28]. EBG structures which consist of periodic arrangements of dielectric material and metal conductors manipulate the propagation of electromagnetic waves in specific frequency. However, typical periodic EBG structures occupy a large area on a ground plane. This affects the installation of other electronic components. In comparison to EBG structures, the DGS is relative small and easy to fabricate as few slots or slits etched in the existing ground plane. However, unless carefully designed it may take up significant area of the ground plane, and more importantly fail to suppress the surface current on ground plane. Therefore, it is still a very challenging task to reduce the size of DGS and EBGs whilst suppressing the surface current for compact mobile terminal devices.

In this project, novel designs of DGS and EBG structures are designed and demonstrated to decouple different closely placed antennas, such as PIFAs, printed monopoles and UWB monopoles. Initially, a dual-element modified PIFA array operating at 1.9GHz is proposed and optimized. A pair of optimized linear slits is inserted on the ground plane and significantly reduce mutual coupling by suppressing the surface current between the two closely placed PIFAs. However, due to their

length and shape, the slits occupy large area of the ground plane. A miniaturised convoluted slit is optimised to have a small footprint and are positioned close to the edges of the ground plane thereby occupying very little space. A transmission minimum is obtained by virtue of the resonance of the convoluted slits resulting in a significant reduction of the mutual coupling across the operating frequency band of the antennas. The convoluted slits are also employed to reduce coupling of the human body to the antenna array.

Although the convoluted slits are much smaller in comparison to the linear slits, their dimensions still need to be further miniaturised to accommodate the practical applications such as compact wireless terminals. Recently, a novel miniaturized Complementary Metallodielectric Electromagnetic Band Gap Structure (CMEBG) was presented, offering a small structural footprint and a wide bandwidth for the band gap region [29]. A novel double-layer miniaturised slit-patch EBG structure based on the CMEBG is proposed to reduce the mutual coupling between antenna array elements. The dimensions and shapes of the proposed EBG structures are optimised to produce maximum miniaturisation thereby occupying very little area on a compact ground plane. Following investigations of the double-layer EBG structure, a dual-element CPW-fed printed monopole antenna array operating at 2.45GHz is designed to further evaluate the performance of the proposed double-layer EBG structure. Also, the double-layer slit-patch EBG structures reduce the mutual coupling for a dual-element UWB planar monopole array operating from 3GHz to 6GHz. Based on this, the size of UWB planar monopole array has a significant reduction, as compared to the original design without slit-patch EBG structure.

In summary, the DGS structures in this thesis illustrate practical approaches to reduce mutual coupling between antenna elements for compact wireless terminals. And the double-layer EBG structures miniaturise the dimensions of the slits etched on the ground plane.

1.4 Chapter Outlines

The thesis is organized into six chapters as follows:

Chapter 2: This chapter presents the introduction to MIMO systems and their channel capacities. Three different types of small antennas for mobile terminals are described. Two special structures (EBG and DGS), together with their advantages and disadvantages, are discussed in detail.

Chapter 3: This chapter addresses linear and convoluted slits. The characteristics of a dual-element PIFA (Planar Inverted-F Antenna) array (such as: S-parameters, surface current distribution and radiation pattern) are presented and analyzed. The novel linear slits and convoluted slits are proposed and optimized to reduce the mutual coupling between the two closely spaced PIFAs. The fabricated prototype models are measured to evaluate the simulated results. Ultimately, the detuning of the PIFA array caused by the human body is assessed both with and without the proposed convoluted slit structure.

Chapter 4: This chapter introduces a miniaturized double-layer slit-patch EBG structure and its transmission characteristics. A microstrip line excitation is initially presented for the efficient analysis and design of the proposed double-layer slit-patch EBG structures. A modified printed monopole and its dual elements array are mounted on a compact substrate for a wireless terminal device operating at 2.46GHz. The proposed slit-patch EBG structures significantly reduce the mutual coupling between two antennas and yield a maximum miniaturization of the antenna array thereby occupying very little space in a compact wireless terminal device. Furthermore, a dual-element modified UWB planar monopole array operating from 3GHz to 6 GHz is studied to demonstrate the versatility of the proposed slit-patch EBG structure.

Chapter 5: This chapter describes another type of slit-patch EBG structure comprising convoluted slits and conducting patches. Simulated transmission responses for different conducting patch widths are presented. Multiple identical slit-patch EBG structures are proposed to extend the bandwidth of the transmission response. The new slit-patch EBG designs reduce the mutual coupling between two PIFAs placed on a compact ground plane below -20dB at the resonance of the antennas. Four identical slit-patch EBG structures are presented to further reduce the correlation coefficient between the two PIFAs.

Chapter 6: This chapter presents the conclusion and some thoughts for future work.

References

- [1] Global Wireless Telecommunications Carriers Market Research Report Jul 2012, <http://www.ibisworld.com/industry/global-wireless-telecommunications-carriers.html>
- [2] T. S. Rappaport, "Wireless Communications Principles and Practice," Second Edition, 2010, pp. 13-55.
- [3] S. Parkvall, E. Dahlman, A. Furuskär, Y. Jading, M. Olsson, S. Wänstedt, and K. Zangi, "LTE Advanced – Evolving LTE towards IMT-Advanced," *Vehicular Technology Conference*, 21–24 September 2008.
- [4] D. Rouffet, S. Kerboeuf, L. Cai, V. Capdevielle, "4G Mobile Technical Paper," *Alcatel Telecommunications Review* 2nd Quarter 2005, www.alcatel.com/atr
- [5] J. Winters, "On the capacity of radio communication system with diversity in a rayleigh fading environment," *IEEE Journal on Selected Areas in Communications*, vol. 5, no. 5, pp. 871-878, June 1987.

- [6] G. Foschini, "Layered space-time architecture for wireless communication in a fading environment when using multi-element antennas," *Bell Labs Technical Journal*, vol. 1, no. 2, pp. 41-59, 1996.
- [7] G. Foschini, and M. Ganst, "On the limits of wireless communication in a fading environment when using multiple antennas," *Wireless Personal Communications*, vol. 6, no. 3, pp. 311-335, March 1998.
- [8] I. E. Telatar, "Capacity of multi-antenna gaussian channels," *European Transactions on Telecommunications*, vol. 10, no. 6, pp. 585-595, November 1999.
- [9] M. Gans, N. Amitay, Y. S. Yeh, T. D. H. Xu, R. Valenzuela, T. Sizer, R. Storz, D. Taylor, W. MacDonald, C. Tran, and A. Adamiecki, "Outdoor blast measurement system at 2.44 GHz: calibration and initial results," *IEEE Journal on Selected Areas in Communications*, vol. 20, no. 3, pp. 570-586, April 2002.
- [10] P. Kyritsi, "Multiple element antenna systems in an indoor environment," Ph.D. thesis, Stanford University, USA, 2001.
- [11] P. Kyritsi, P. Wolniansky, and R. A. Valenzuela, "Indoor blast measurements, in Multiaccess, Mobility and Telstar for Wireless Communications," K. A. Publishers, Ed., vol. 5, 2000, pp. 4960.
- [12] D. Chizhik, J. Ling, P. Wolniansky, R. Valenzuela, N. Costa, and K. Huber, "Multiple-input multiple-output measurements and modeling in manhattan," *IEEE Journal on Selected Areas in Communications*, vol. 21, no. 3, pp. 321-331, April 2003.
- [13] W. L. Stutzman, and G. A. Thiele, "Antenna Theory and Design," New York Wiley, 2nd Edition, 1998.
- [14] Fletcher, P. M., M. Dean, and A. R. Nix, "Mutual coupling in multi-element array antennas and its influence on MIMO channel capacity," *IEE Electronics letters*, Vol. 39, No. 4, 342-344, 2003.
- [15] Skafidas, E. and R. J. Evans, "Antenna effects on the capacity of MIMO

- communications systems in Rayleigh channels,” *Proc. of IEEE Personal Indoor and Mobile Radio Communications*, Vol. 1, 617–621, 2004.
- [16] McNamara, D. P., M. A. Beach, and P. N. Flescher, “Experimental investigation into the impact of mutual coupling on MIMO communication systems,” *Proc. of Int. Symp. on Wireless Personal Multimedia Communications*, Vol. 1, 169–173, Sep. 2001.
- [17] Borja, C., A. Algans, M. Royo, J. Anguera, and C. Puente, “Impact of the antenna technology and the antenna parameters on the performance of MIMO systems,” *Proc. of IEEE Antennas and Propagation Symposium*, Vol. 2, 507–510, 2003.
- [18] Y. Gao, X. Chen, Z. Ying, and Clive. Parini, “Design and Performance Investigation of a Dual-Element PIFA Array at 2.5 GHz for MIMO Terminal,” *IEEE Trans. Antennas and Propag.*, 55, (12), 2007, pp. 3433-3441.
- [19] C.C. Chiau, X. Chen, and C.G. Parini, “A Miniature Dielectric-Loaded Folded Half-Loop Antenna and Ground Plane Effects,” *IEEE Antennas and Wireless Propagation*, vol. 4, pp. 459-462, 2005.
- [20] Y. Gao, C. C. Chiau, X. Chen and C. G. Parini, “Modified PIFA and its Array for MIMO Terminals,” *IEE proceeding on Microwaves, Antennas and Propagation*, Volume 152, Issue 4, Page(s):253-257, August 2005.
- [21] R. Makinen, V. Pynttari, J. Heikkinen, and M. Kivikoski, “Improvement of antenna isolation in hand-held devices using miniaturized electromagnetic band-gap structures,” *Microwave Opt. Technol. Lett.* vol. 49, no 10, pp. 2508 –2513, 2007.
- [22] F. Yang, and Y. Rahmat-Samii, “Microstrip Antennas Integrated With Electromagnetic Band-Gap (EBG) Structures: A Low Mutual Coupling Design for Array Applications,” *IEEE Transactions on Antennas and Propagation*, pp. 2936-2944. Oct. 2003.
- [23] C.C. Chiau, X. Chen, and C.G. Parini, “A Sandwich Multi-period EBG

- Structure for Microstrip Patch Antennas,” *Microwave and Optical Technology Letter*, vol. 46, no. 5, pp. 437-440, 5 Sept 2005.
- [24] M. Karaboikis, C. Soras, G. Tsachtsiris, and V. Makios, “Compact Dual-Printed Inverted-F Antenna Diversity Systems for Portable Wireless Devices,” *IEEE Antennas and Wireless Propagation*, vol. 3, 2004, pp. 9-14.
- [25] C.-Y. Chiu, C.-H Cheng, R.D. Murch, and C. R. Rowell, “Reduction of mutual coupling between closely packed antenna elements,” *IEEE Antennas and Wireless Propagation*, Vol. 55, No. 6, pp. 1732 – 1738, Jun. 2007.
- [26] T. Kokkinos, E. Liakou, and A. P. Feresidis, “Decoupling Antenna Elements of PIFA Arrays on Handheld Devices,” *IET Electronics Letters*, 44 (25), 2008, pp. 1442-1444.
- [27] R.G. Vaughan and J.B. Andersen, “Antenna diversity in mobile communications,” *IEEE Trans. Vehicular Technology*, vol. 36, pp. 147-172, Nov 1987.
- [28] H.L. Xu, Y. G. Lv, X.G. Luo, and C. Du, “Method for Identifying the Surface Wave Frequency Band-Gap of EBG Structures”. *Microwave and Optical Technology Letters*, Vol. 49, pp. 2668–2672, November 2007.
- [29] A.P. Feresidis, G. Apostolopoulos, N. Serfas, J.C. Vardaxoglou, “Closely coupled metallodielectric electromagnetic band-gap structures formed by double-layer dipole and tripole arrays,” *IEEE Transactions on Antennas and Propagation*, Vol.52, pp.1149-1158, May 2004.

Chapter 2

MIMO Systems on Compact Wireless Terminals

2.1 Introduction

In this chapter, the theoretical background of this thesis is presented and explained. Initially, the channel capacity of wireless communication system is described. Definitions of SISO (Single Input Single Output) and MIMO (Multiple Input Multiple Output) systems are given, and their channel capacities are explained. By employing multiple antennas at the transmitter and receiver, the channel capacity of a MIMO system increases with the number of antenna elements increasing [1]. However, due to stringent space limitations, when the MIMO system is implemented in a compact wireless terminal device, it becomes difficult to employ multiple antennas whilst maintaining the performance of the antenna array [1]. In comparison to a single antenna for a SISO system, multiple antennas which are employed for MIMO system must have compact size, low profile and meet some additional requirements such as good isolation and lower correlation. In this thesis, three different types of antennas will be implemented respectively to form antenna arrays, namely PIFAs (Planar Inverted F Antennas), printed CWP-fed monopoles, and UWB (Ultra-wideband) monopoles, and these are described in section 2.3. In sections 2.5 and 2.6, an extensive overview of EBG and DGS is given. The properties and applications of the two structures are explained. Finally, an overview of the electromagnetic modeling

tools utilized throughout the thesis, based on CST Microwave Studio, is provided in section 2.7.

2.2 Wireless Channel and Capacity

Wireless communication technologies have experienced an explosive growth to meet the rapidly increasing requirement for wireless multimedia services and wireless computer networking. Modern wireless communication systems are required to increase their channel capacity, QoS (Quality of Service), reliability and coverage. However, in conventional wireless communication systems, the SISO systems which employ one antenna both at the transmitter and receiver cannot support enough channel capacity for the demand of wireless communication systems without additional radio spectrum and transmission power [2]. The channel capacity of SISO with an AWGN (Additive White Gaussian Noise) was first defined by Claude Shannon [2, 3]. It is shown to be [4]:

$$C = W \log_2 \left(1 + \frac{P}{WN_0} \right) \quad (2.1)$$

where W is the channel bandwidth, P is the received mean power, and N_0 is the noise power spectral density. This equation illustrates that the channel capacity of a SISO system is dependent on the transmission bandwidth and the SNR ($P/(WN_0)$) value. For a SISO system with a fixed bandwidth (W), the channel capacity only depends on the SNR. Meanwhile, the radio spectrum is an extremely scarce and valuable commodity for all wireless communication systems.

The application of multiple antennas at both the transmitter and the receiver through multipath channels defined as MIMO system, has been proposed as a method of improving the channel capacity [5]. In a MIMO system, at the transmitter, multiple

antennas send multiple streams through uncorrelated channels. At the receiver terminal, the multiple streams are received by multiple antennas and sorted to obtain the original stream of data using a special signal algorithm [6]. The received signal vector $r(t)$ is defined by:

$$r(t) = [r_1(t), r_2(t), \dots, r_{n_r}(t)]^T \quad (2.2)$$

where $r_{n_r}(t)$ is the signal at the n_r -th receiver element and $[\cdot]^T$ denotes the transpose operation. Similarly, the transmitted signals is defined as:

$$s(t) = [s_1(t), s_2(t), \dots, s_{n_t}(t)]^T \quad (2.3)$$

where $s_{n_t}(t)$ is the signal at the n_t -th transmitter element. A usage of such a channel can be described by the following matrix equation, using the relation of the vector $r(t)$ to $s(t)$ [7]:

$$r(t) = H(t)s(t) + n(t) \quad (2.4)$$

where the H ($n_r \times n_t$) are the MIMO radio channel matrix, n_r and n_t are the numbers of the transmitters and receivers, $n(t)$ is the additive noise matrix between transmitters and receivers. For example, two antennas were employed at both transmitter and receiver ends shown in Figure 2.1. The received signal is derived as:

$$r_1(t) = H_{11}(t)s_1(t) + H_{12}(t)s_2(t) + n_1(t) \quad (2.5)$$

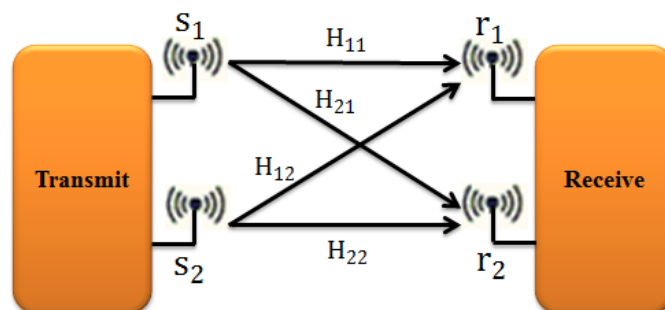


Figure 2.1 Multiple channels of a 2×2 MIMO system

Generally, the MIMO channel can be analysed as a set of sub-channels, and the sub-

channels eigenvector is used for calculating the capacity of the MIMO channel. When the transmit power is equally allocated to all antenna elements, the total capacity of a MIMO system has been derived as [8-10]:

$$C = W \log_2 \det \left(I + \frac{H^H H S}{n_t N} \right) \quad (2.6)$$

where W is the single sub channel bandwidth, S is the received mean power, \det is the determinant, N is the noise power on each receiver antenna, and I denotes the identity matrix. H^H is the Hermitian transpose of H . Compared to the channel capacity of a SISO system [11], the capacity of a MIMO system achieves almost the sum of n SISO channels [12]. Hence, when both n_t (number of transmit antennas) and n_r (number of receiver antennas) increase, the capacity increases linearly with respect to $\min\{n_t, n_r\}$. The capacity of a MIMO system has an enormous improvement over the single channel system, as shown in Figure 2.2.

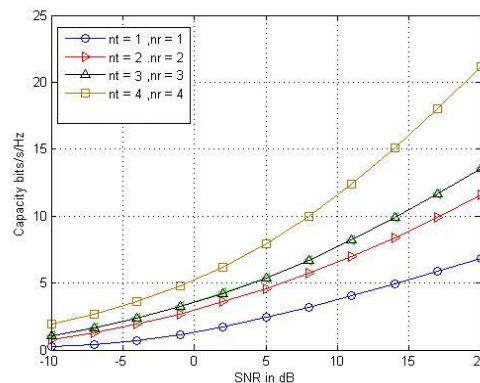


Figure 2.2 MIMO channel capacity for different number of antenna elements [8]

2.3 Compact Mobile and Wireless Terminal Antennas

Recently, two trends of antenna designs for compact portable terminal devices are evidenced [13]: the first one demands that the antenna is smaller, built-in, and supports multiple communication systems such as GSM, UMTS and WLAN; the

second one demands that the antenna system supports absolute quality and quantity of transmission data for various users' requirements. As introduced in the last section, the MIMO system employs multiple antennas at both the transmitter terminal and receiver terminal ends. The channel capacity of a MIMO system increases with the number of antennas at the transmitter and receiver terminal increasing [9]. In order to accommodate multiple antennas in compact wireless terminal, the built-in antennas should meet certain essential factors such as: minimum occupied volume, light weight, adequate bandwidth, isotropic radiation characteristics, and low fabrication cost [14]. A major factor is that the antenna array should have low mutual coupling between the individual elements. When multi antennas are placed close to each other, high mutual coupling appear and affect the performance of the antenna array such as the radiation patterns, input impedance of antenna elements and channel capacity [15-17]. The impact of mutual coupling between two dipoles for different antenna separation is presented in Figure 2.3. The radiation patterns of antenna 1 have significant difference with the separation (d) decrease [18]. Therefore, when multiple antenna elements are employed to form a MIMO system on compact wireless terminal device, antenna geometry and the position of antenna elements in the array need to be optimised for reducing mutual coupling level between antenna elements. Three widely used antennas which are applied for mobile and wireless terminals such as PIFA, printed CPW-fed monopole and UWB monopole antenna are presented in this section.

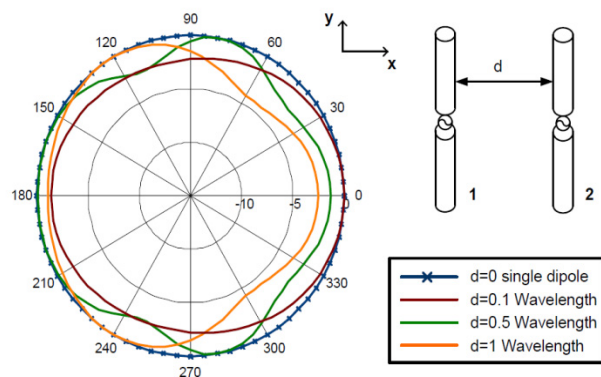


Figure 2.3 Radiation patterns of one dipole in a dual-element antenna array for different separations (d) [18]

2.3.1 Planar Inverted-F Antenna

In last ten years, with the volume and weight of mobile terminal devices decreasing, the antenna design for handsets has undergone an evolution from extendable to internal. The evolution process from monopole to PIFA (Planar Inverted-F Antenna) is presented in Figure 2.4. The monopole was the most common antenna for the handset in the 1980's. However, with the development of mobile communication technology, the monopole antenna is not suitable for compact modern mobile terminal devices due to its high profile. The ILA (Invert-L Antenna) is the simplest improvement of the monopole. This antenna has a low profile, including a short vertical part and a longer horizontal part. The ILA is difficult to impedance match to a feed line because the impedance of ILA consists of a low resistance and a high reactance caused by the horizontal part close to ground plane. An L-shaped stub was added close to the feeding pin, and a new antenna named as IFA (Inverted-F Antenna) was formed to improve the matching characteristics of ILA [13]. Nevertheless, both the ILA and IFA have narrow impedance bandwidth because of their small radiation elements. Finally, the PIFA has emerged by using a planar patch as the radiation elements to increase the bandwidth of antenna [19].

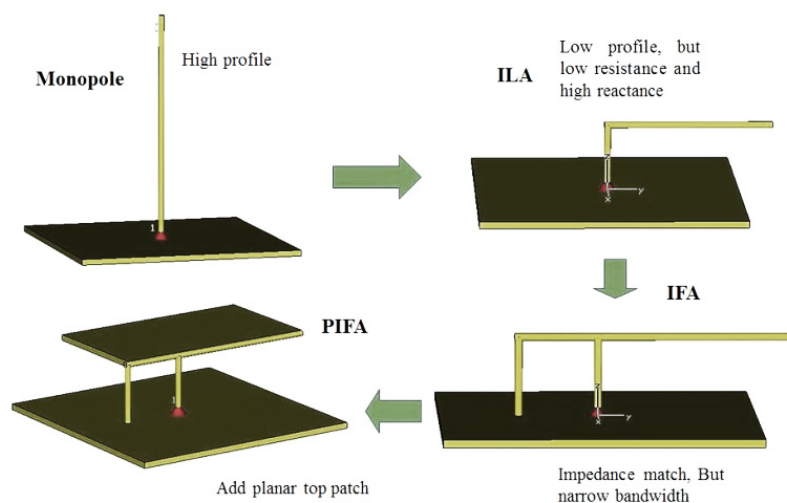


Figure 2.4 The evolution process from monopole to PIFA [19]

As presented in Figure 2.5, the PIFA consists of a shorting point, a feeding point and a planer radiating patch. It has compact dimensions and resembles a letter F which faces down. There are two dimensional values, the width and length of the radiating patch, which affect the resonant frequency of the antenna derived by [20]:

$$f = \frac{c}{4(L+W)} \quad (2.7)$$

where, f is the resonant frequency, c is the speed of the light in the free space, L and W are the length and width of antenna radiating element.

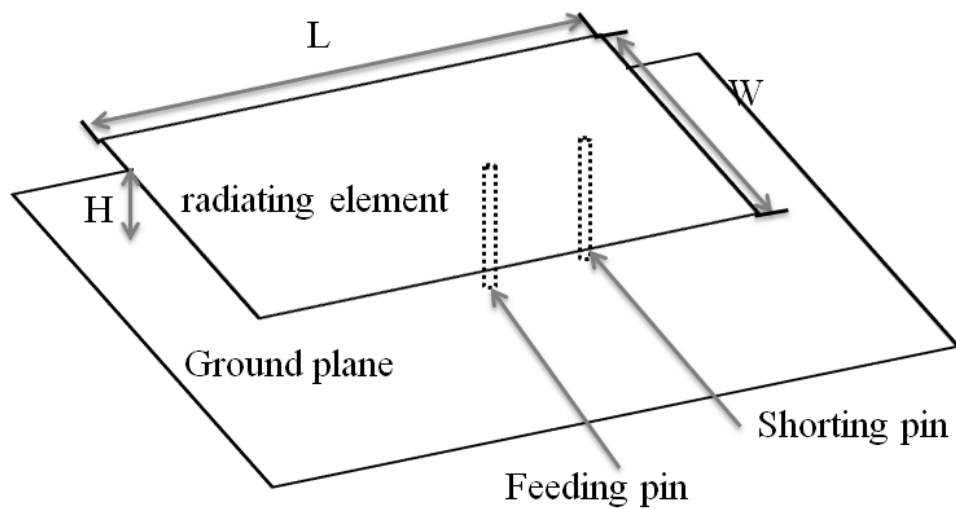


Figure 2.5 Configuration of a Planar Inverted-F Antenna

Compared to a conventional antenna, the PIFAs have been presented to support a multiband system by implementing some promising radiating top patches [21-23]. PIFAs are able to widen bandwidth by adding a parasitic element at the open end [24, 25]. In personal communication systems, PIFAs effectively reduce the backward radiation and electromagnetic energy toward the users' head in comparison to some conventional mobile terminal antennas like monopoles and whip antennas which present omnidirectional radiation [20]. The PIFAs have been widely applied to various wireless communication devices for their advantageous characteristics.

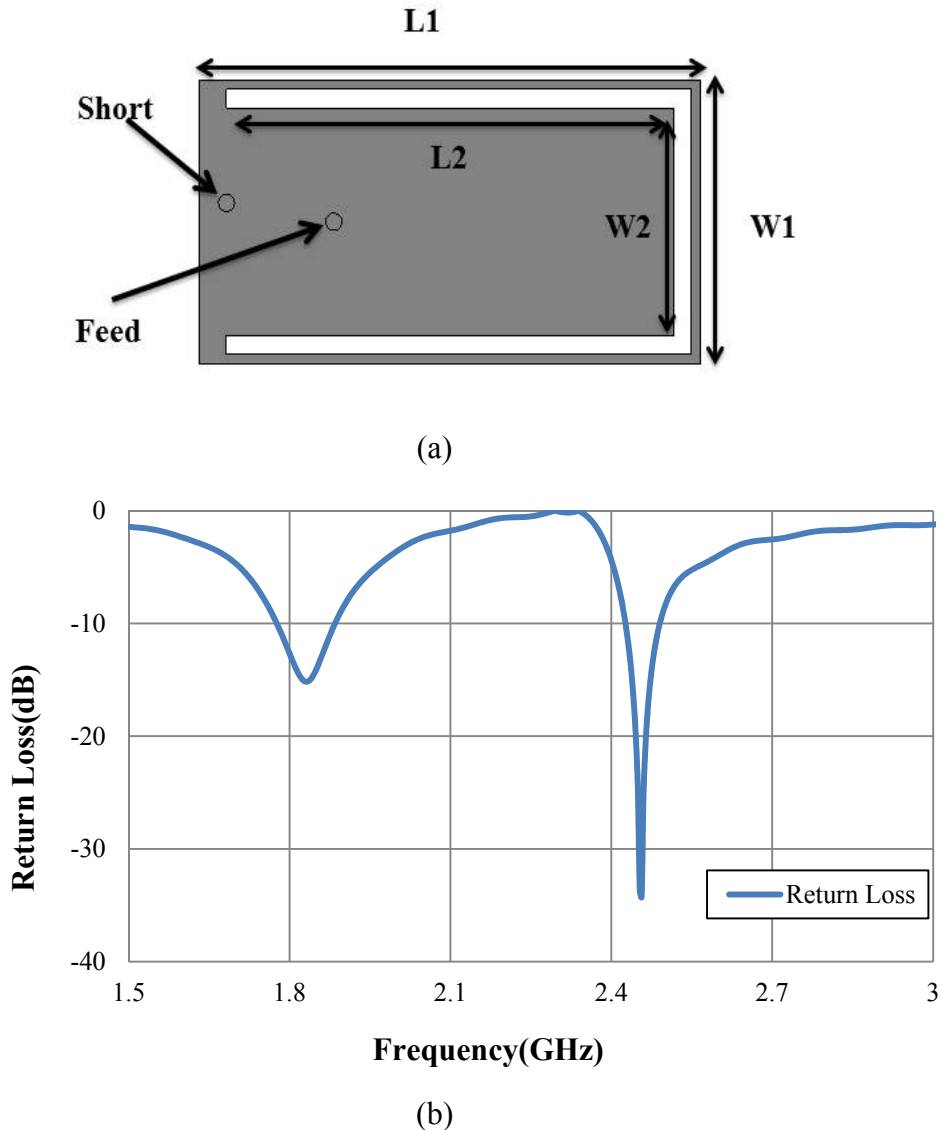


Figure 2.6 (a) The geometry and (b) Return Loss of the dual-band PIFA with a U-shape slot patch

A dual-band PIFA which operates for GSM and WLAN is presented in Figure 2.6(a). This design employs an embedded U-shaped slot in the radiating top patch. In the top patch, a small inner rectangular patch with dimension $L_2 \times W_2$ for operating around 2450 MHz is obtained. The external rectangular patch with dimension $L_1 \times W_1$ is for 1800MHz band operation. The simulated return loss of this PIFA is presented in Figure 2.6(b). This kind of multi-band PIFA has been widely used for different mobile terminals by the mobile terminal manufacturers [20].

2.3.2 Printed CPW-fed Monopole

Conventional monopoles were widely implemented in the past for the applications of the mobile phone as external antennas. However, these antennas have high profile and increase the overall volume of a mobile phone. Novel very low-profile monopole antennas were designed to be printed on substrates as a built-in antenna. This monopole is always fed by CPW (Coplanar Waveguide) line. The radiating element, CPW line and ground plane are printed on the same side of the dielectric substrate [26, 27]. The geometry of a square planar monopole with a 50Ω CPW line is described in Figure 2.7. It is obvious that the CPW-fed printed monopole is best suited to be fabricated as a separate antenna module for a wireless compact terminal like laptop or table PC [26-29]. The characteristics of the proposed CPW-fed printed monopole are determined by several design parameters [30]. The feed gap (H) and the width of the ground plane (W) will significantly affect the input impedance and the operating bandwidth [30]. The dimension of the radiating element determines the first resonant frequency. This kind of printed CPW-fed monopole will be studied to form a MIMO antenna array in Chapter four.

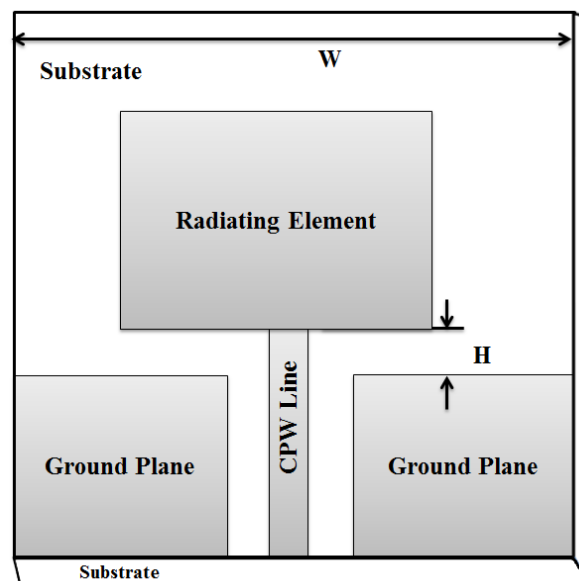


Figure 2.7 Geometry of a CPW-fed printed monopole

2.3.3 UWB Monopole Antenna

UWB (Ultra WideBand) technology has attracted much attention since the FCC (Federal Communications Commission) allowed the free license of the frequency spectrum 3.1-10.6GHz to UWB systems at low power usage in 2002 [31]. In comparison to other wireless communication standards, the UWB system has the maximum bandwidth, the minimum transmission energy and a lower multipath interference as shown in Figure 2.8 [32]. There are five kinds of applications over the UWB frequency spectrum [33]: short range wireless communication system, radars for detecting vehicles, robotics position and movement, communication systems for the military, UWB short pulse radars for inner inspection in medical and underground exploration. The UWB communication technology is principally studied to constitute a new wireless communication system which supports relative larger bandwidth in comparison to conventional wireless systems which have narrow percent bandwidth defined as the ratio of absolute bandwidth to center frequency: $(\frac{f_H-f_L}{f_c})$.

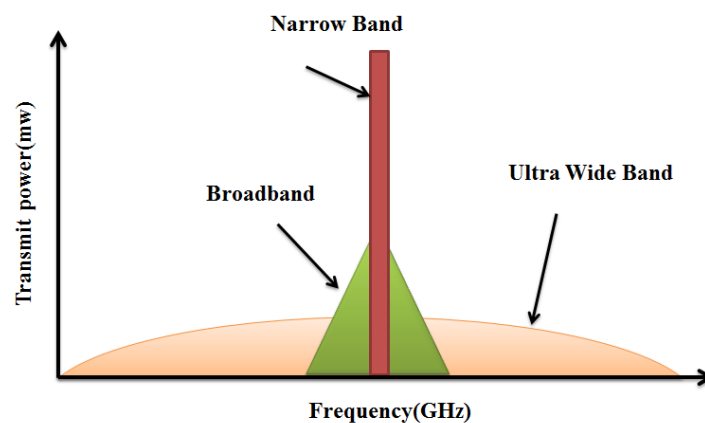


Figure 2.8 The relation between UWB and other wireless communication systems[32]

The various kinds of wireless communication systems are presented in Figure 2.8. As the UWB systems operate in the same spectrum that some existing wireless communication systems have occupied, interference will occur. Stringent regulations for UWB have been set by organizations and governments to improve the

compatibility between UWB and other communication systems [33]. In a small coverage, the UWB system which operates at the minimum power level is not disturbed by severe interference from other existing narrow band communication systems which operate in the assigned frequency band. In the near future, UWB technology will be applied to PCS in the 4G project [34].

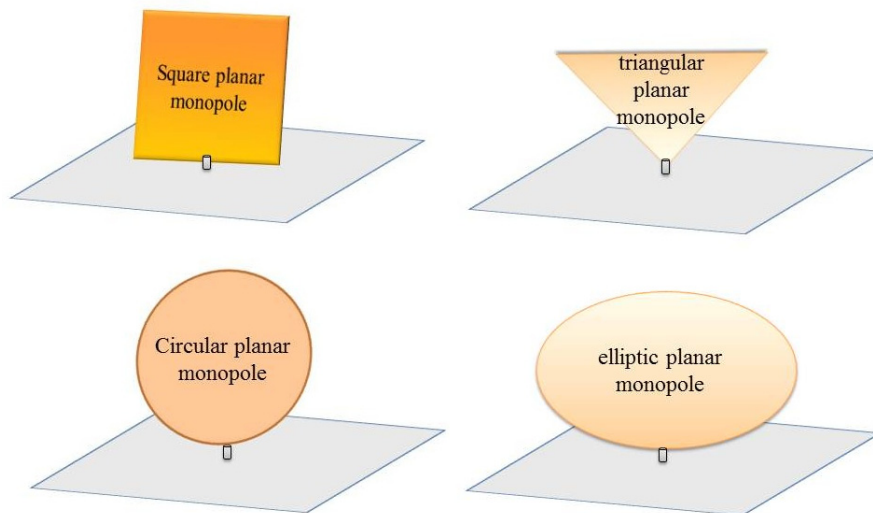


Figure 2.9 Different UWB Planar monopoles [39]

Planar UWB monopoles have received much attention for their attractive characteristics such as their consistent polarization and radiation pattern parameters [35-38]. The radiating elements of a planar UWB monopole, fed by either a coplanar waveguide line or a microstrip line, are made into various shapes for different applications such as: square, circular, elliptic, triangle and so on, as shown in Figure 2.9[39]. Initially, in order to suppress horizontal currents on ground plane and to obtain a stable omni-radiation pattern, the radiating elements are perpendicular to their ground planes. However, it is difficult to mount the antenna module into a compact wireless device. Therefore, the radiating elements and their feed lines are printed on the same side of a dielectric substrate. Nevertheless, strong surface current are generated and widely spread over the PCB [40]. The radiation from the current on the PCB will seriously damage the antenna radiation parameter and produce high

mutual coupling between antenna elements when multiple planar UWB monopoles are employed to form MIMO systems. Suppressing the surface current on a PCB will be studied in Chapter four.

2.4 Mutual Coupling and Correlation

Mutual coupling refers to the electromagnetic interactions between antenna array elements. When multiple antennas are placed on a compact ground plane to form MIMO system, high surface current appears on the ground plane between antenna elements. In this way, some energy which is transmitted by an antenna is transferred to other nearby antennas. The current on radiating element consists of the current from transmitting antenna and the current induced by other antenna elements [41]. The mutual coupling will affect the radiation patterns and input impedance of antenna elements adjacent to each other due to the small separation between them, as shown in Figure 2.10. The performance of antennas will be degraded due to the strong electromagnetic coupling between them [41]. Compared to a single conventional antenna, the reduction of mutual coupling between antenna elements is an essential consideration in the design of an antenna array for a small wireless terminal.

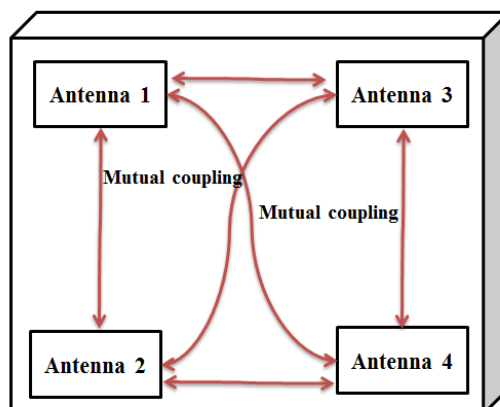
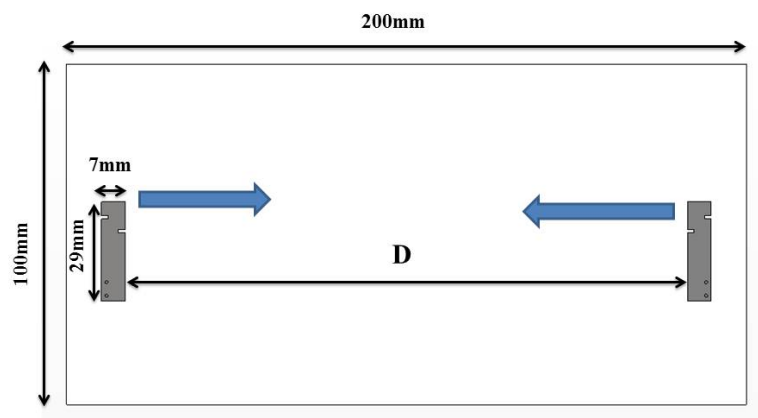
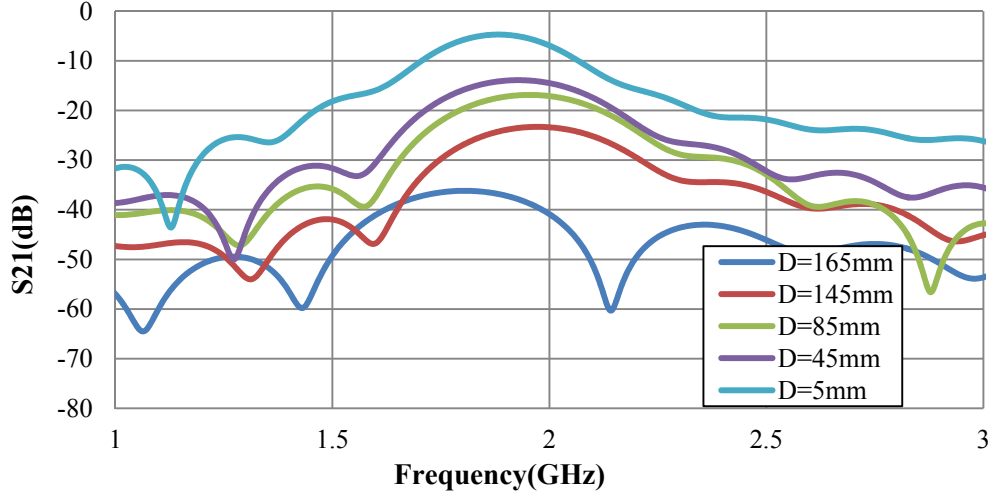


Figure 2.10 Mutual coupling between antenna elements on a compact ground plane

In this project, a 2x2 MIMO system is modeled by using a scattering matrix (S-parameters). The S21 is evaluated as the mutual coupling of a dual-element antenna array. Here, a number of simulations are presented to verify the relation between mutual coupling and the separation between the elements. The configuration of a dual-element PIFA array is presented in Figure 2.11(a). The antennas are optimized to resonate at 1.95GHz and mounted with a variable interelement separation (D) on the ground plane. Figure 2.11(b) shows the simulated mutual coupling (S21) between two antennas for different separations. When the two PIFAs are closer, higher surface current appears between antennas. Therefore, the mutual coupling increases with separation (D) decreasing. When multiple antennas are implemented on compact wireless terminals, it is an unavoidable problem that the inadequate separation between antenna elements will result in high mutual coupling which ultimately affects the performance of the antenna array [41, 42]. Several techniques have been proposed for the reduction of mutual coupling between closely spaced antennas on compact grounds, such as novel optimized antenna designs [43], and the use of EBG structures [44]. The application of single [45] or multiple [46] defects (slots or slits) on the ground plane has also attracted significant interest due to the ease of fabrication and applicability with different antenna types. All these techniques significantly reduce the mutual coupling by suppressing surface current on ground plane.



(a)



(b)

Figure 2.11 (a) The configuration of PIFAs on a 200mm×100mm ground plane and (b) Simulated S21 with various separations (D) between two PIFA elements

When multiple antenna array elements are mounted into a compact wireless terminal device, due to the small internal spacing, high mutual coupling will introduce additional correlation between wireless channels and reduce channel capacity of MIMO system [47-50]. There are two main methods of calculating the correlation between antennas. One method is obtained from the S-parameters of the antenna terminals [51]. Another method is obtained from the far-field radiation pattern [52]. The envelope correlation of a two-element antenna array could be calculated using equation (2.8) [53] or equation (2.9) [51]

$$\rho_e = \frac{|S_{11}^* S_{12} + S_{21}^* S_{22}|^2}{(1 - (|S_{11}|^2 + |S_{21}|^2))(1 - (|S_{12}|^2 + |S_{22}|^2))} \quad (2.8)$$

$$\rho_e = \frac{\left| \iint_{4\pi} \vec{F}_1(\theta, \phi) \cdot \vec{F}_2^*(\theta, \phi) d\Omega \right|^2}{\iint_{4\pi} |\vec{F}_1(\theta, \phi)|^2 d\Omega \iint_{4\pi} |\vec{F}_2(\theta, \phi)|^2 d\Omega} \quad (2.9)$$

where $\vec{F}_i(\theta, \phi)$ is the far-field pattern of the antenna system with antenna I excited (other ports are terminated in a 50Ω match). The EM field of external sources and the antenna radiation patterns affect the envelope correlation [54]. When the antenna system is placed in a uniform distribution of EM field, the calculation of

correlation which utilises equation (2.8), based on the S-parameters, is very quick and suitable for obtaining good approximations [54]. If not, the equation (2.8) will introduce an error, because the equation (2.8) does not include the radiation efficiencies of antennas [54]. Equation (2.9), based on the far-field pattern of the antenna system, provides a more accurate correlation between antennas although it is more complicated.

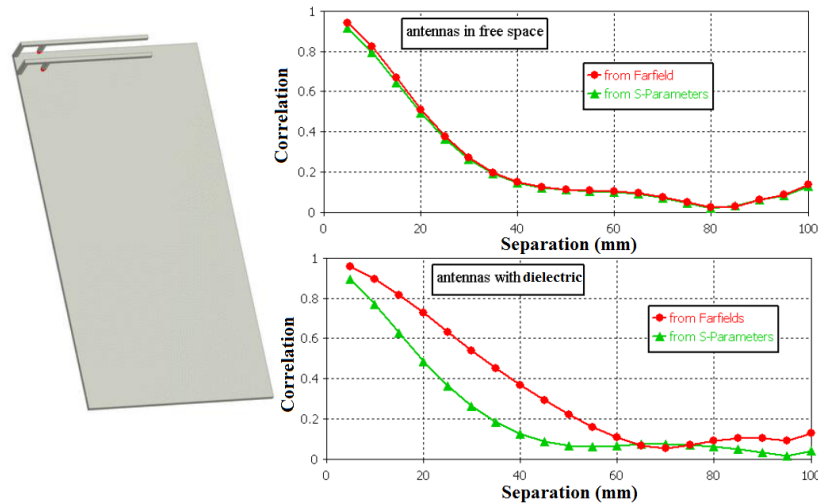


Figure 2.12 Correlation coefficient between two IFAs over different separations [55]

Figure 2.12 shows an example of correlation values between two closely spaced IFAs on a mobile handset ground plane, where the values have been calculated using the two different methods mentioned above, namely equations (2.8) and equation (2.9) [55]. When the antenna system is in free space, the results which are calculated from two equations are almost the same. When a dielectric object is close to the antenna array, the method based on the far-field pattern presents the better description of correlation although the equation is more complicated.

2.5 EBG Structures

EBG structures evolved from the PBG (Photonic Band-gap) structure which is proposed to prevent the propagation of light in specific frequencies [56]. PBG

structures are artificially made structures either in two or three dimensions [57, 58]. Initially, PBG concepts were only applied in an optical regime [59]. Because of their advantageous characteristics, PGB structures have been widely applied in microwave and millimeter-wave regions to suppress electromagnetic wave propagation in specific frequencies [60, 61]. Hence they have been renamed to EBG structures. EBGs are defined as the “artificial periodic objects that prevent the propagation of electromagnetic waves in a specified band of frequency for all incident angles and all polarisation states” [62].

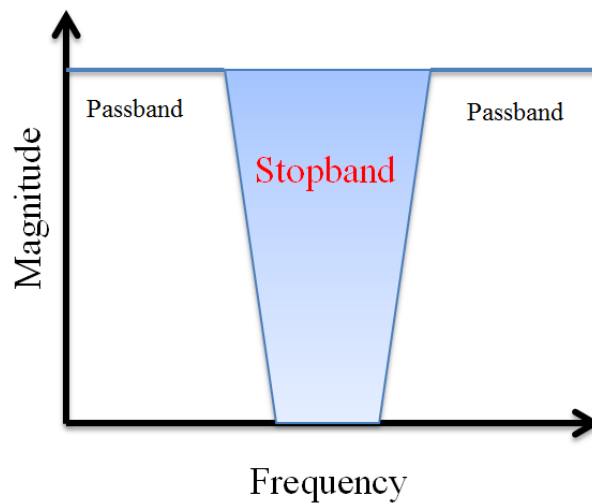
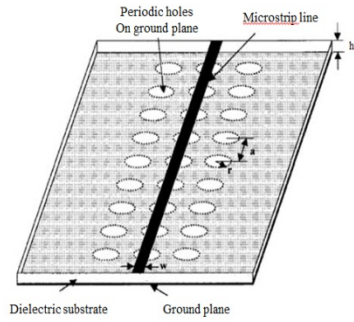
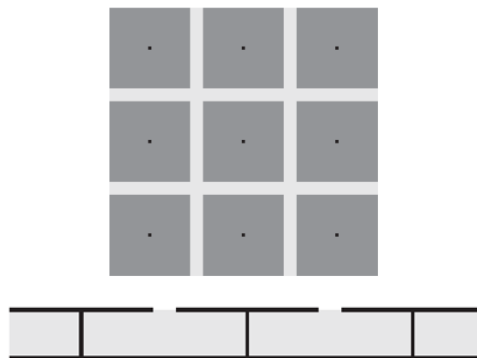


Figure 2.13 The characteristic of an EBG structure

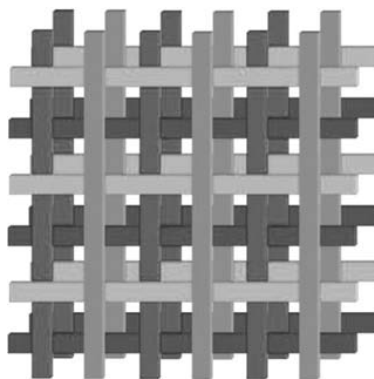
The EBG structure generally consists of a periodic arrangement of dielectric material and metal conductors. Based on their structural geometry, EBG structures are sorted into three groups: (1) one-dimensional transmission line structures, (2) two-dimensional planar surface structures, and (3) three-dimensional volumetric structures[63]. Some typical EBG structures which have been applied in microwave circuit design are exhibited below. One microstrip line with periodic holes on the ground plane is shown in Figure 2.14(a) [64]. A mushroom-like surface structure shown in Figure 2.14(b) is an example of the two-dimensional EBG structure[65]. A woodpile structure consisting of square dielectric bars is shown in Figure 2.14 (c) for three-dimensional volumetric EBG structures [66].



(a)



(b)



(c)

Figure 2.14 Three EBG structures: (a) one microstrip line with periodic holes on ground plane [64] (b) a mushroom-like surface structure [65] (c) a woodpile structure consisting of square dielectric bars [66]

EBG structures are usually realized by periodic arrangement of dielectric materials and metallic conductors to achieve stop band effect. By suppressing the surface current on ground plane, EBG structures succeed in reducing the mutual coupling level between antenna elements [44, 67, 68]. However, due to strict space constraints,

EBG structures are very difficultly implemented in compact wireless terminals because they will occupy a large area of ground plane. In next section, another simple structure will be presented to reduce mutual coupling between antenna array elements.

Recently, a novel technique for miniaturizing EBG structures has been proposed [69, 70]. This kind of EBG structures etches a slot array and conducting dipoles on either side of a thin supporting dielectric substrate [71-73]. This double layer slit-patch EBG structure places two layers of conducting elements close to each other to produces strong field and high coupling between the elements. In this way, the effective electrical length of the overall structure increases, resulting in a decrease of the resonant frequency and yielding significant miniaturisation of the slot array.

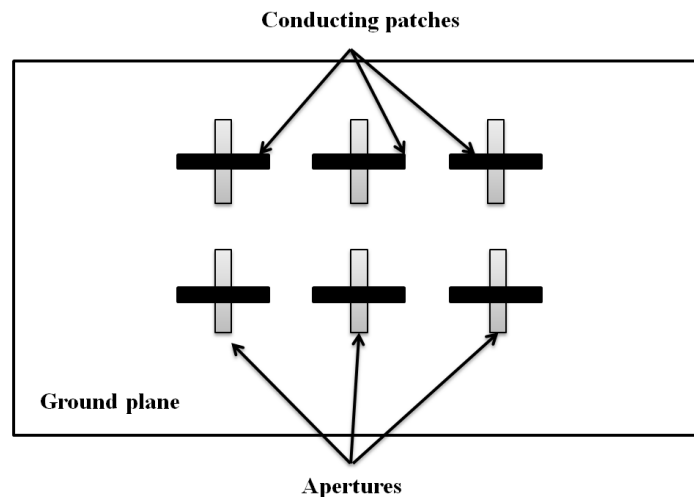


Figure 2.15 Schematic of proposed Complementary Dipole array

A corresponding closely coupled EBG array etched conducting patches and aperture slots on either side of a very thin dielectric layer, as shown in Figure 2.15. The apertures are rotated 90^0 with respect to the conducting patches in order to maximize the coupling between them. Simulated and measured results illustrated that the resonant frequency of the band gap decreases as the width of the conducting patches increases [74]. This structure will be used to miniaturise the size of slits etched on ground plane in chapter four and chapter five.

2.6 Defected Ground Structure

DGS (Defected Ground Structure) is an etched periodic or non-periodic configuration defect in a ground plane [75]. In comparison periodic EBG structure, DGS employ fewer slots or slits to modify the current distribution on the ground plane, because of DGS dimension and its relative position, resulting in the alteration of the characteristics of the transmission response.

The DGS presents different characteristic from their geometries etched on the ground plane. They have been widely applied as various microwave filters such as the low-pass, band-pass and band-stop [76-78]. Recent research has demonstrated that the implementation of several coupled linear slits has succeeded in reducing mutual coupling between closely spaced antenna elements acting as a band-stop filter [79, 80]. Three pair linear slits were etched on a compact ground plane between two closely-packed monopoles to reduce the mutual coupling between the antenna elements, as shown in Figure 2.16. Compared to the original ground plane, the linear slits introduce a significant reduction of mutual coupling between two closely spaced monopoles [80].

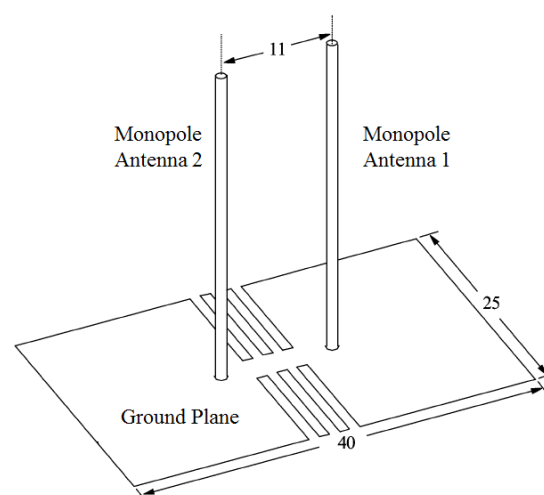


Figure 2.16 Two monopoles antennas on the proposed ground plane [80]

In order to describe the mechanism of linear slits, the surface current distribution is shown in Figure 2.17. Five pairs of linear slits are etched on a ground plane between two antennas. Although two PIFAs are closely placed on the compact ground plane, the slitted patterns succeed in trapping a large portion of current and energy. Less surface current propagate from one antenna to the other one. As described in section 2.4, the mutual coupling is mainly contributed by the flowing surface current between antenna elements. So, the linear slits effectively reduce the mutual coupling between the antenna elements [81]. The DGS will be used as the major method for reducing the mutual coupling for the various antenna configurations in this project.

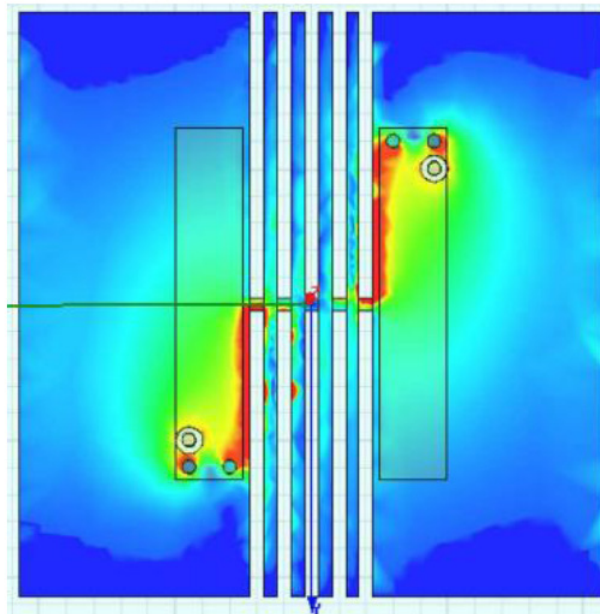


Figure 2.17 The Simulated surface current distribution of a dual-element PIFA array at 2.35 GHz [80]

2.7 CST Microwave Studio

In the last twenty years, with the rapid development of computer science, many powerful simulation software tools have emerged for applications in electromagnetic analysis and design. CST MICROWAVE STUDIO is one of the 3D simulation

software tools which provide a solid modeling front end to simplify the inputting process [81]. CST supports fast and accurate simulations for different electromagnetic devices such as antennas, filters, planar and multi-layer structures. The powerful 3D visual effect of CST simplifies the operational procedures shown in Figure 2.18. After the simulated model has been inputted into the software, a novel automatic meshing program will minimize the error of the simulation results. CST MWS provides a number of different solvers for different applications such as: the transient solver, the frequency domain solver, the integral equation solver, and the eigenmode solver[81].

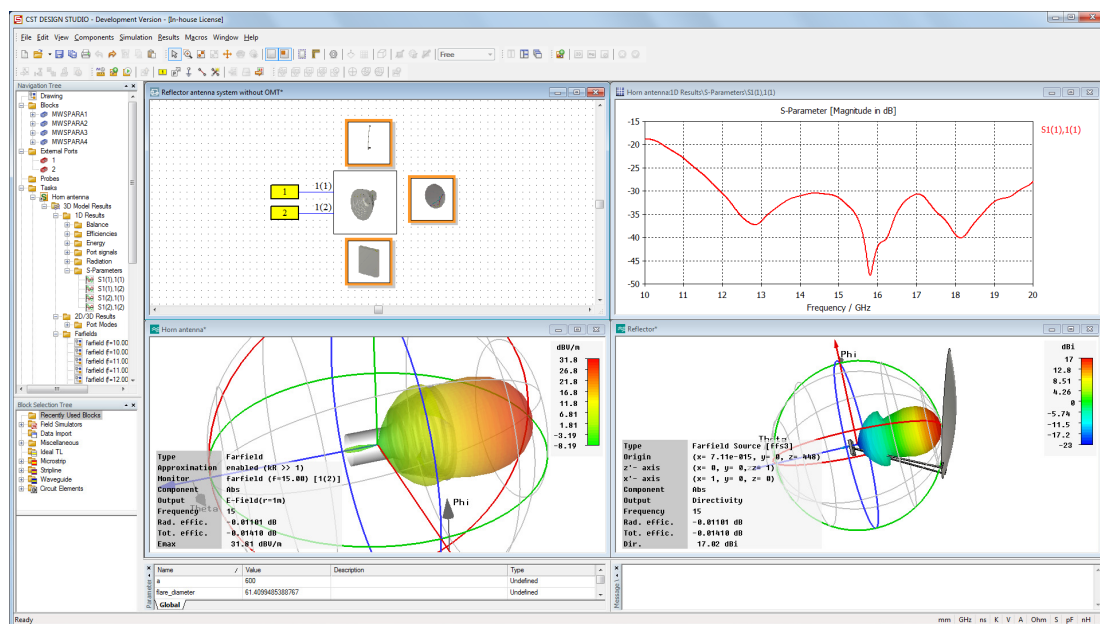


Figure 2.18 CST Microwave studio overview [81]

In this project, the transient solver is the principal tool used to calculate simulated results for the various models. This solver is efficient for calculating S-parameters, electric fields, magnetic fields, surface currents, power flows, current densities and field distributions [81]. The transient solver is based on the Finite Integration Technique (FIT) numerical method which was proposed by Thomas Weiland in 1977 [82]. FIT is a spatial discretisation scheme for solving electromagnetic questions in the time and frequency domain [82]. This approach discretizes the integral form of Maxwell's equations and decomposes the computation domain to a finite number of

staggered grids. Due to the high flexibility in geometric modeling and boundary handling, FIT was used by CST MWS to solve all kinds of electromagnetic problems. However, this method also introduces errors when the simulated model has a curved surface. CST MWS exploits an exclusive efficient method termed as the Perfect Boundary Approximation (PBA) to reduce this kind of error [83]. PBA, by applying sub-cellular analysis for any shaped boundaries, increases the simulation accuracy and reduces the consumed computation resource, as shown in Figure 2.19.

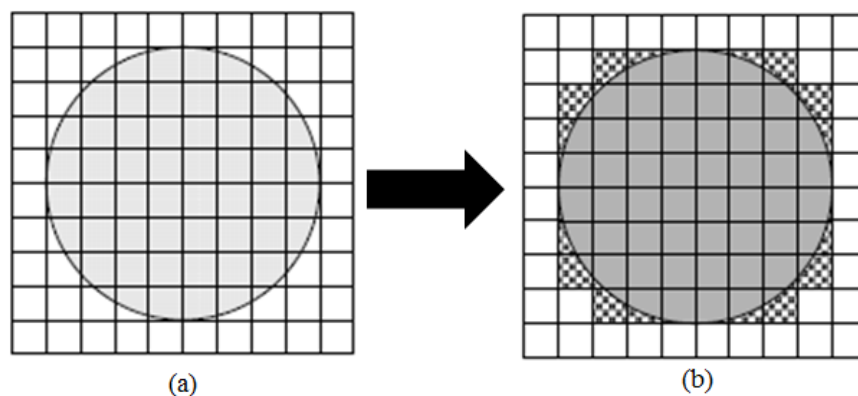


Figure 2.19 Grid approximation of rounded boundaries(a) standard (b) Perfect Boundary Approximation[83]

2.8 Summary

This chapter has presented the theoretical background for the application of MIMO system implemented in compact wireless terminal. The channel capacity of a MIMO system has a significant improvement over the SISO system without increasing the radio spectrum.

Now, the antenna designs for a mobile terminal present two trends: the first one demands that the antenna is smaller, built-in, and supports multiple communication systems; the second one demands that the antenna system supports the absolute quality and quantity of transmission data for various users' requirements. These

demands have forced a rapid evolution of the mobile terminal antenna. However, when multiple antennas employed at the transmitter and receiver in a compact wireless terminal, the mutual coupling between antenna elements is a big challenge because of the small separation between antennas. Therefore, some DGS structures will be presented to reduce the mutual coupling, which are discussed in Chapter 3.

Novel, miniaturised, closely coupled Electromagnetic Band Gap Structures have been presented to miniaturise the dimensions of the EBG structures etched on the ground plane. The proposed structure employs two layers of conducting elements and apertures placed on either side of a thin supporting dielectric substrate for producing a strong field and high coupling between them. Based on this, the electrical length of the overall structure effectively increases, resulting in a resonant frequency of EBG structure decrease. This means that the dimension of the EGB etched on the ground plane could be reduced by implementing this double-layer structure. Some slit-patch EBG structures are conducted in Chapter 4 and Chapter 5.

References

- [1] G. J. Foschini, and M. J. Gans, “On limits of wireless communications in a fading environment when using multiple antennas,” *Wireless Personal Communications*, vol. 6, pp. 311-335, March, 1998.
- [2] C. E. Shannon, “A Mathematical Theory of Communication,” *Bell System Tech. J.*, Vol. 27, June 1948.
- [3] C. E. Shannon, “Communication in the Presence of Noise,” *Proceeding of the IEEE*, Vol. 86, No. 2, February 1998, pp. 447–458.
- [4] T. S. Rappaport, “Wireless communications: principles and practice,”

- Prentice Hall, 2002. pp.5-50.
- [5] E. Biglieri, R. Calderbank, A. Constantinides, A. Goldsmith, A. Paulraj, and H. V. Poor, "MIMO Wireless Communications," Cambridge University Press 2007 pp.1-20.
- [6] D. Pearce, "Personal and mobile communication," University of York, September 2005. pp. 17-64.
- [7] J. N. Franklin, "Matrix Theory," General Publishing Company, Toronto, 1993.
- [8] A. Goldsmith, "Wireless Communication," Stanford University, 2005, pp. 299-327.
- [9] T. L. Marzetta, and B. M. Hochwald, "Capacity of a mobile multi-antenna communication link in Rayleigh flat fading," *IEEE Trans. Information Theory*, vol. 45, no. 1, Jan. 1999, pp. 139-157.
- [10] Z. Q. Yun, "MIMO Capacity Calculation and Fading Estimation for Indoor/Outdoor Wireless Communication Environments," *IEEE transaction*, 0-7803-8197-1/03, 2003.
- [11] T. M. Cover, and J. A. Thomas, "Elements of Information Theory". John Wiley & Sons, 1991. pp. 183-222.
- [12] I. Berenguer, X. D. Wang. "Space-Time Coding and Signal Processing for MIMO Communications," *J.comput. Sci. & Technol*, vol. 18, No. 6, pp. 689-702.
- [13] K. Fujimoto. "Mobile Antenna Systems Handbook," Artech House, INC 2008 pp. 1-21.
- [14] H. Morishita, Y. Kim, and K. Fujimoto, "Design Concept of Antennas for Small Mobile Terminals and the Future Perspectives," *IEEE Antenn. Propag. Mag.*, Vol. 44, No. 5, 2002, pp. 30– 42.
- [15] Gupta, I. J. and A. A. Ksienski, "Effect of mutual coupling on the performance of adaptive arrays," *IEEE Trans. on Antennas and Propagation*, Vol. 31, No. 5, 785–791, 1989.

- [16] Borja, C., A. Algans, M. Royo, J. Anguera, and C. Puente, "Impact of the antenna technology and the antenna parameters on the performance of MIMO systems," *Proc. of IEEE Antennas and Propagation Symposium, APS03*, Vol. 2, 507–510, 2003.
- [17] Ozdemir, M. K., H. Arslan, and E. Arvas, "Mutual coupling effect in multi-antenna wireless communication systems," *Proc. of IEEE Global Telecommunications conference*, Vol. 2, 829–833, 2003.
- [18] C. A. Balanis, Ed., "Antenna Theory: Analysis and Design," Wiley 2 edition, 1997.
- [19] K. Hirasawa and M. Haneishi, Eds., "Analysis, Design, and Measurement of Small and Low-Profile Antennas," Artech House, 1992. pp. 4-27.
- [20] K. L. Wong, "Planar antennas for wireless communications," 2003, Canada, pp. 26-69.
- [21] P. Song, P. Hall, H. Ghafouri-Shiraz, and D. Wake, "Triple-band planar inverted-F antenna," *IEEE Antennas and Propagation Society International Symposium*, vol. 2, July 1999, pp. 908-911.
- [22] W.-S. Chen, T.-W. Chiou, and K.-L. Wong, "Compact pifa for gsm/dcs/pcs triple-band mobile phone," *IEEE Antennas and Propagation Society International Symposium*, vol. 4, June 2002, pp. 528-531.
- [23] P. Ciaisi, R. Staraj, G. Kossiavas, and C. Luxey, "Compact internal multiband antenna for mobile phone and wlan standards," *Electronics Letters*, vol. 40, no.15, pp. 920-921, July 2004.
- [24] H. Mishima, and T. Taga, "Mobile antennas and duplexer for 800 mhz band mobile telephone system," *IEEE Antennas and Propagation Society International Symposium*, vol. 18, June 1980, pp. 508-511.
- [25] H. Nakano, R. Suzuki, and J. Yamauchi, "Low-profile inverted-f antenna with parasitic elements on an infinite ground plane," *IEE Proceedings - Microwaves, Antennas and Propagation*, vol. 145, no. 4, pp. 321-325, August 1998.

- [26] Y. Kim, and D.-H. Kwon, "CPW-fed planar ultra wideband antenna having a frequency band notch functions," *Electron. Lett.*, 2004, 40, (7), pp. 403–405.
- [27] S.-Y. Suh, W. Shutzman, W. Davis, A. Waltho, and J. Schiffer, "A novel CPW-fed disc antenna," *IEEE Antennas Propag. Soc. Symp.*, 20–25 June 2004, Vol. 3, pp. 2919–2922.
- [28] T. Yang, and W.A. Davis, "Planar half-disk antenna structures for UWB communications," *IEEE Antennas Propag. Soc. Symp.*, 20–25 June 2004, Vol. 3, pp. 2508–2511.
- [29] H. Yoon, H. Kim, K. Chang, Y.J. Yoon, and Y.-H. Kim, "A study on the UWB antenna with band-rejection characteristic," *IEEE Antennas Propag. Soc. Symp.*, 20–25 June 2004, Vol. 2, pp. 1784–1787.
- [30] J. Liang, "Study of CPW-Fed Planar Monopole Antenna for Wideband Applications," *IEEE Proc. Microwaves Ant. Propag.*, Vol. 153, No. 6, December 2004, pp. 210–214.
- [31] Federal Communications Commission (FCC), "Revision of Part 15 of the Commission's Rules Regarding Ultra Wideband Transmission Systems," First Rep. and Order, ET Docket 98-153, FCC 02-48, Adopted: Feb. 2002; Released: Apr. 2002.
- [32] R. Fleming, and C. Kushner, "CMOS Ultra-Wideband Localizers for Networking in the Extreme," Presentation to DARPA. Retrieved, JAN 18, 2001 from www.darpa.mil.
- [33] G. F. Ross, "The transient analysis of multiple beam feed networks for array Systems," Ph.D. thesis, Polytechnic Institute of Brooklyn, Brooklyn, NY, 1963.
- [34] E. Baccarelli, M. Biagi, C. Pelizzoni, and P. Bellotti, "A novel multi-antenna impulse radio UWB transceiver for broadband high-throughput 4G WLANs," *IEEE Comm. Lett.*, vol. 8, July 2004, pp. 419-421.

- [35] J. Liang, L. Guo, C.C.Chiau, X. Chen, and C.G.Parini, "Study of CPW fed circular disc monopole antenna for ultra-wideband applications," *IEE Proceedings on Microwaves, Antennas & Propagation*, vol. 152, Dec 2005, no. 6, pp. 520-526.
- [36] J. Liang, C Chiau, X. Chen and C.G. Parini, "Study of a Printed Circular Disc Monopole Antenna for UWB Systems", *IEEE Trans. On Ant. and Prop.*, vol. 53, no. 11, pp.3500-3504, Nov. 2005.
- [37] K. L. Wong, C. H. Wu, S. W. Su, "Ultrawide-band square planar metal-plate monopole antenna with a trident-shaped feeding strip," *IEEE Transaction. on Antenna. and Propagation.*, vol. 53, 2005,no. 4, pp.1262 – 1269.
- [38] C.-C. Lin, Y.-C. Kan, L.-C. Kuo, and H.-R. Chuang, "A planar triangular monopole antenna for UWB communication," *IEEE Microwave and Wireless Components Letters*, vol. 15, no. 10, pp. 624-626, Oct. 2005.
- [39] Kin-Lu Wong, "Ultrawide-band square planar metal-plate monopole antenna with a trident-shaped feeding strip," *IEEE Transactions on Antennas and Propagation*, vol. 53 , Issue:4 pp.1262 – 1269, April 2005
- [40] L. Liu, Y.F. Weng, S. W. Cheung, T. I. Yuk, and L. J. Foged, "Modeling of cable for measurements of small monopole antennas", *Loughborough Antennas & Propagation Conference*, 14-15 November 2011, Loughborough, UK.
- [41] P.N. Fletcher, M. Dean, and A. R. Nix, A.R. "Mutual coupling in multi-element array antennas and its influence on MIMO channel capacity," *Electron. Lett.*, 2003, 39, (4), pp. 342–344.
- [42] S. Lu, T. Hui, and M. Bialkowski, "Optimizing MIMO channel capacities under the influence of antenna mutual coupling," *IEEE Antennas Wireless. Propag. Lett.*, 2008, 7, pp. 287–290.
- [43] Y. Gao, X. Chen, Z. Ying, and Clive Parini, "Design and Performance Investigation of a Dual-Element PIFA Array at 2.5 GHz for MIMO

- Terminal,” *IEEE Trans. Antennas and Propag.*, 55, (12), 2007, pp. 3433-3441.
- [44] R. Makinen, V. Pynttari, J. Heikkinen, and M. Kivikoski, “Improvement of antenna isolation in hand-held devices using miniaturized electromagnetic band-gap structures,” *Microwave Opt. Technol. Lett.* vol. 49, no 10, pp. 2508 –2513, 2007.
- [45] M. Karaboikis, C. Soras, G. Tsachtsiris, and V. Makios, “Compact Dual-Printed Inverted-F Antenna Diversity Systems for Portable Wireless Devices,” *IEEE Antennas Wireless. Propag. Lett.*, vol. 3, 2004, pp. 9-14.
- [46] C.-Y. Chiu, C.-H Cheng, R.D. Murch, and C. R. Rowell, “Reduction of mutual coupling between closely packed antenna elements”, *IEEE Trans. Antennas and Propag.*, Vol. 55, No. 6, pp. 1732 – 1738, Jun. 2007.
- [47] J. W. Wallace, and M. A. Jensen, “The Capacity of MIMO wireless systems with mutual coupling,” *Proceedings of IEEE VTC’ 03.* 2002; 2: 696–700.
- [48] A. Derneryd, and G. Kristensson, “Signal correlation including antenna coupling,” *Electronics Letters* 2004; 40(3): 157–158.
- [49] M. Karaboikis, C. Soras, G. Tsachtsiris, V. Makios, “Compact dual printed inverted-F antenna diversity systems for portable wireless devices,” *IEEE Antennas and Wireless Propagation Letters* 2004; 3: 9–14.
- [50] B. Clerckx, D. Vanhoenacker-Janvier, C. Oestges, and L. Vandendorpe, “Mutual coupling effects on the channel capacity and the space-time processing of MIMO communication systems,” *Proceedings of ICC ’03.* *IEEE International Conference on Communication*, Vol. 4 2003, 2638–2642.
- [51] R. G. Vaughan, and J. Bach Andersen, “Channels, Propagation and Antennas for Mobile Communications,” *The IEE*, UK, 2003. ISBN 0 85296 0840.

- [52] R. G. Vaughan, and J. Bach Andersen, "Antenna diversity in mobile communication," *IEEE Transactions on Vehicular Technology* 1987; 36:149–172.
- [53] J. Blanch, J. Romeu, and I. Corbella, "Exact representation of antenna system diversity performance from input parameter description," *Electronics Letters* 2003; 39: 705–707.
- [54] J. Thaysen, K. B. Jakobsen, "Design considerations for low antenna correlation and mutual coupling reduction in multi antenna terminals," *European transactions on telecommunicationseuro. Trans. Telecomm.* 2007; 18:319–326.
- [55] CST MIMO Antenna Simulation, UGM 2009 Darmstadt <http://www.cst.com/Content/Documents/Events/UGM2009/3-1-4-MIMO-Antenna-Simulation.pdf>.
- [56] E. Yablonovitch, "Photonic band-gap structures," *J. Opt Soc. Am. B.*, vol. 10, no. 2, pp. 283-295, Feb. 1993.
- [57] E Yablonovitch, "Photonic Crystal: Semiconductor of light," *Scientific American*, pp. 47-55, 2001.
- [58] P. S. L. Russel, "Photonic band gaps" *Physics World*, Aug 1992, pp.37-42.
- [59] E. Yablonovitch, "Photonic crystals," *Journal of Modern Optics*, 1994, vol. 41, No 2, pp.173-194.
- [60] J. Shumpert, T. Ellis, G. Rebeiz, and L. Katehi, "Microwave and millimeterwave propagation in photonic band-gap structure," AP-S/URSI, pp. 678, 1997.
- [61] E. R. Brown, and O. B. McMahon, "Large electromagnetic stop bands in metallodielectric photonic crystals," *Applied Physics Letters*, Vol. 67, Oct 1995, pp. 2138.
- [62] Y. Rahmat-Samii and H. Mosallaei, "Electromagnetic band-gap structures: classification, characterization and applications," *Proceedings of IEE-ICAP symposium*, pp. 560–4, April 2001.

- [63] F. Yang, and Y. Rahmat-Samll, “Electromagnetic Band Gap Structures in Antenna Engineering,” Cambridge University, 2008, pp.1-54.
- [64] V. Radisic, Y. Qian, R. Coccioli, and T. Itoh, “Novel 2-D photonic bandgap structure for microstrip lines,” *IEEE Microw. and Guided Wave Lett.*, vol. 8, no. 2, 69–71, 1998.
- [65] D. Sievenpiper, L. Zhang, R. F. J. Broas, N. G. Alexopolus, and E. Yablonovitch, “High-impedance electromagnetic surfaces with a forbidden frequency band,” *IEEE Trans. Microwave Theory Tech.*, vol. 47, 2059–74, 1999.
- [66] E. Ozbay, A. Abeyta, G. Tuttle, M. Tringides, R. Biswas, T. Chan, C. M. Soukoulis, and K. M. Ho, “Measurement of a three-dimensional photonic band gap in a crystal structure made of dielectric rods,” *Phys. Rev. B, Condens. Matter*, vol. 50, no. 3, 1945–8, July 1994.
- [67] M. F. Abedin, M. Ali, “Effects of a Smaller Unit Cell Planar EBG Structure on the Mutual Coupling of a Printed Dipole Array” *IEEE Antennas And Wireless Propagation Letters*, VOL. 4, 2005, pp. 274-276.
- [68] H.S. Farahani, M. Veysi, M. Kamyab, A. Tadjalli, “Mutual Coupling Reduction in Patch Antenna Arrays Using a UC-EBG Superstrate,” *IEEE Antennas And Wireless Propagation Letters*, VOL. 9, 2010, pp. 57-59
- [69] E. A. Parker, A. N. A. El Sheikh, “Convolutated array elements and reduced size unit cells for frequency-selective surface,” *IEEE Proceedings Microwaves, Antennas and Propagation*, Volume 138, Issue 1, Feb 1991 pp:19-22.
- [70] S. Tse, B. S. Izquierdo, J. C. Batchelor, and R. J. Langley “Reduced sized cells for electromagnetic bandgap structures,” *Electronic Letters*, Volume 40, Issue 22, 28 Oct, 2004 pp: 1391-1392.
- [71] A. P. Feresidis, G. Apostolopoulos, N. Serfas, and J. C. Vardaxoglou, “Closely Coupled Metallodielectric Electromagnetic Band-Gap Structures

Formed by Double-Layer Dipole and Tripole Arrays,” *IEEE transactions on antennas and propagation*, vol. 52, no. 5, may 2004.

- [72] J. C. Vardaxoglou and D. Lockyer, “Modified FSS response from two sided and closely coupled arrays,” *Electron. Lett.*, vol. 30, no. 22, pp.1818–1819, 1994.
- [73] D. S. Lockyer and J. C. Vardaxoglou, “Reconfigurable FSS response from two layers of slotted dipole arrays,” *Electron. Lett.*, vol. 32, no. 6, pp. 512–513, 1996.
- [74] G. Apostolopoulos, A. P. Feresidis, G. Goussetis, J. C. Vardaxoglou, “Complementary Metallo-Dielectric Electromagnetic Band Gap Structures,” *Microwave Conference, 2005 European*, vol. 2 Issue 4-6 Oct. 2005.
- [75] L. H. Weng, Y. C. Guo, X. W. Shi, and X. Q. Chen, “An overview on defected ground structure,” *Progress In Electromagnetics Research B*, Vol. 7, 173–189, 2008.
- [76] C. Insik, and L. Bomson, “Design of defected ground structures for harmonic control of active microstrip antenna,” *IEEE Antennas Propag. Soc. Int. Symp.*, vol. 2, 852–855, 2002.
- [77] J. S. Park, J. H. Kim, J. H. Lee, et al., “A novel equivalent circuit and modeling method for defected ground structure and its application to optimization of a DGS low-pass filter,” *IEEE Microwave Symposium Digest, 2002 IEEE MTT-S International*, vol. 1, 417–420, 2002.
- [78] G.-L. Wu, W. M., X.-W. Dai, et al., “Design of novel dual-band bandpass filter with microstrip meander-loop resonator and DGS,” *Progress in Electromagnetics Research*, PIER 78, 17–24, 2008.
- [79] T. Kokkinos, E. Liakou, and A. P. Feresidis, “Decoupling Antenna Elements of PIFA Arrays on Handheld Devices,” *IET Electronics Letters*, 44 (25), 2008, pp. 1442-1444.

- [80] C.-Y. Chiu, C.-H Cheng, R.D. Murch, and C. R. Rowell “Reduction of Mutual Coupling Between Closely-Packed Antenna Elements”. *IEEE Transactions on Antennas and Propagation*, 2007, June. 1732-1737.
- [81] CST MICROWAVE STUDIO® 2008 – Workflow and Solver Overview
<http://www.cst.com/Content/Products/DS/Overview.aspx>
- [82] T. Weiland, “A Discretization Method for the Solution of Maxwell's Equations for Six-Component Fields,” *Electronics and Communications AEUE*, vol. 31, no. 3, pp. 116–120, 1977.
- [83] CST Studio Suite developed by Computer Simulation Technology 2010.

Chapter 3

Linear and Convoluted Slits on Ground Plane

3.1 Introduction

The theoretical background regarding the multiple antennas used for compact wireless terminal devices has been introduced in Chapter two. In a MIMO system, multiple antennas are employed at both the transmitter and receiver to significantly increase the channel capacity. In comparison to the requirements of a single antenna for a compact wireless terminal, such as minimum occupied volume, light weight, adequate bandwidth, isotropic radiation characteristic, and low fabrication cost [1,2], the application of multiple antennas needs to meet some additional conditions, such as good isolation, diversity performance for the multiple antennas, enough space in-between for other electric components[2]. In order to implement a multiple-element antenna array into compact wireless terminals, the dimensions and relative position of antenna elements need to be rigorously designed and tested to achieve low mutual coupling between the elements. In this chapter, the geometry of one single PIFA operating at 1.9GHz is proposed and optimised. One dual-element antenna array based on the configuration and dimension of the single antenna is presented. Novel linear slits and convoluted slits are inserted in the ground plane to introduce a

transmission minimum in the coupling path between two close spaced PIFAs and produce a significant reduction of the mutual coupling within the operating frequency band of the antennas. The prototypes of the PIFA array with the proposed linear and convoluted slits have been fabricated in order to validate experimentally the proposed designs. Ultimately, the miniaturized convoluted slit structures integrated into a compact ground plane have been presented to reduce the coupling of the human body to antennas.

3.2 Planar Inverted – F Antenna Design and Simulation

The wireless and mobile terminal market has an explosive development in last ten years. Meanwhile, a lot of new antennas have emerged to be implemented in wireless and mobile terminal devices [3-6]. These antennas have an evolution from extendable antenna to internal antenna; PIFAs and other built-in antennas have replaced the monopoles [7, 8]. In this section, a Planar Inverted-F Antenna (PIFA) and its dual-element array are proposed and optimized to further evaluate the electromagnetic properties of some defected ground structures on the ground plane. The antenna system is designed to operate within the 1.7-2.1GHz frequency band for a 3G system. As mentioned in Chapter two, in a MIMO system, the separation between antenna array elements should be more than a half wavelength in order to achieve a good isolation between them. However, it is difficult to obtain low mutual coupling when two PIFAs are implemented on a conventional ground plane for a compact mobile terminal device. A novel approach for reducing the electromagnetic coupling between antenna elements is presented in the following sections.

3.2.1 Antenna Geometry Design

As mentioned in Chapter two, the resonant frequency of a PIFA is determined by several important factors. According to the equation given here [9]:

$$f = \frac{c}{4(L+W)} \quad (3.1)$$

Where, the length L and width W of radiating element will determine the resonant frequency (f) of the antenna. The distance between the feeding pin and the shorting pin also affects the antenna's resonating properties through altering the surface current flowing path on the radiating patch [9]. The antenna operation frequency range is defined within 1.7-2.1GHz, so the central frequency should be around 1.9GHz.

Due to the proposed antennas being established in one compact mobile handset, owing to the practical situation, the height of the PIFA radiating patch is defined as 10mm. After a series of simulations, the dimensions of the radiating patch are defined as 29mm length and 7mm width to make the antenna operate in the desired frequency range and leave enough room for the other electronic components in the compact mobile device. In order to obtain more bandwidth and reduce the size of radiating element, some slits or slots are etched on the radiating patch. Initially, five different configurations of radiating patches are studied, as shown in Figure 3.1.

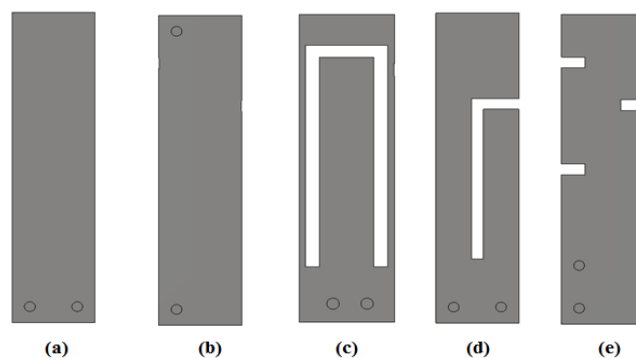


Figure 3.1 The five different PIFA configurations: (a) simple PIFA, (b) simple PIFA with the shorting pins on the top edge, (c) U-slotted PIFA, (d) L-slitted PIFA, (e) PIFA with 3 slits

Figure 3.2 represents the simulated return loss (S_{11}) of the antennas corresponding to the different configurations shown in Figure 3.1. The simple PIFA in schematic (a) resonated at 1.86GHz. After the shorting pin was moved to the top edge of the radiating patch in Figure 3.1(b), the resonant frequency of the PIFA shifted to 3.2GHz. The U-slotted PIFA introduced a dual band which resonated in both 1.95 and 3.7GHz as in schematic (c). And the L-slotted PIFA resonated in both 1.88GHz and 3.27GHz. However, the upper frequency bands of schematic (b) and (c) did not satisfy the requirement of the communication system ($S_{11} < -6\text{dB}$). By adding three linear slits on the radiating patch, the resonant frequency of the last PIFA (e) matched the desired frequency 1.9 GHz and had 150MHz bandwidth.

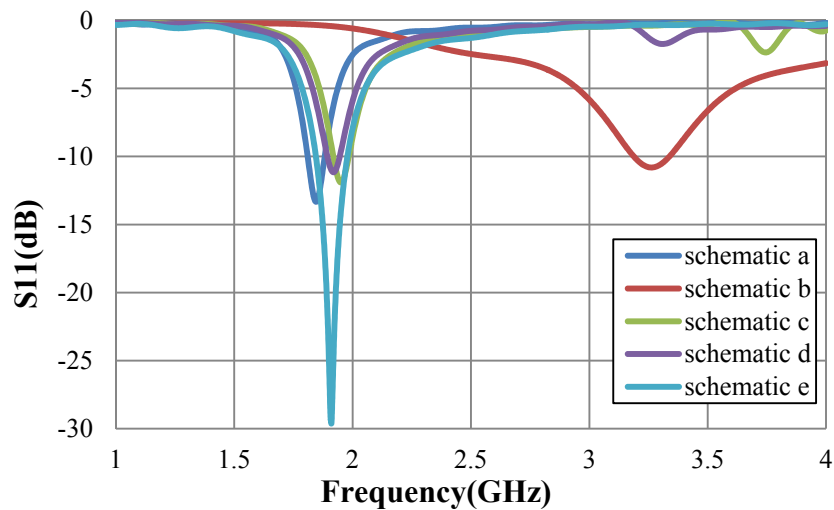


Figure 3.2 Return loss results (S_{11}) of PIFAs corresponding to different PIFA configurations shown in Figure 3.1

Figure 3.3 shows the geometry of a modified radiating patch. It comprises one PEC (Perfect Electric Conductor) patch with two etched circles and two $2 \times 1\text{mm}^2$ linear slits. The distance between the two circles is 4mm. The first circle is connecting the shorting pin. The second circle denotes the feeding pin for connecting one coaxial cable. The total length of the radiating patch is 72mm, approximately half wavelength when the PIFA is resonant at 1.9GHz.

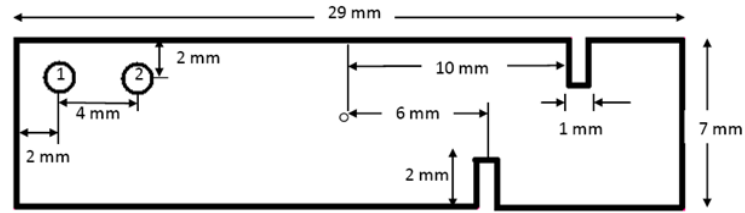


Figure 3.3 Geometry of the PIFA radiating patch

The proposed PIFA is placed on a compact ground plane with dimensions $100 \times 40 \text{ mm}^2$ for a mobile terminal, and is printed on a 1.55mm-thick FR-4 dielectric substrate ($\epsilon_r=4.5$), as shown in Figure 3.4. The antenna is supported by one coaxial cable and a shorting pin. The coaxial cable directly drills through the substrate and the ground plane to avoid touching the PEC (Perfect Electric Conductor) layer on the ground plane. This will reduce the influence, caused by the dimension of the ground plane, which causes the antenna performance to deteriorate sharply. The diameter of the coaxial cable is 1.5mm. The outer radius of the metallic shield is 2mm. The resistance of the cable is defined as 50Ω .

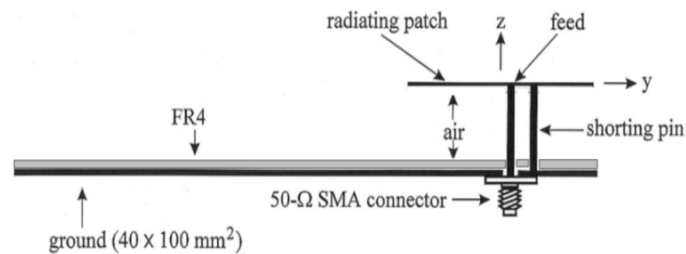


Figure 3.4 Geometry of the antenna system

3.2.2 Single Modified PIFA Design

The modified PIFA is placed on the $100 \times 40 \text{ mm}^2$ ground plane. By using CST Microwave StudioTM (CST MWS), the simulated return loss (S11) of the PIFA is shown in Figure 3.5. A sharp minimum of S11 is obtained around 1.9GHz, with a

good matching of the desired frequency band. The effective impedance bandwidth ($|S_{11}| > 6\text{dB}$) of the antenna is from 1.76 to 2.05 GHz.

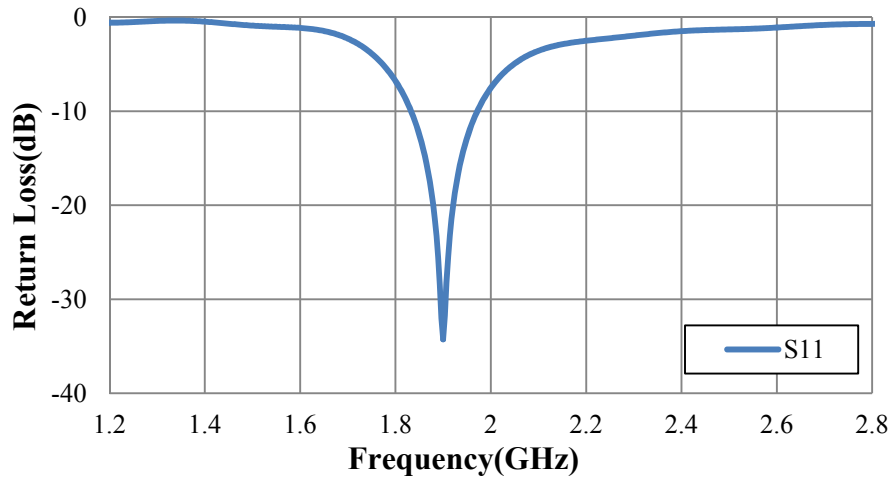


Figure 3.5 Simulated return loss (S11) of the modified PIFA

The current distribution on the ground plane at the resonant frequency 1.9GHz was obtained from simulation software, as shown in Figure 3.6. The surface current seems to propagate along the edges from one side of the ground plane to the other side. The surface current will produce high mutual coupling between the antenna elements when two or more antennas are implemented on the ground plane.

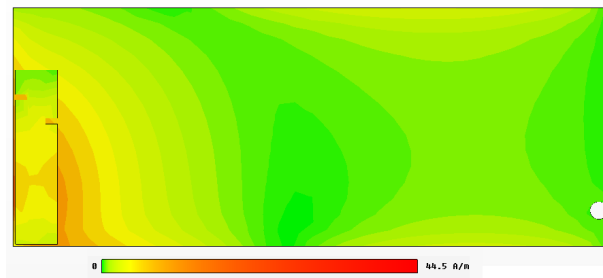


Figure 3.6 Current distribution of a PIFA on ground plane at 1.9GHz

3.2.3 Dual-element PIFA Array Design

A dual-element PIFA array based on the configuration and dimension of the single PIFA element was proposed and optimized in this section. The antenna array is mounted on the ground plane (100x40 mm²). In order to leave enough room for

battery and other electronic components, the two PIFAs are respectively placed near the two edges of the ground plane. Meanwhile, the separation between antenna array elements will be increased to obtain lower mutual coupling. The configurations and dimensions of the PIFAs are the same as the single one shown in Figure 3.3. Four different positions of the PIFAs are displayed in Figure 3.7.

In the first three configurations of the PIFA array, the separations between two PIFAs are 92mm in schematic (a), 93mm in schematic (b) and 82mm in schematic (c). The spacing between the two antennas is only 32mm in schematic (d). In first three schematics, the separations between the two antennas are slightly more than a half wavelength, which satisfies the typical distance of $\lambda/2$ for achieving a low mutual coupling between antenna elements [10].

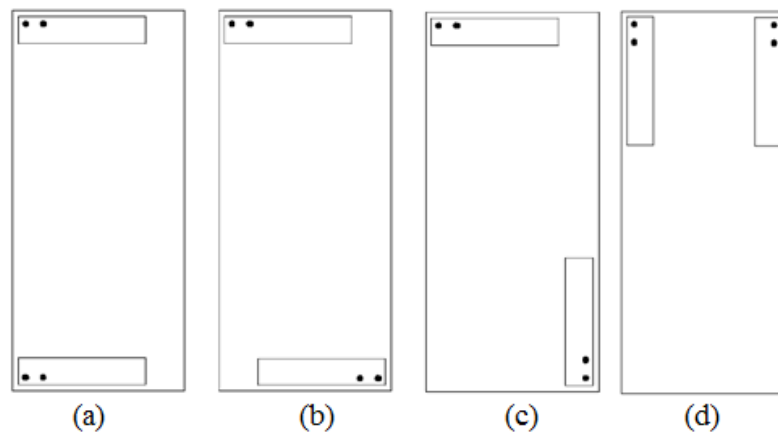
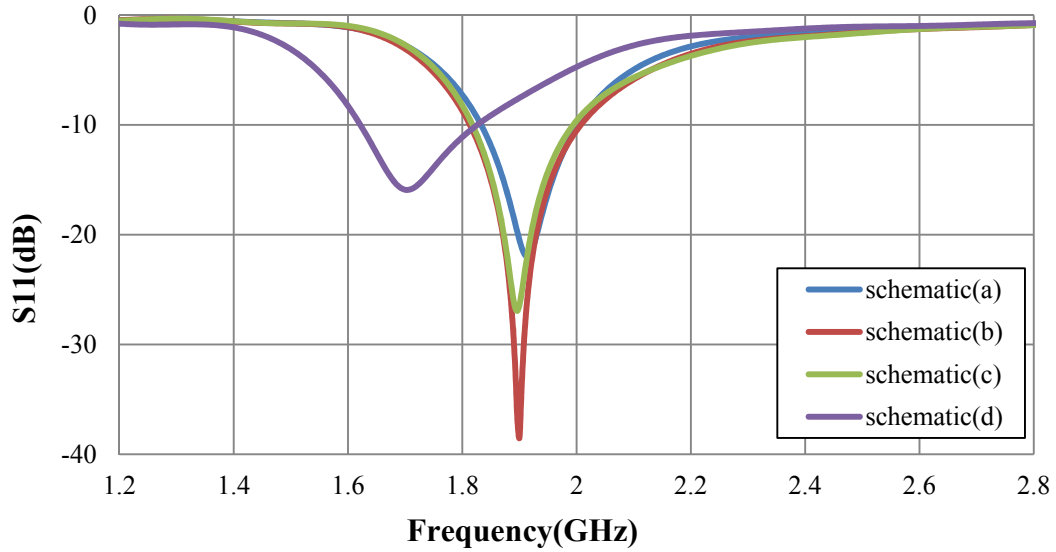
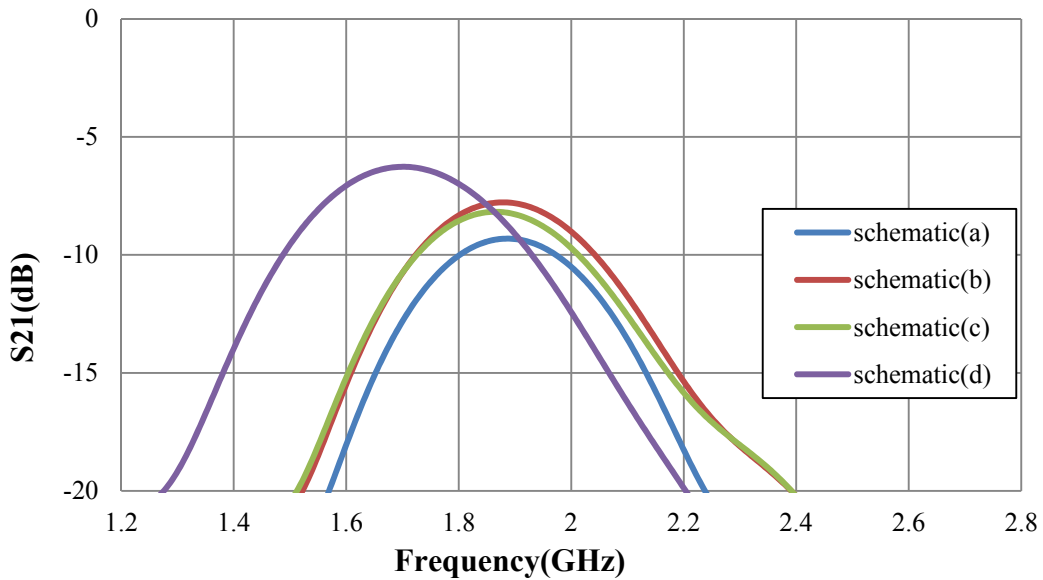


Figure 3.7 Four different configurations for the position of two antennas

The simulated S-parameters of the PIFA arrays for the four configurations are shown in Figure 3.8. All the return losses of antenna 1 (S11) are around 1.9GHz except schematic (d), as shown in Figure 3.8 (a). It is obvious that the high mutual coupling significantly affects their resonant frequencies when the antennas are very closely placed to each other. In all four configurations, at the resonance of the antennas, their mutual couplings are over -10dB. Because schematic (a) has lowest mutual coupling (S21) in comparison to the other schematics, this configuration of antenna array will be further investigated in the following sections.



(a)



(b)

Figure 3.8 (a) S11 and (b) S21 for four different configurations of the two array shown in Figure 3.7

The simulated surface current distribution on the ground plane at the resonant frequency (1.9GHz) is presented in Figure 3.9. It was noticed that the surface current is widely spread on the ground plane when the antennas are excited. The current are around the area underneath the radiating elements and propagates along the edges of ground plane thus producing a high mutual coupling between antenna elements. In the four configurations, schematic (a) and schematic (b) have the biggest separation

between two the PIFA elements. However, due to the different orientation of the antennas (open ends of PIFAs on opposite sides), less current propagates from one PIFA to the other one, resulting in a lower mutual coupling in schematic (a). This is in agreement with the conclusion obtained from the simulated S-parameters shown in Figure 3.8. So this configuration, whereby two identical PIFAs are symmetrically placed on the opposite edges, will be applied in this chapter.

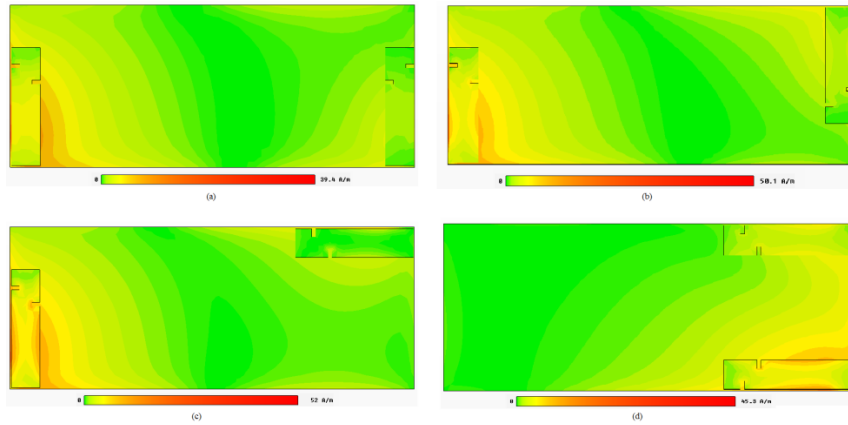


Figure 3.9 Surface current induced by the PIFAs at 1.9GHz

3.3 Linear Slits on Ground Plane

As discussed in last section, the separation between multiple antennas is an important parameter which affects the mutual coupling. However, when the multiple antennas are mounted in small mobile terminals, due to the finite inner-space, the mutual coupling between closely packed antenna elements becomes a critical issue which affects the performance of antenna system. Here, a novel structure for reducing the electromagnetic coupling between two closely packed PIFAs is presented in this section.

3.3.1 Linear Slit Etched on Ground Plane

From the current distribution presented in Figure 3.9 and the simulated S-parameters shown in Figure 3.8, it is noted that the mutual coupling between the antenna elements is higher when more surface current flow from one antenna to the other one. Therefore, in order to substantially reduce the mutual coupling, single or multiple DGS (slits) etched on the ground plane have attracted significant interest due to the ease of fabrication and applicability with different antenna types [11, 12]. Four different ground plane configurations are presented in Figure 3.10.

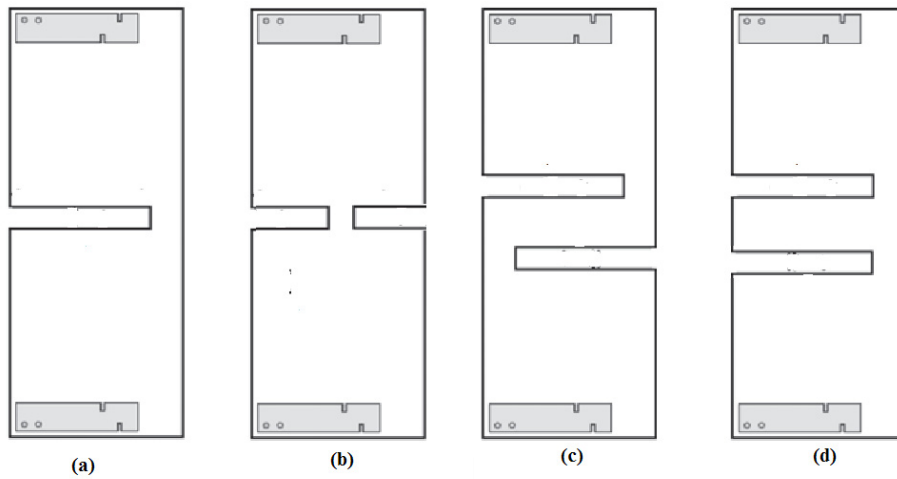


Figure 3.10 Four configurations of slits on the ground plane

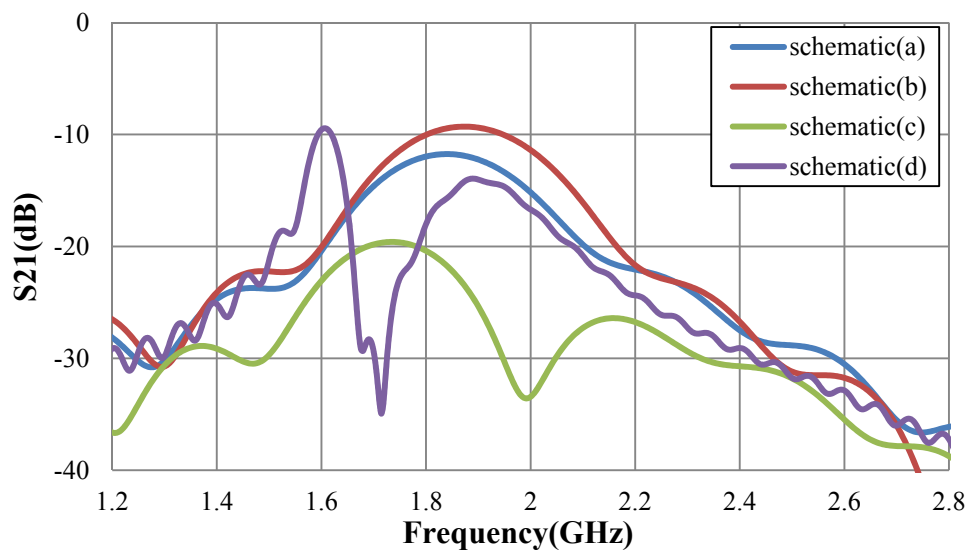


Figure 3.11 Simulated mutual coupling results (S₂₁) of four configurations

Figure 3.11 shows the simulated mutual couplings (S21) corresponding to the structures in Figure 3.10. The S21 achieves a little improvement in schematic (a) and (b) in comparison to the original ground plane without slits. The schematic (c) produces an encouraging result although the resonant frequency of the slits shifts to 2GHz, where the mutual coupling significantly reduces to -33dB. The resonance of schematic (d) shifts towards low frequency and its bandwidth (-20dB) is much less than the schematic(c). The current distribution is presented in Figure 3.12. As the surface current propagates along two edges of ground plane, the two linear slits which are inserted in the two edges of ground plane in schematic (c) make less current propagates from one side of the ground plane to the other side. Therefore, the ground plane configuration of schematic(c) will be applied in this chapter.

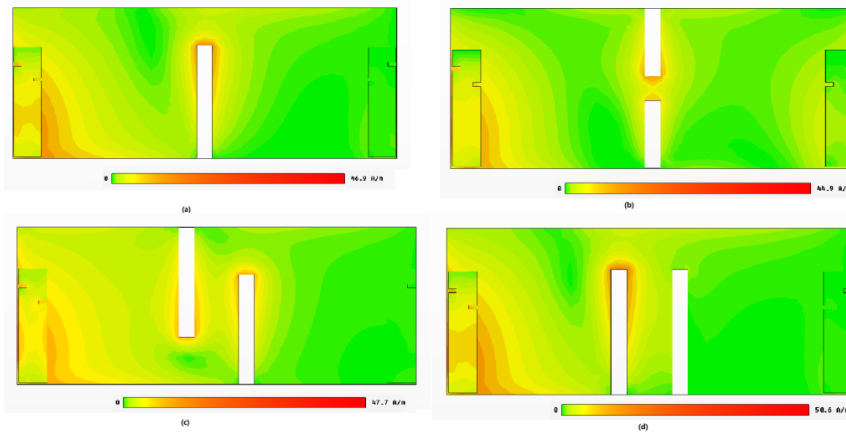


Figure 3.12 Current distributions for the four configurations at 1.9GHz

Because the distance between two PIFAs placed on the ground plane is approximately a half-wavelength apart, the electromagnetic coupling between the antenna array elements is mainly caused by the surface current on the ground plane. According to a significant research, linear slits acting like $\lambda/4$ stub filters improve the isolation characteristics between antennas [12]. The design with two slits inserted at two edges of the ground plane between the two antennas is shown in Figure 3.13. In this structure, two critical factors, the length of slits and the distance between them, determine the inter-element spacing and the effect of suppressing the surface current between the two PIFAs.

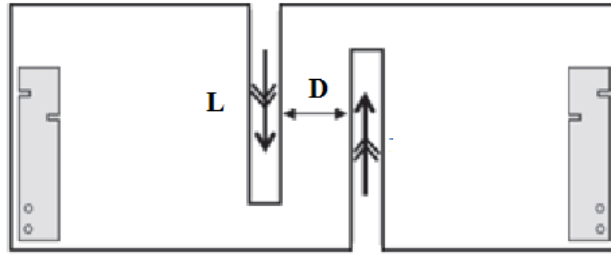


Figure 3.13 Two slits inserted at two edges of the ground plane

The first parametric study is the alteration of the slit length to validate the effect of the proposed linear slit structures. The length of the slits is approximate to quarter wavelength. The simulated transmission responses (S21) for different slit lengths are presented in Figure 3.14. It is noticed that the S21 is just -11.4dB at resonant frequency when the slit length is 29 mm. When the length is over 30mm, the mutual coupling has a significant reduction. With the slit length increasing, the resonance slightly shifts towards low frequency while their mutual couplings are slightly inversely proportional to the length. In order to most match the resonant frequency of the PIFA, the length is chosen to be 30mm.

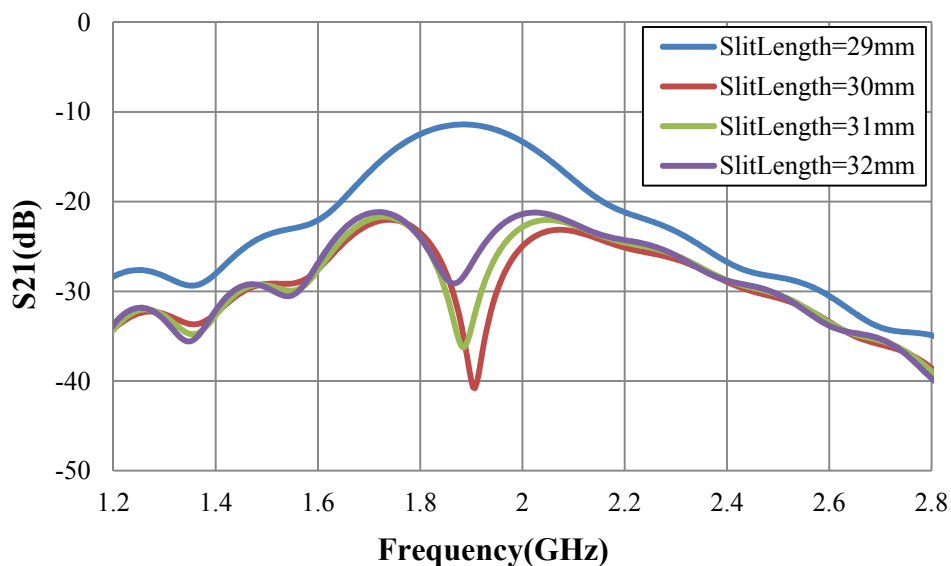


Figure 3.14 S21 of antenna array for different slit lengths

The second parametric study is to validate the distances between the two linear slits. It affects the resonant frequency of linear slits. Figure 3.15 shows the simulated S21

for different distance. Their resonant frequencies slightly shift from 1.89GHz to 1.91GHz with the distance increasing. When the distance between two slits is 12mm, the pair of slits resonates at 1.903GHz. The mutual coupling between the two PIFAs drop below -50dB and introduce transmission zero($S_{21} < -20\text{dB}$) across the operating band of PIFAs [13].

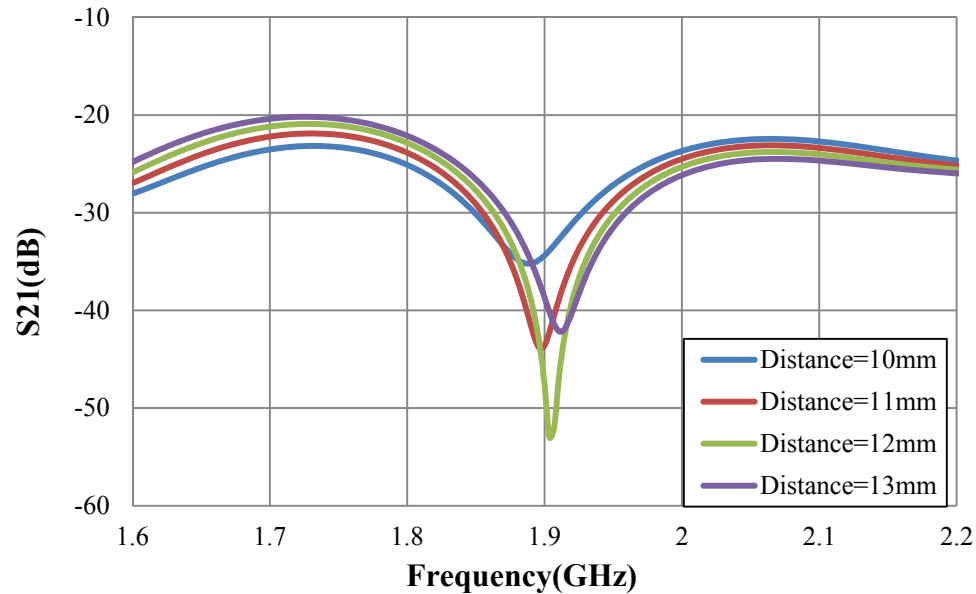


Figure 3.15 S_{21} of antenna array for different distance between two slits

After the slit length and distance are optimized, the simulated S-parameter of the dual-element antenna array is presented in Figure 3.16. The resonance of the second PIFA slightly shifts from 1.89GHz to 1.93GHz due to the asymmetric configuration of the slits on the ground plane. In order to present the effect of slits to antenna resonance, the dimensions of PIFAs is not retuned. Nevertheless, both antennas are well matched ($S_{11} < -6\text{ dB}$ and $S_{22} < -6\text{ dB}$) at the resonant frequency of the two slits. These simulated results show that a transmission zero ($S_{21} < -20\text{dB}$) is introduced in the coupling path between the two radiating elements, reducing the electromagnetic coupling between them to particularly low values [13]. The mutual coupling (S_{21}) between the two PIFAs drops to -43dB at the resonant frequency 1.9 GHz

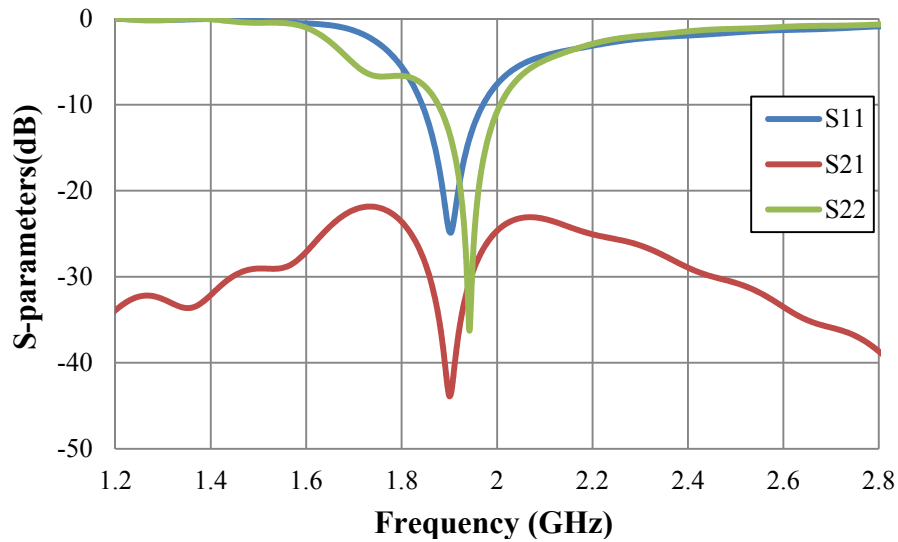


Figure 3.16 S-parameter of proposed slit on the ground plane

After insertion of the coupled linear slits, in comparison to the original antenna system, the S21 value reduces to below -20dB across the operating frequency band of the PIFAs, as shown in Figure 3.17. The mutual coupling shows a significant reduction from -9dB to -43dB at the resonance of the antennas. These results demonstrate that the pair of optimised linear slits introduces a good isolation between the antenna array elements.

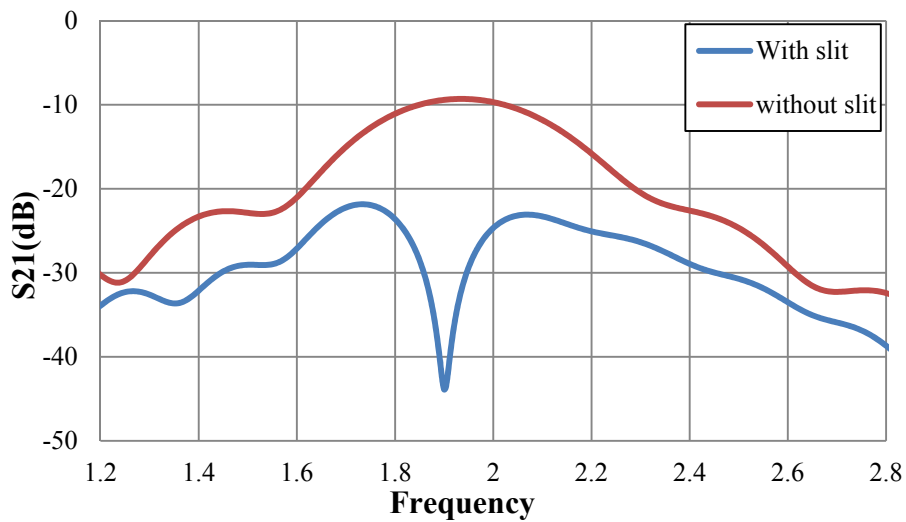


Figure 3.17 Simulated S21 with and without the two linear slits

The simulated current flow produced by the antennas at 1.9GHz on the ground plane is presented in Figure 3.18(a). The most current flow is around the area underneath the antenna radiating element and propagates via the edge of the ground plane.

However, the two coupled slits result in less current propagating across them. It is evident that strong opposite currents are excited in the slits, resembling an odd mode resonance of the two-slit configuration and resulting in strong electric fields normal to the ground shown in Figure 3.18(b). Hence, by optimizing the distance between them, they can be made to resonate at the desired frequency. It is evident that due to the opposite directions of the magnetic fields through the two slits, a strong magnetic field loop is formed between the two slits, depicted in Figure 3.18(c). This is a clear indication of the magnetic coupling that is established between the two proposed slits and further enhances the resonances, resulting in the sharp minimum in the S21 response.

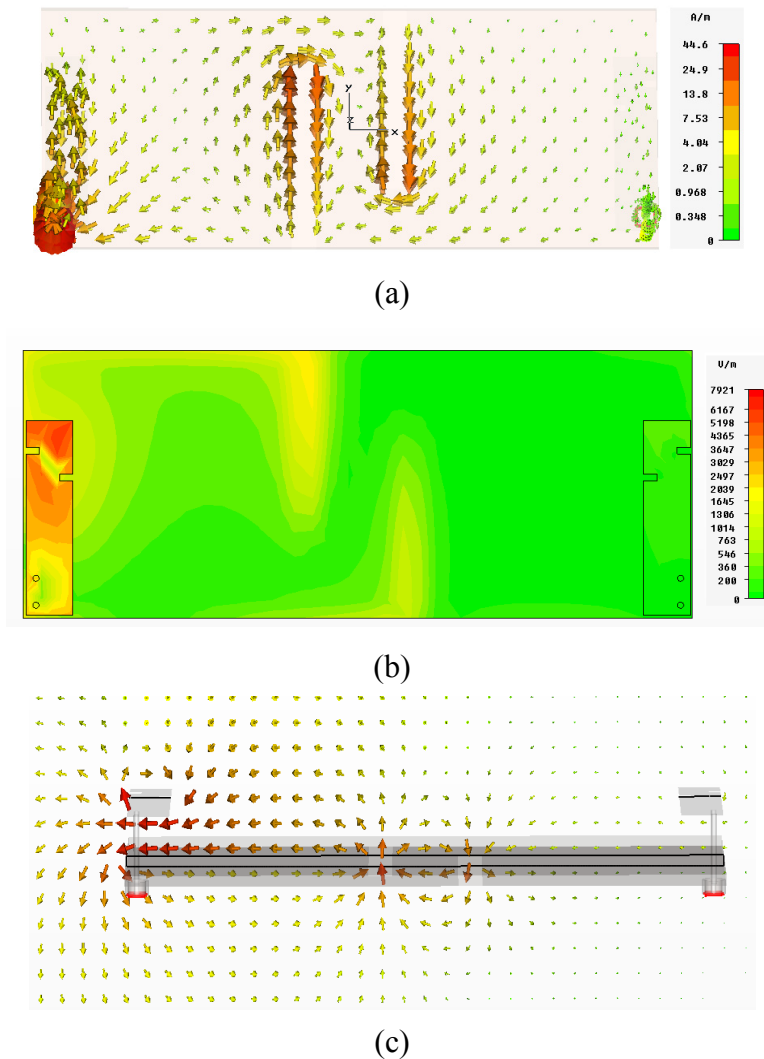


Figure 3.18(a) Current flow (b) Electric field on the ground plane (c) Magnetic loop between two linear slits at resonant frequency

It is noted that the optimised coupled slits are expected to radiate. Therefore, the radiation patterns of the examined antenna arrays in the presence of the resonating slits have been studied and have been found to be slightly different to those of the array without the slits. This is shown in Figure. 3.19, where the radiation patterns for the two cases have been plotted. The pattern of the proposed structure is slightly more omni-directional (directivity of 3.5dBi compared to 4.5dBi). The total efficacy of the antenna system has improved from 85.7% to 93.5%, due to the reduced S21 and hence the reduction of the power coupled from one PIFA to the other. It is thus well suited for mobile handset applications.

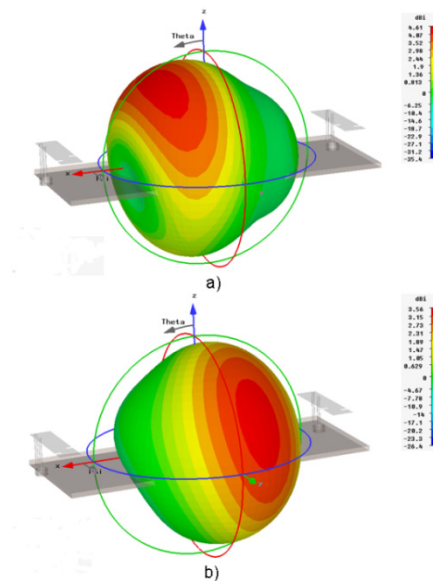


Figure 3.19 Simulated radiation patterns of (a) the original array configuration when PIFA1 (the left element) is excited and (b) the decoupled array in the presence of the slits, when the same element is excited

3.3.2 Fabrication and Measurement

Based on the optimized simulated configuration, two prototypes of a dual-element antenna array (the original ground plane and the one with the linear slits) were fabricated and measured in the laboratory at Loughborough University, as shown in Figure 3.20. An anritsu 37000D vector network analyzer recorded the S-Parameters data from the prototypes.



Figure 3.20 Prototype system using the proposed slitted ground plane

The measured S-parameter of a dual-element PIFA array on a conventional ground plane without linear slit is shown in Figure 3.21. By comparison to the measured and simulated data, the centre resonance frequencies of proposed PIFA arrays are slightly shifted from 1.9GHz to 1.86GHz (PIFA1) and 1.84GHz (PIFA2). The measured S21 reaches a maximum of -10.5dB which is better than the simulated result. These minor discrepancies between simulated and measured results are due to fabrication imperfections in the manual soldering of the feeding and shorting pins of the PIFAs. Figure 3.22 illustrates the measured S-parameter of the PIFA array with the proposed linear slit structure. The measured return loss of Antenna 1 (S11) is different to that of Antenna 2. This is due to the two linear slits not being completely symmetrical on the ground plane. However, both antennas are well matched ($S_{11} < -6\text{dB}$ and $S_{22} < -6\text{dB}$) and the mutual coupling (S21) drops to -47.58 dB at the resonant frequency of the slits (1.921GHz), instead of the simulated resonance (1.9GHz). Finally, the measured mutual coupling between the antenna elements in the proposed design is significantly reduced, in comparison to the original design of a dual-element PIFA array on a conventional ground plane, across the whole operating frequency band of the PIFAs.

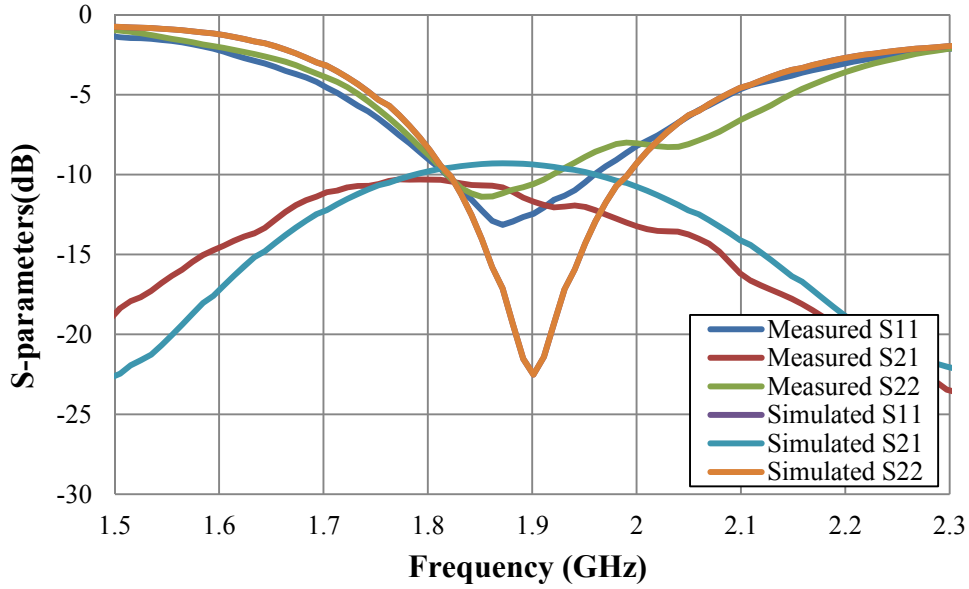


Figure 3.21 Simulated and measured S-parameters for the prototype with the conventional ground plane

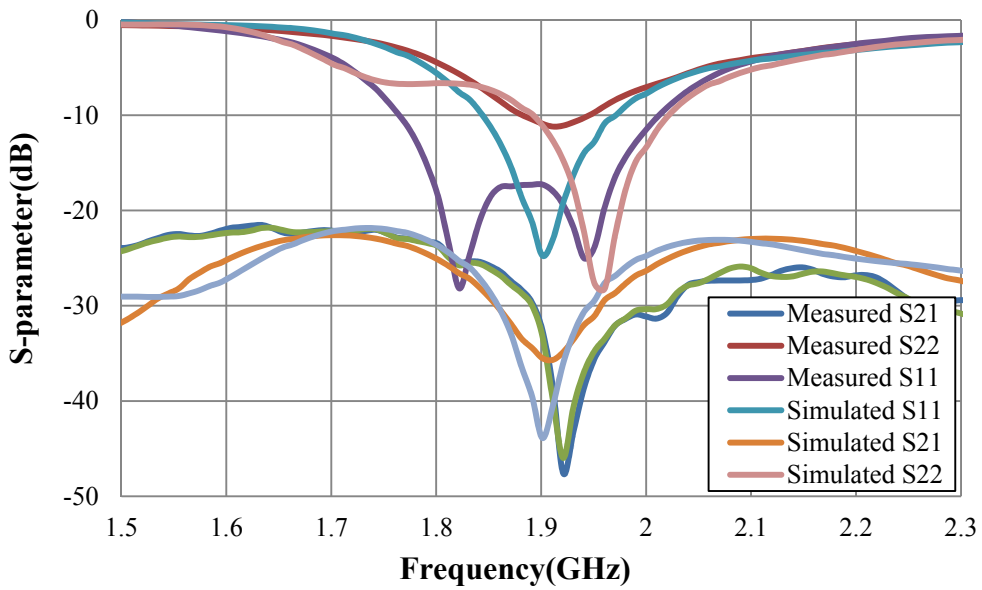


Figure 3.22 Simulated and measured S-parameters the prototype with the proposed linear slits

3.4 Convoluted Slits on Ground Plane

In the last section, the two coupled quarter-wavelength linear slits produce a significant reduction of the mutual coupling between the two PIFAs and introduce a

transmission zero across the operation frequency for a typical handheld device. However, due to their length and position, they occupied a relatively large area on the ground plane between the two antennas, which is impractical in many realistic designs of handheld devices. Therefore, novel miniaturised convoluted slits are proposed and optimized in this section. The configuration and dimension of the proposed PIFAs are the same as above.

3.4.1 Single Convoluted Slit on Ground Plane

In order to investigate the impact of the proposed convoluted slits, a series of simulations have been carried out in CST software package. Their length, width and position are studied and optimized. Initially, one single convoluted slit is etched close to the top edge of the ground plane as a miniaturized element, as shown in Figure 3.23. The first parametric study is the alteration of slit length to validate the effect of the proposed slit structure. The simulated transmission responses (S21) for different slit lengths are presented in Figure 3.24. With the slit length increasing, the resonance shifts towards a lower frequency while their mutual couplings are below -19dB. In order to match the resonant frequency of the PIFA, the value of the slit length is 36mm.

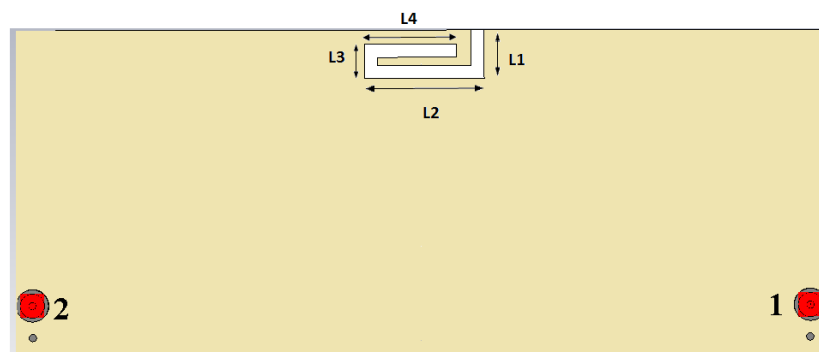


Figure 3.23 Single miniaturized slit inserted in the ground plane

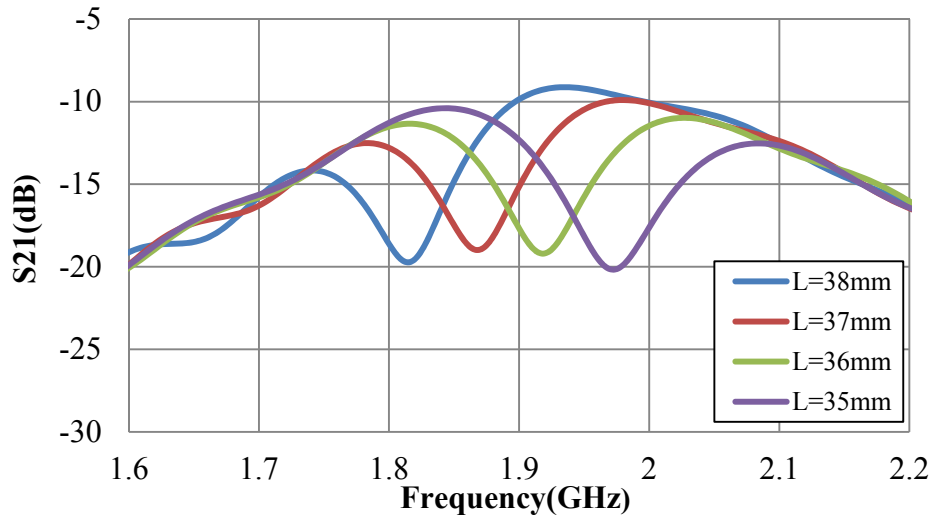


Figure 3.24 Mutual coupling of antenna array for different slit length

The second parametric study is to validate the width of convoluted slits. Figure 3.25 illustrates the simulated transmission responses (S_{21}) for different widths. Their resonant frequencies slightly shift from 1.9GHz to 1.935GHz when the width of the slit increases from 1mm to 1.75mm. The impedance matching of the proposed convoluted slit shows an improvement without significantly losing its bandwidth when the width is decreased. Finally, the value of the slit width which makes the couple slit resonate at 1.9175GHz is found to be 1.25mm.

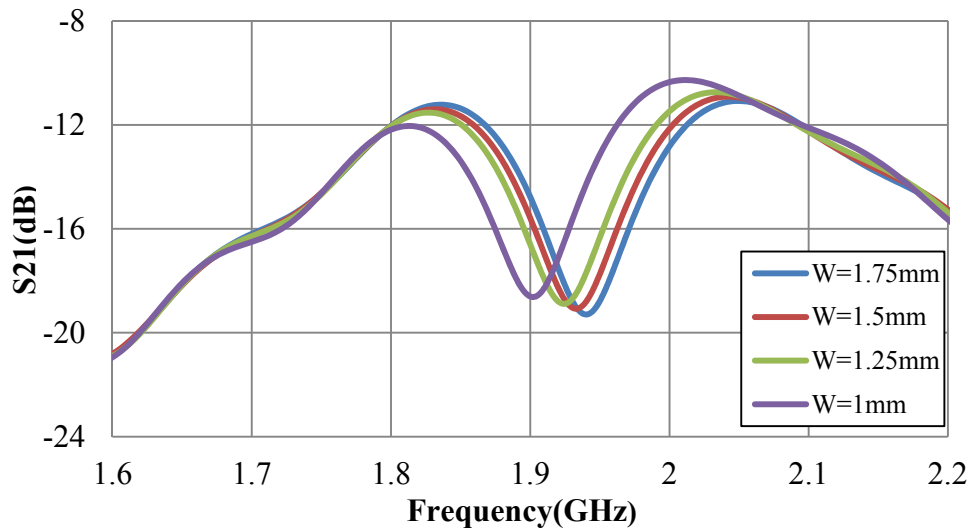


Figure 3.25 Mutual coupling of antenna array for different slit width

After a series of simulations in CST Microwave Studio, the dimensions of the slit were optimised in order to match the operating frequency band of the PIFAs. The

final dimensions are $L_1=6\text{mm}$, $L_2=14\text{mm}$, $L_3=5\text{mm}$, $L_4=11\text{mm}$, and the slit width is 1.25mm . The simulated S-parameter of the PIFAs in the presence of the single slit on the top edge of the ground plane is shown in Figure 3.26. The mutual coupling between two PIFAs is reduced from -9dB to -19dB at 1.9175GHz in comparison to a conventional ground plane without the slit (shown in Figure 3.17). Furthermore, it is noticed that the return loss (S_{11} and S_{22}) of the two PIFAs are different due to the asymmetric shape of the convoluted slit. However, both antennas remain well matched at the resonant frequency of the slit.

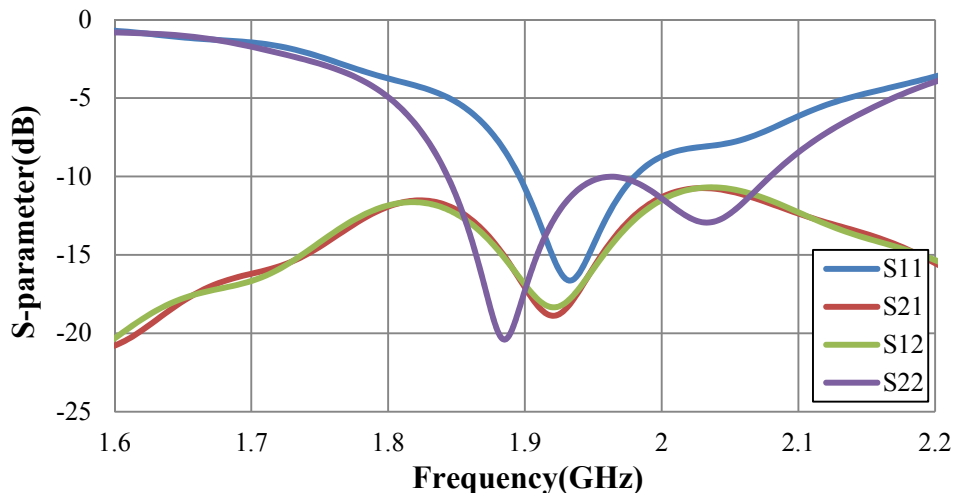
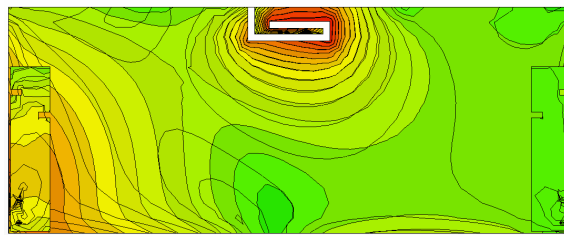
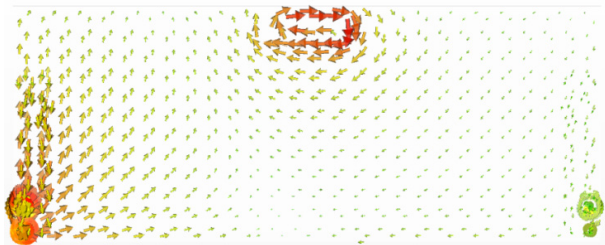


Figure 3.26 S-parameters of antenna array PIFAs with a convoluted slit on top edge of ground plane



(a)



(b)

Figure 3.27 (a) Current distribution and (b) Current flow on the ground plane when a single slit etched close to top edge

The surface current on the ground plane at the resonant frequency (1.92GHz) in the presence of one convoluted slit is shown in Figure 3.27. It is evident that the current is amassed in the area underneath the radiating patch and less current propagates via the single top slit to the other antenna. Although the convoluted slit is adjacent to the wider edge of the ground plane and takes up less area, the single slit still traps a large portion of current, resulting in a good isolation between the two antenna elements.

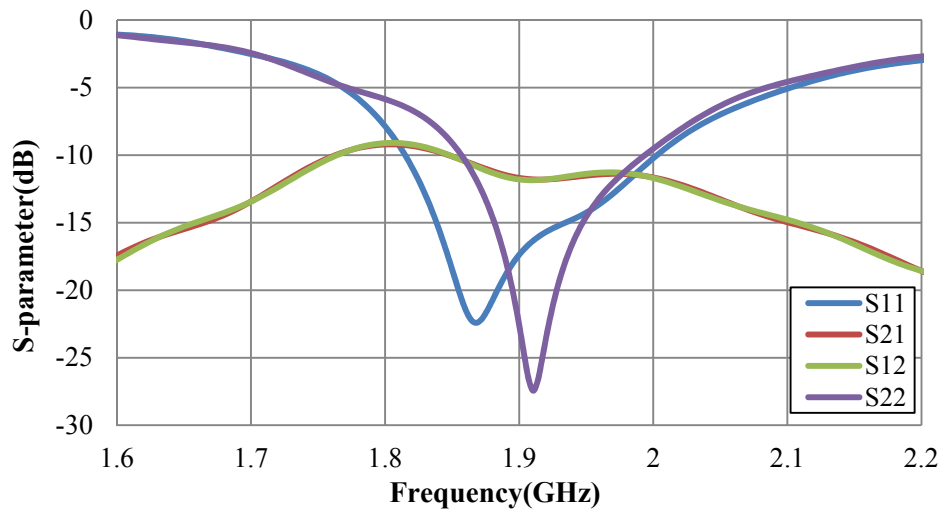
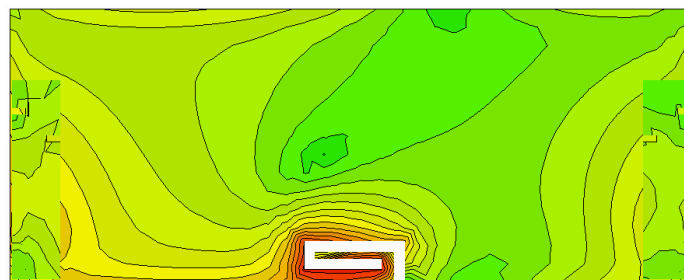
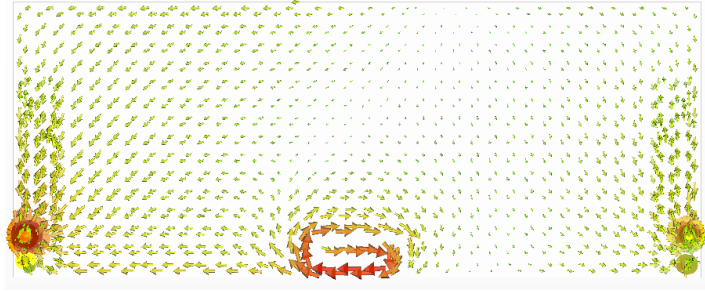


Figure 3.28 S-parameters of antenna array with a convoluted slit on bottom edge of ground plane

The proposed convoluted slit is then positioned at the bottom of the ground plane. The width and length of the slit are kept the same as above. Figure 3.28 shows that the S21 at 1.9 GHz is just -12 dB which is worse than the top one. The difference of S21 for the two different positions is attributed to the open ends of PIFAs close to top edge and more current propagate along the top edge. In Figure 3.29, a large amount of current are widely spread on the ground plane, resulting in a high mutual coupling between the antennas.



(a)



(b)

Figure 3.29 (a) Current distribution and (b) Current flow on the ground plane when the slit is etched close to bottom edge

3.4.2 Dual Convoluted Slits on Ground Plane

The previous study showed that the single convoluted slit which is placed at the top side succeeded in reducing the mutual coupling. In order to further reduce the mutual coupling, two convoluted slits are etched on the ground plane as shown in Figure 3.30. A series of studies such as the length, width and position of the two slits will be presented. The optimized dimensions of the proposed convoluted slit are: $L_1=6\text{mm}$, $L_2=14\text{mm}$, $L_3=5\text{mm}$. The L_4 will be optimized to make the slits resonate within the desired operating frequency band of the PIFAs.

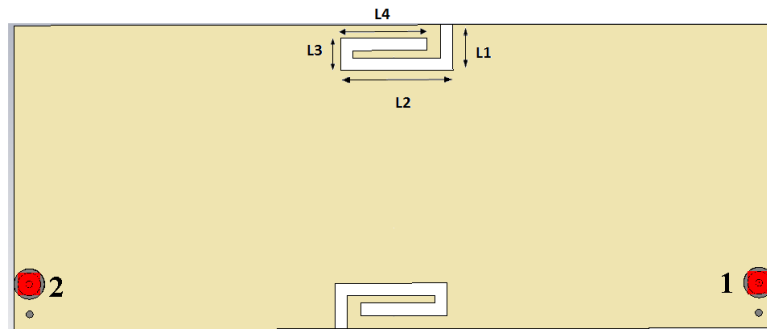


Figure 3.30 Proposed miniaturised convoluted slits

Figure 3.31 illustrates the simulated mutual coupling (S_{21}) accompanied by the alteration of slit length. As the length of L_4 increases from 9.4mm to 12.4mm, the minimum of S_{21} which corresponds to the resonance of the slit shifts from 2 GHz to

1.86GHz while their minimums of S_{21} are below -24dB. Figure 3.32 illustrates the simulated return loss (S_{11}) of antenna 1 with different slit lengths. All their resonated frequencies of PIFA are around the desired frequency (1.9GHz), regardless of the alteration of slit length. Finally, the most satisfactory result of L_4 is 11.4mm to make the slits resonant at 1.91GHz. In fact, the two convoluted slits also resonate at other frequency about 5.2GHz which is far away from the desired frequency 1.9GHz.

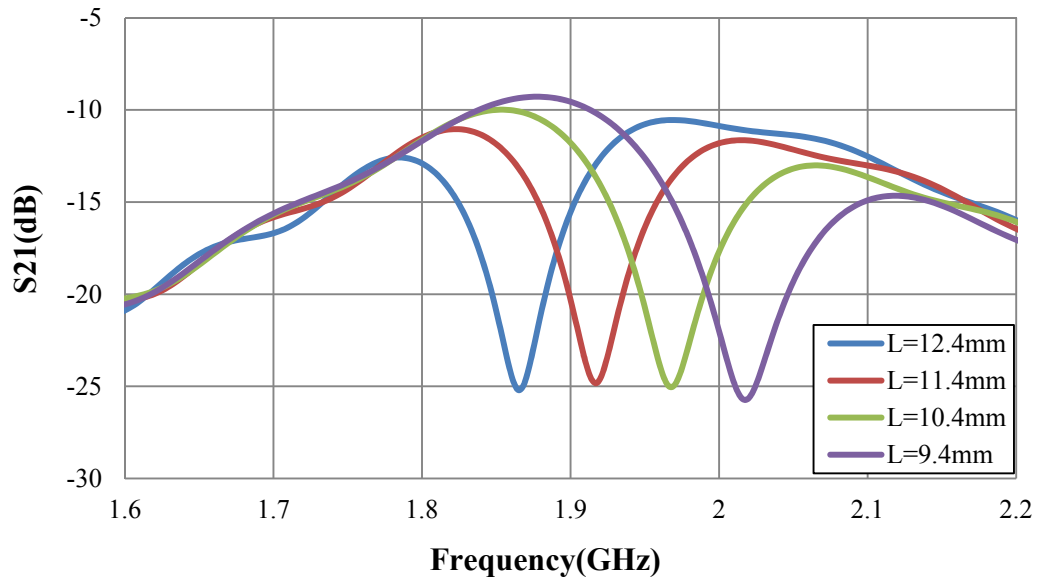


Figure 3.31 Mutual coupling (S_{21}) of antenna array for different slit lengths

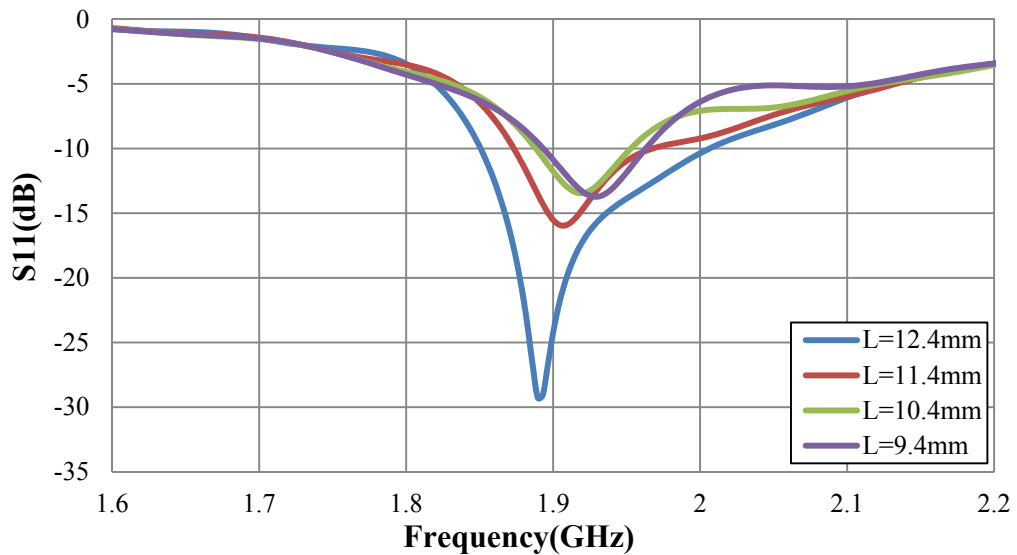
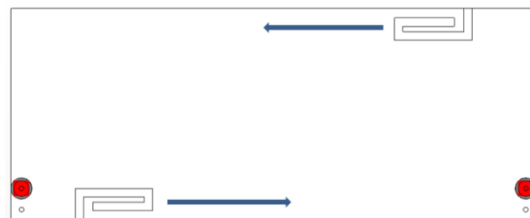
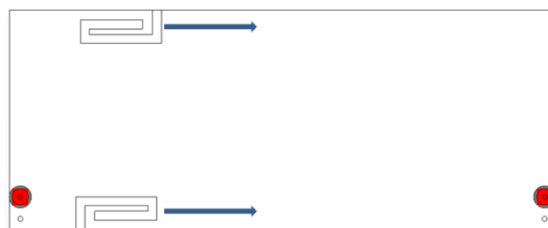


Figure 3.32 Return Loss (S_{11}) of antenna 1 for different slit lengths

In the previous simulations, the convoluted slits are placed at the middle of the wider edge. In order to investigate the effect of slit positions, the two convoluted slits are employed, having different positions on the ground plane. The slits are constantly smooth shifting along the X axis along two different directions: in the opposite direction in Figure 3.33(a), and in the same direction in Figure 3.33(b). The slits are shifted by 0mm, 16mm, 24mm, 36mm, 44mm, and 60mm respectively. When the slits are shifting along the opposite direction, the resonance of the slit shifts to lower frequencies with the slits close to each other, as shown in Figure 3.34(a). When the two slits move along the same direction, all S21 minimums corresponding to the resonance of the slit are below -23dB around the desired frequency (1.91GHz), except in one position (M=60mm), as shown in Figure 3.34(b). The proposed convoluted slits do not significantly lose their bandwidth with different positions on the ground plane. The reason for the production of the different results in the two motion directions will be explained below. However, these results are encouraging since the miniaturised convoluted slit structure can maintain a good performance for reducing mutual coupling at most of positions along the wider edges of the ground plane. It is well suitable for the design for a compact handset.

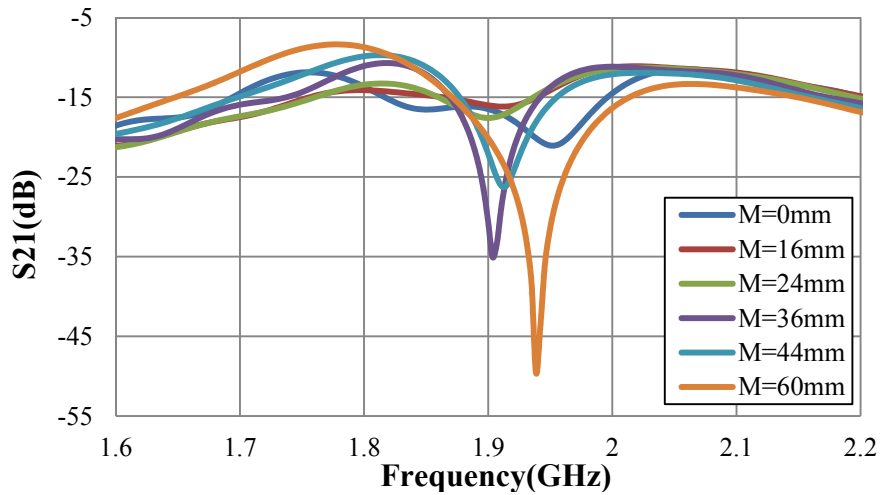


(a)

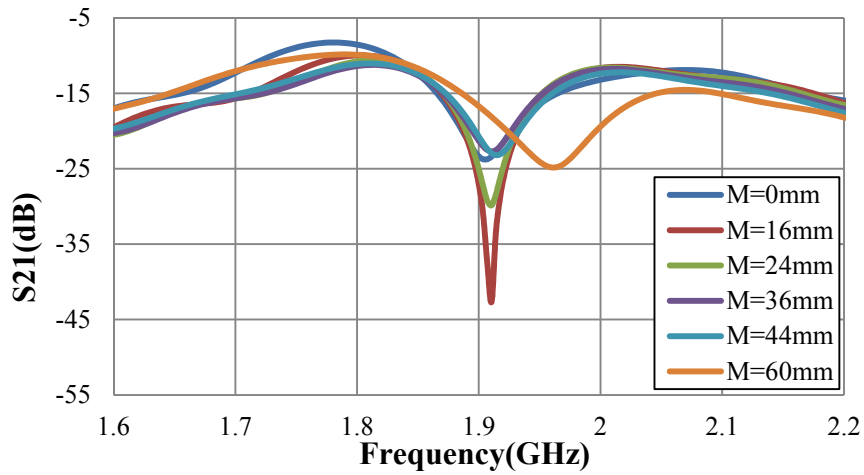


(b)

Figure 3.33 Slits shift along the x-axis in (a) opposite direction, (b) same direction



(a)



(b)

Figure 3.34 Mutual coupling (S_{21}) of antenna array when slits shifted along the x-axis in (a) the opposite direction, (b) the same direction

After the length and width of the slits are optimized, placing these two convoluted slits at the middle of the ground plane, the simulated S-Parameter of antenna array is depicted in Figure 3.35. In comparison to the case of the PIFA array without slits shown in Figure 3.17, a sharp transmission minimum is obtained at 1.92GHz, while the S_{21} reduced to -27dB. Simulations have shown that inserting a second convoluted slit opposite the first one, produces virtually no changes to the resonant frequency of slits. The significant further reduction of the mutual coupling in the presence of two convoluted slits is attributed to the nature of the slits' resonances, which is investigated in following text by inspecting surface currents and the magnetic fields.

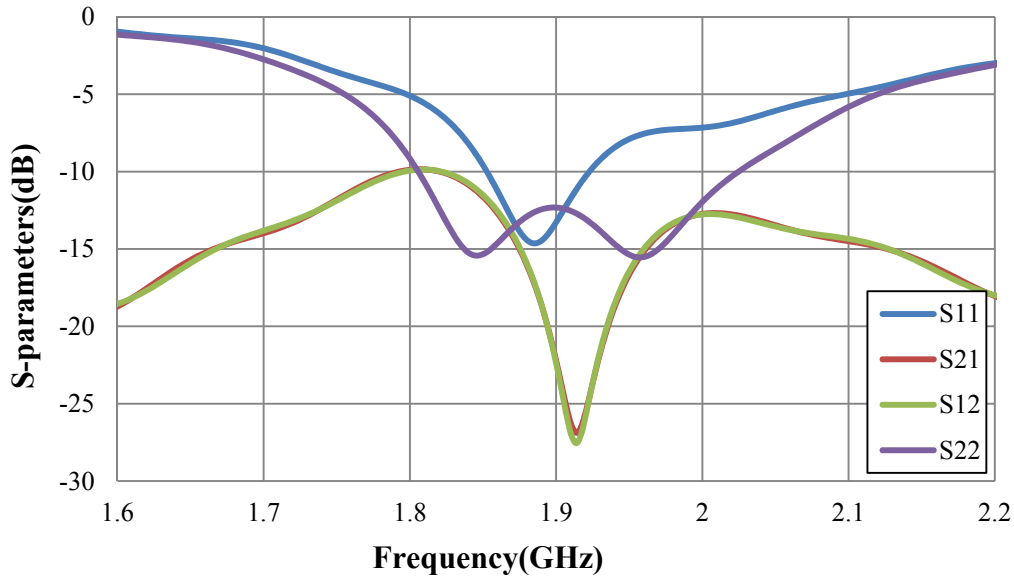


Figure 3.35 S-parameters of the PIFA array with the convoluted slits

The current flows on the ground plane at the resonant frequency of the proposed slits are presented in Figure 3.36. As is evident, the two slits are able to trap most of the current on the ground plane. Although the slits are close to the edges and take up little space on the ground plane, there is very little current flowing across the space between the slits. On the top slit, current flows around the slit in a clockwise direction. In contrast, on the bottom slit, the current is anti-clockwise. This creates strong magnetic fields of opposite direction normal to the two slits. The magnetic fields in the plane which are normal to the ground and crossing the centres of the two slits is plotted in Figure 3.37. It is evident that due to the opposite directions of the magnetic fields through the two slits, a magnetic field loop is formed between the two slits. This is a clear indication of the magnetic coupling that is established between the two proposed slits and further enhances the resonances, resulting in the sharp minimum in the S21 response. It also presents the reasons why the resonances of convoluted slits are anchored around the desired frequency when they are constantly smooth shifting along the same direction as shown in Figure 3.34(b)

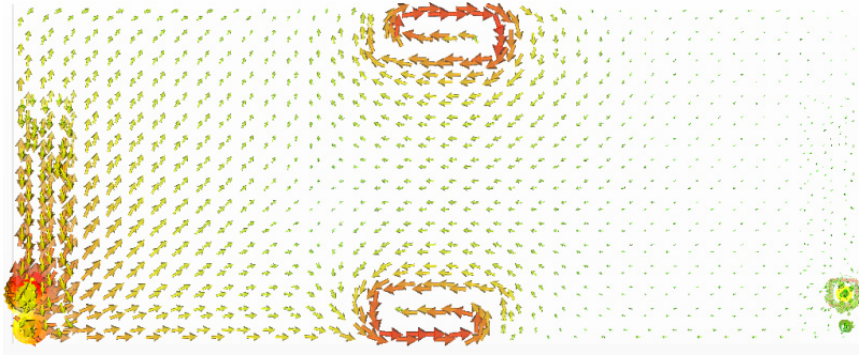


Figure 3.36 Simulated surface current flow on the ground plane in the presence of the resonating slits at 1.92GHz

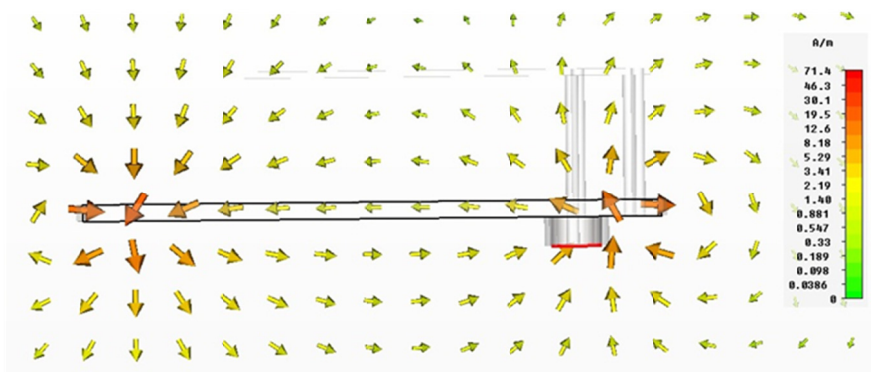


Figure 3.37 The magnetic field distribution in the plane normal to the ground and through the centres of the two slits. Maximum magnetic field of opposite direction flows through the two slits

The radiation efficiency of the PIFAs at 1.92GHz is about 98% without the slits and reduces to about 93% in the presence of the slits, due to the additional resonant currents and associated losses. The total efficiency has also been calculated from equation (3.2) [14] using the simulated results and is shown in Figure 3.38

$$\eta_{tot} = \eta_{rad}(1 - |S_{21}|^2 - |S_{11}|^2) \quad (3.2)$$

It is evident that although the radiation efficiency slightly decreases in the presence of the slits, the total efficiency is slightly higher, due to the reduced S21 and hence the reduction of the power which is coupled from one PIFA to the other. At 1.92GHz the total efficiencies are approximately 89% and 87.1% with the slits and 86% without the slits.

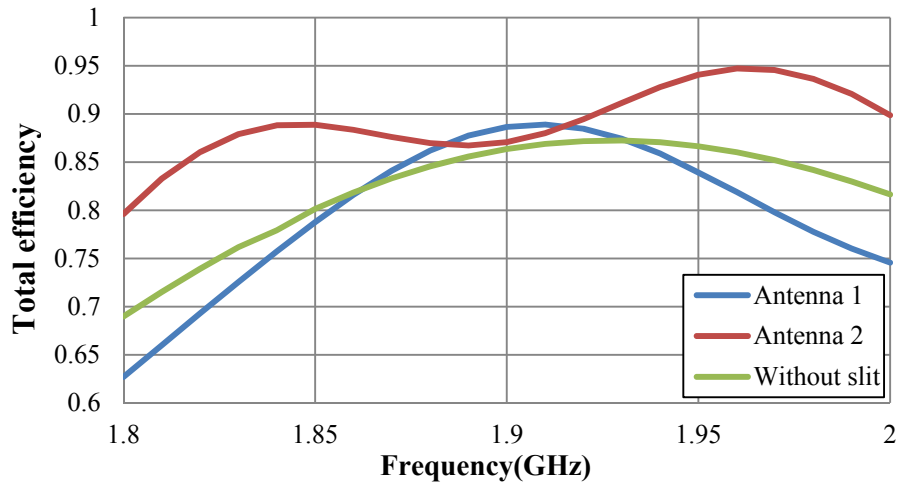


Figure 3.38 Simulated total efficiency of antennas

3.4.3 Fabrication and Measurement

A prototype of the configuration employing the two convoluted slits has been fabricated in order to experimentally validate the proposed design, as shown in Figure 3.39. The measured S-parameters without and with the proposed slits are also presented in Figure 3.40 for comparison. These results validate that, in the presence of the convoluted slits, a minimum is obtained in the mutual coupling between the two antennas, at exactly 1.92GHz corresponding to the resonance of the proposed slits. The PIFAs' resonances are very slightly shifted. These minor discrepancies are due to fabrication imperfections in the manual soldering of the feeding and shorting pins of the PIFAs. Nevertheless, at the resonance of the slits (1.92GHz) both antennas are well matched ($S_{11} < -10$ dB and $S_{22} < -10$ dB) and the mutual coupling drops to -26dB. Furthermore, the measured S21 between the antennas in the proposed design is significantly reduced, as compared to the original design, for the whole operating bandwidth of the PIFAs.

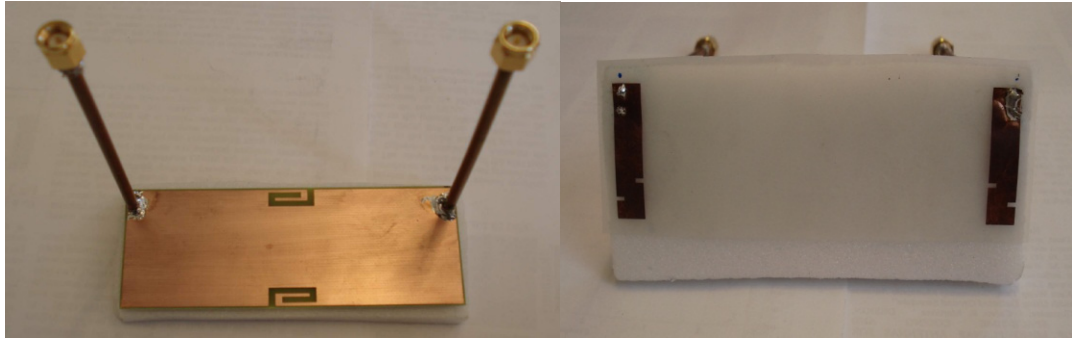
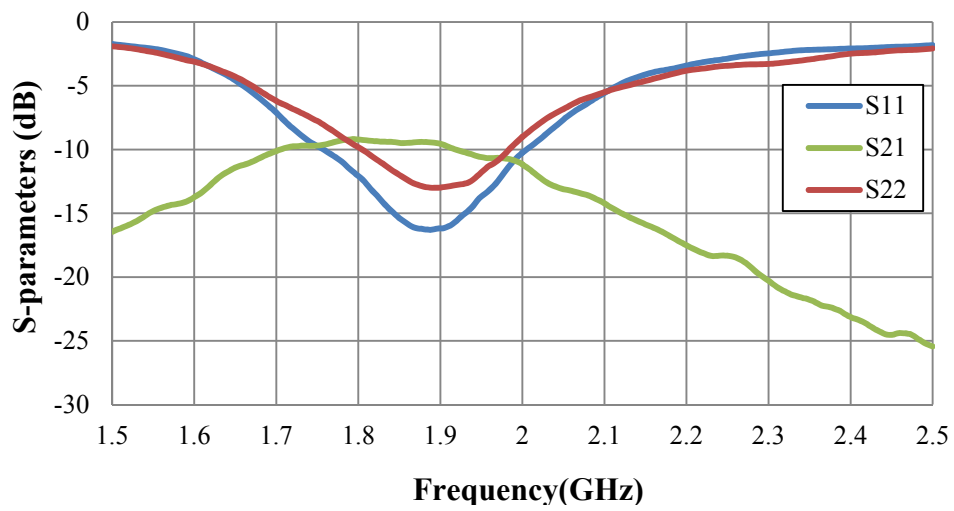
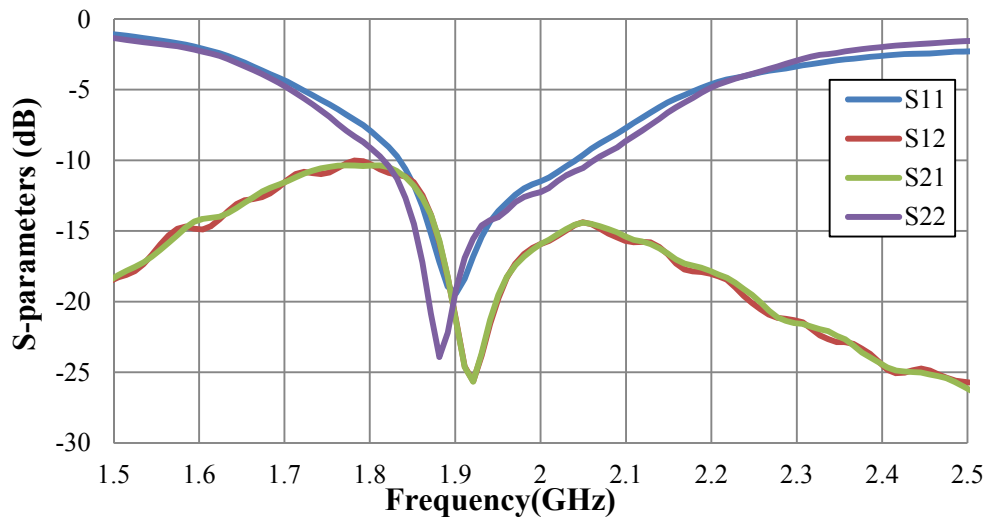


Figure 3.39 Prototype of antenna system using the proposed slitted ground plane



(a)



(b)

Figure 3.40 Measured S-parameters of antenna array (a) without slit, (b) with slit

The antenna radiation efficiency has been assessed experimentally using the Wheeler cap method [14] and the total efficiency η_{tot} was calculated from equation (3.2) using the measured S-parameters. A prototype of the PIFA system employing the two convoluted slits has been measured to experimentally validate the proposed properties of convoluted slits, as shown in Figure 3.41. The measured total efficiency values in the presence of the optimized slits are 90% for PIFA1 and 88% for PIFA2 which are in agreement with the simulations. Without the slits the total efficiency was measured 80% shown in Figure 3.42. In comparison to the simulated results shown in Figure 3.39, the measured total efficiency of the antenna array without the slits has a reduction from 86% to 79.5% at the resonance of the antennas.

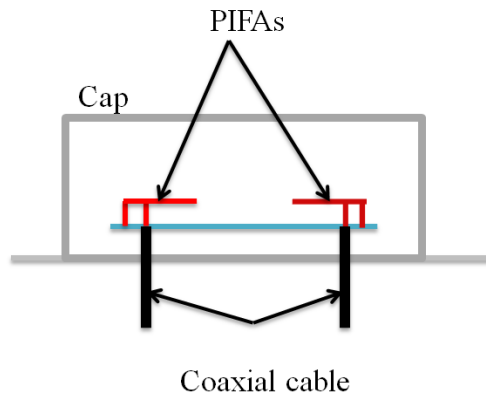


Figure 3.41 PIFA array within a wheeler cap [14]

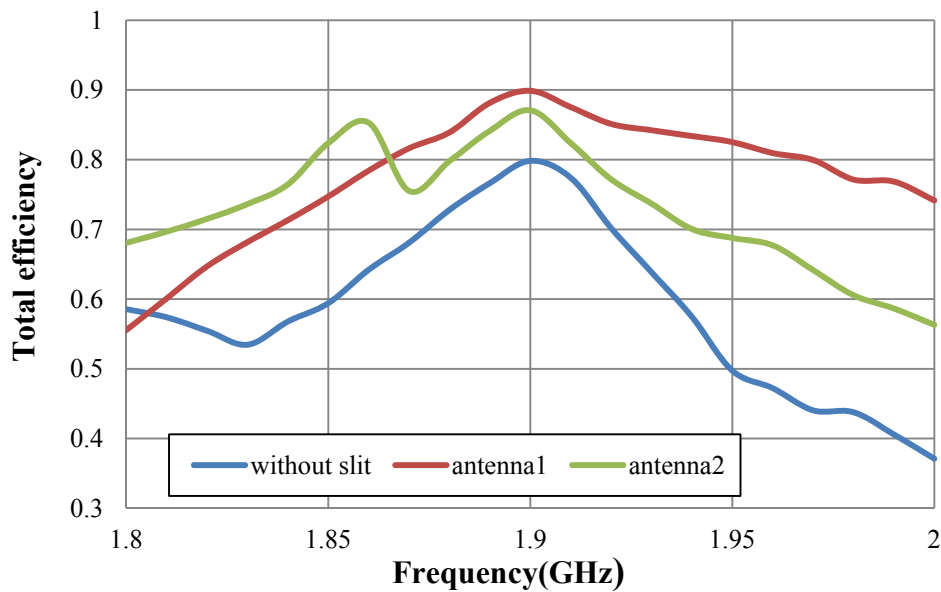


Figure 3.42 Measured total efficiency of antennas with and without slits

A novel approach for reducing the electromagnetic coupling between two PIFAs has been presented. The proposed technique is based on the insertion of miniaturized convoluted slits close to the edges of the ground plane. The dimensions of the convoluted slits have been optimised using full-wave simulations. A transmission minimum was obtained by virtue of the resonance of the slits resulting in a significant reduction of the mutual coupling across the operating bandwidth of the antennas. The magnetic fields and surface currents on the ground plane were studied, validating the nature of the slits' resonance.

3.4.4 Effect of Human Body on Radiation Properties of PIFAs

In personal communications, the electromagnetic interaction between built-in mobile phone antennas and nearby biological body is a key consideration [15]. Some of the literature demonstrates that the interaction will significantly degrade the antenna radiation pattern and other characteristics [16, 17]. The miniaturized convoluted slit structure etched on the ground plane is proposed to reduce the effect of human body on the radiation properties of antenna while achieving a minimum mutual coupling between antenna array elements. A dual-element PIFA array with two convoluted slit will be evaluated when a box model of a human hand or head are relatively close to the antenna system.

In order to simulate the effect of a hand on the dual-element PIFAs array, the hand model was modelled by the one box model. The model is characterized by permittivity epsilon equal to 38.63, the loss tangent is 0.008, and conductivity $S=1.21 \text{ S/m}^2$. The configurations of PIFAs and convoluted slits are the same as the case in the previous section. The box model of the hand is placed above the PIFA system with the overall dimensions $60\text{mm}\times 60\text{mm}\times 20\text{mm}$ as shown in Figure 3.43. In order to present the effect of a hand on a dual-element PIFA array with two convoluted slits, the

hand(box model) is placed increasingly close to the antenna system at smaller distances S from the the radiating patch of the PIFA.

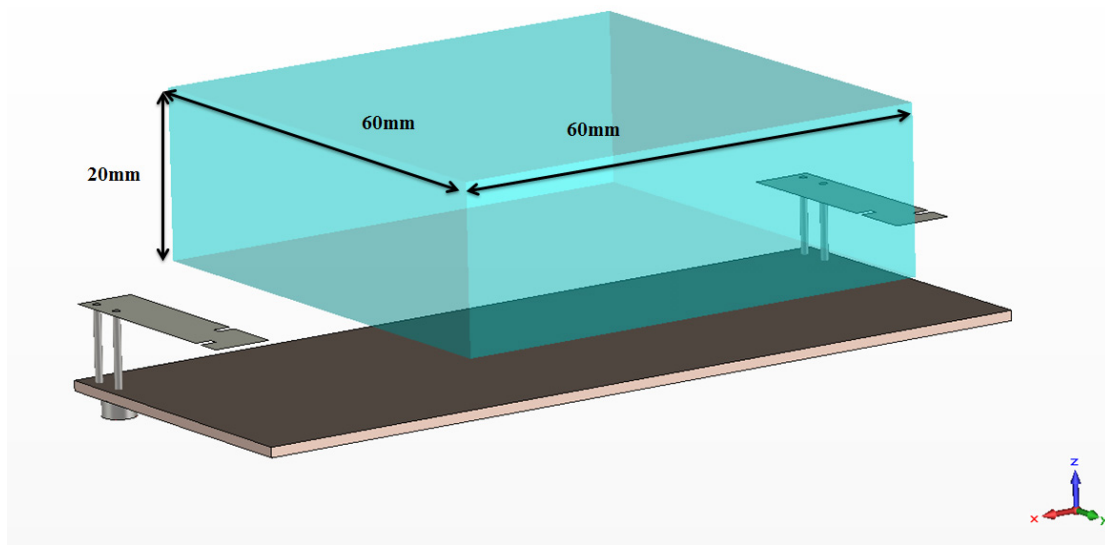
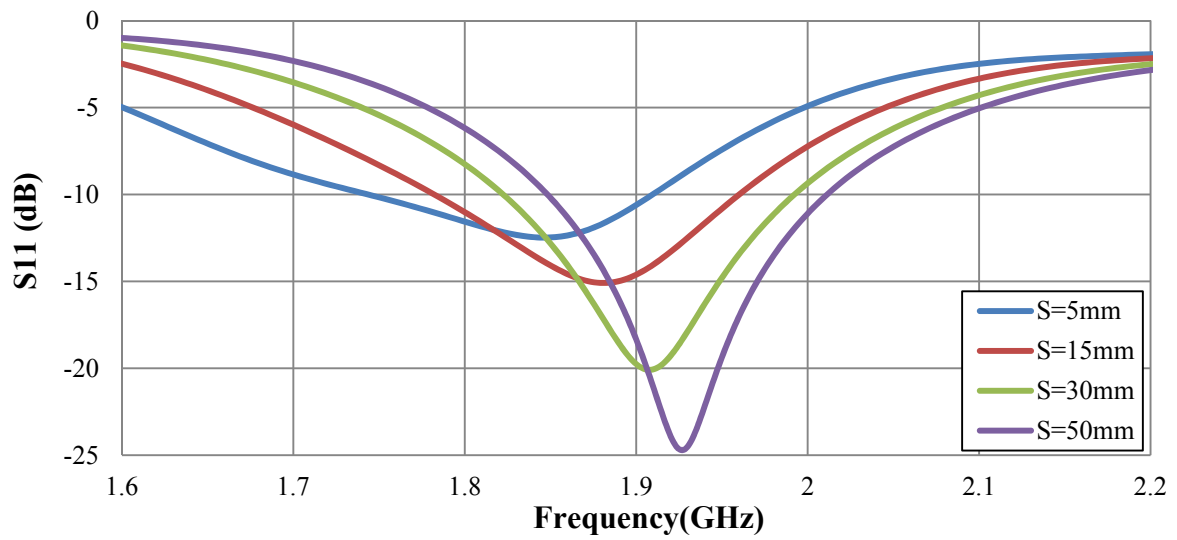


Figure 3.43 Simulated model of a hand on the ground plane with two PIFAs

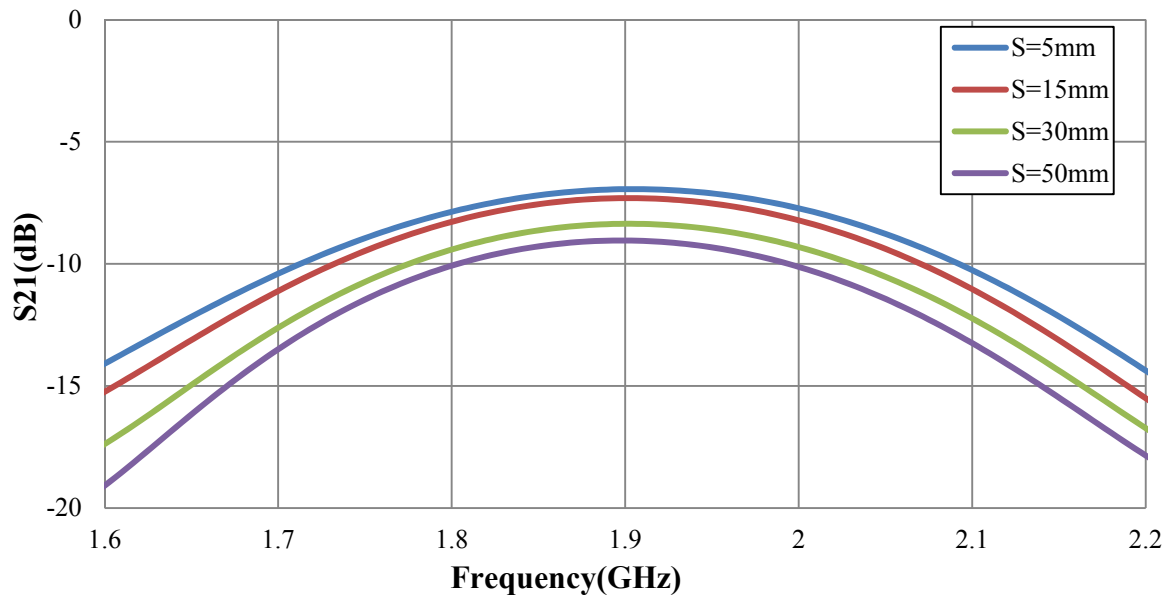
The effect of a hand on the performance of the dual-element PIFAs array without the convoluted slit is initially presented. The hand (box model) is right above the ground plane and higher than the antenna radiating patch by 5mm on the Z -axis, owing to the practical situation such as the case of the handset or something else. In order to simulate a real hand holding a mobile phone, the hand (box model) is placed by increasing the smaller distances S from the the radiating patch of PIFA along the Z -axis.

After a series of simulations with increasing distance(s) from 5mm to 50mm, Figure 3.44(a) shows the return loss of the antenna 1 with a conventional ground plane held by a human hand for different distances. It is noted that the resonance of the antenna shifts towards lower frequencies with the hand (box model) close to the PIFA array. It is caused by the high permittivity object (hand) close to the antenna array [18]. The hand model reflects more energy transmitted from antennas to the ground plane. The mutual coupling between the two PIFAs, shown in Figure 3.44(b), is over -10dB at the

resonant frequency of antennas for all distances between the hand (box model) and the PIFA radiating patch.



(a)

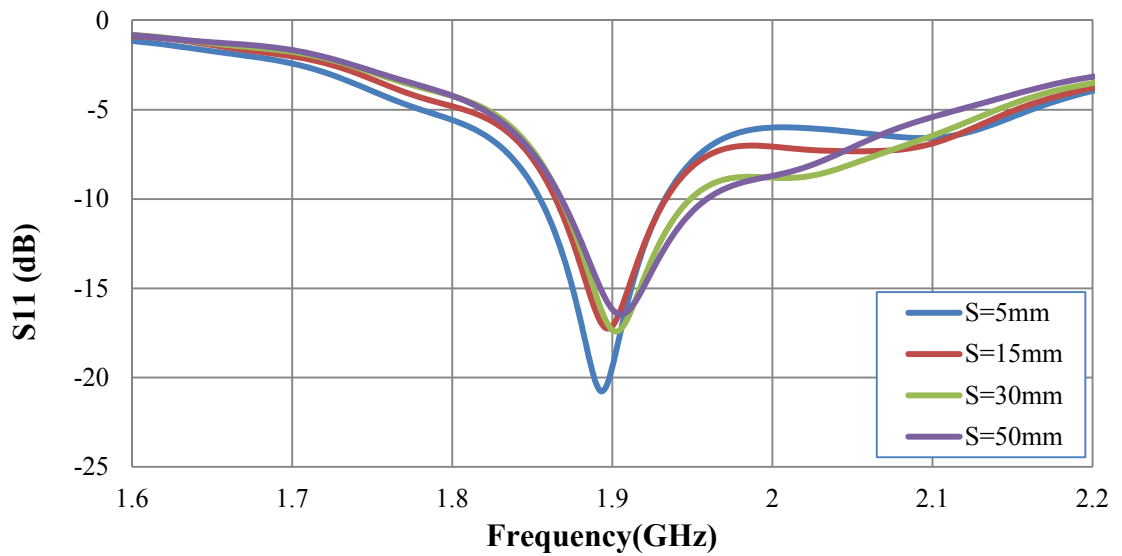


(b)

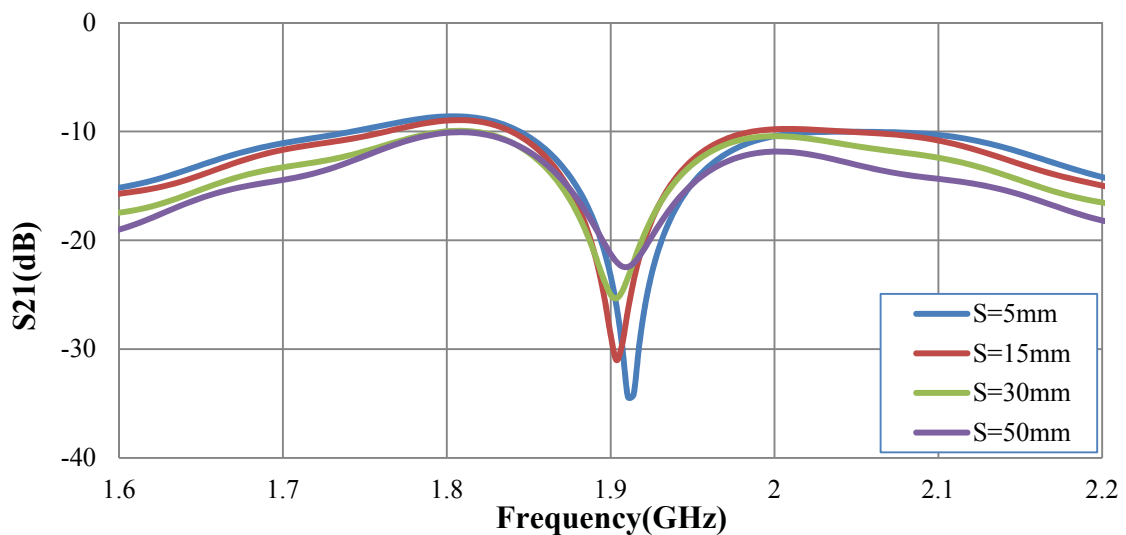
Figure 3.44 (a) Reflection coefficient(S_{11}) of antenna 1 and (b) Mutual coupling(S_{21}) of the antenna system with a conventional ground plane in the presence of the hand at different distances S from the antenna

After the miniaturized convoluted slits are inserted in the ground plane, with the PIFA array held by a human hand, the simulated return loss and mutual coupling of the antenna system for different distances are presented in Figure 3.45. In comparison

to the case without the convoluted slits in Figure 3.44, the resonant frequencies of the antenna 1 are constantly around the desired frequency. Meanwhile, the mutual coupling between the antenna array elements shows a significant reduction for all distances below -22dB at the resonance of the antenna. These results demonstrate that miniaturized convoluted slits produce a good isolation, whether the mobile handset is in free space or held by a hand. It also illustrates that the proposed convoluted slits succeed in reducing the PIFA array detuning from a hand.



(a)



(b)

Figure 3.45 (a) Reflection coefficient (S_{11}) of antenna 1 and (b) Mutual coupling (S_{21}) of the antenna system with the convoluted slit in the presence of the hand at different distances S from the antenna

Since a mobile phone is relatively close to the head when a user is on the phone, one homogeneous box model of the head is proposed. The head box model is placed at the back of the ground plane with the overall dimensions 200mm×150mm×50mm, as shown in Figure 3.46. The model is characterized by permittivity epsilon equal to 38.63, loss tangent is 0.008 and conductivity $S=1.21S/m^2$. In order to present the effect of the hand and head on a dual-element PIFA array with two convoluted slits, the head (box model) was placed relatively close to the antenna system at increasingly smaller distances S from the ground plane along the Z -axis. It should be noted that the distance is defined as the separation between the ground plane and the head surface. The hand (box model) is right above the ground plane and higher than the antenna radiating patch by 5mm on the Z -axis, owing to the practical situation such as the case of a handset or something else. The head model is 5mm apart from the ground plane and has a rotation angle with respect X -axis equal to 10 degree, which approximates the posture in which people use a mobile handset.

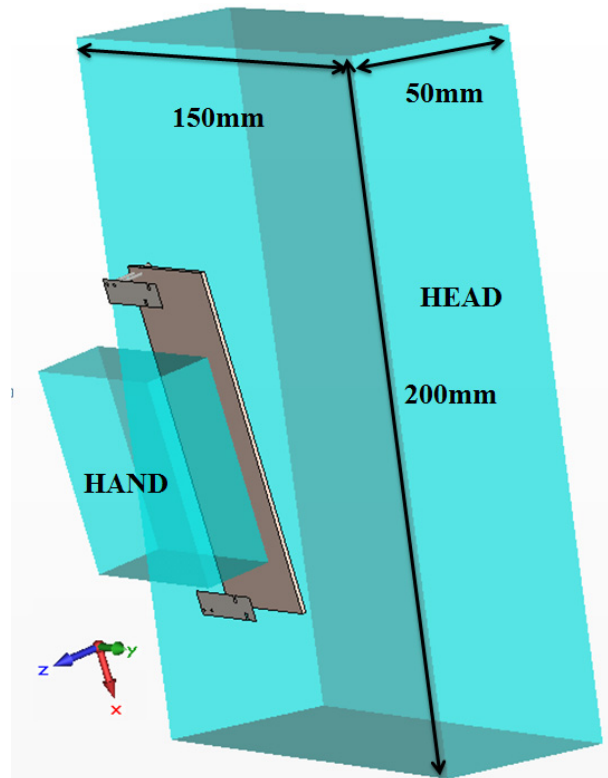
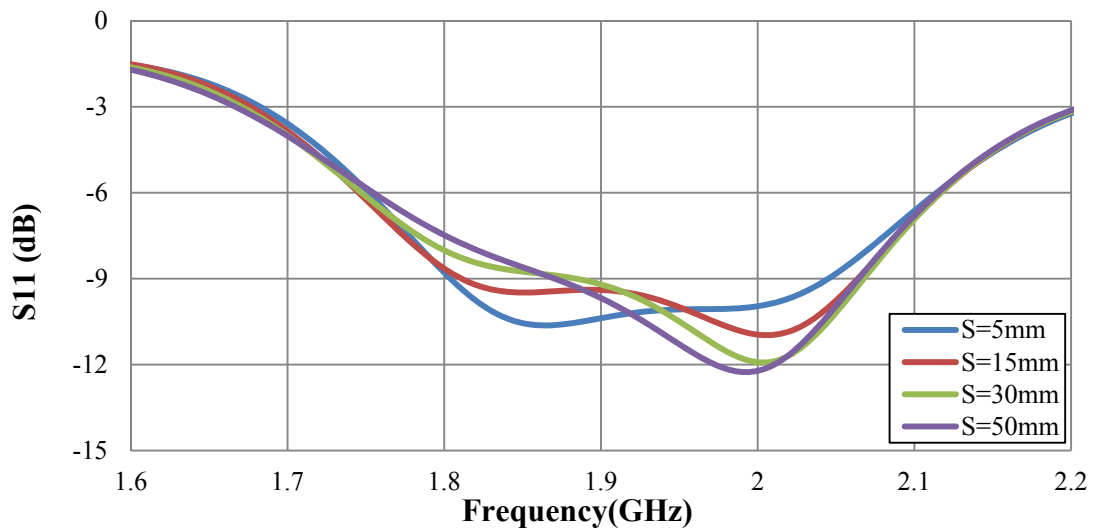
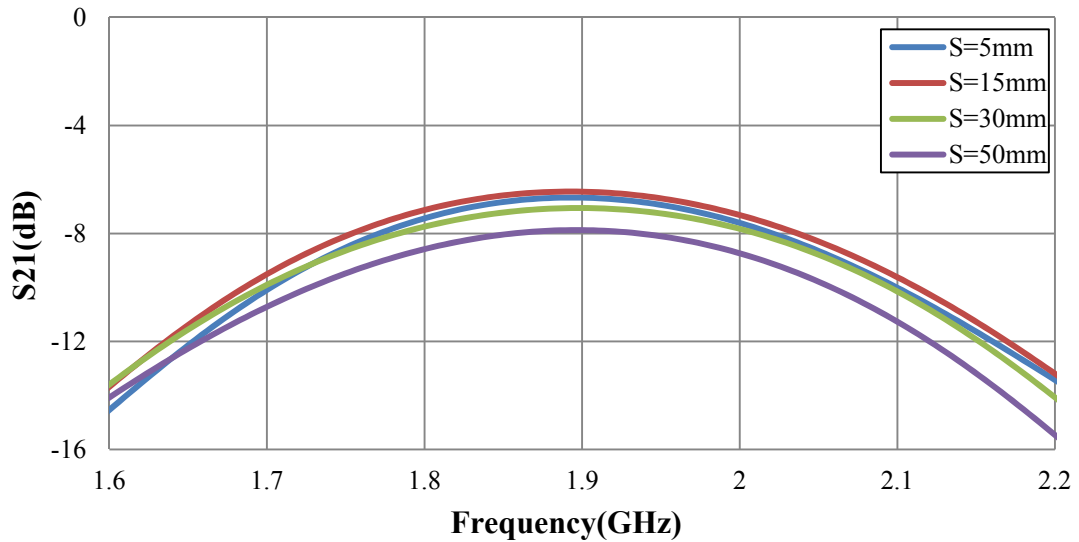


Figure 3.46 Simulated model of hand and head with two PIFAs in the presence of the proposed convoluted slits

After performing simulations with increasing distance(S) from 5mm to 50mm, the simulated return loss of the PIFA array with a conventional ground plane held by a human hand close to the user's head is presented in Figure 3.47(a). Due to the detuning occurring, as a result of the coupling of the human body's high permittivity, the resonance of the antenna shifts towards low frequencies with the head (box model) close to the ground plane. The mutual couplings between two PIFAs, shown in Figure 3.47(b), are over -8dB at the resonant frequency of antennas for all distance (S).



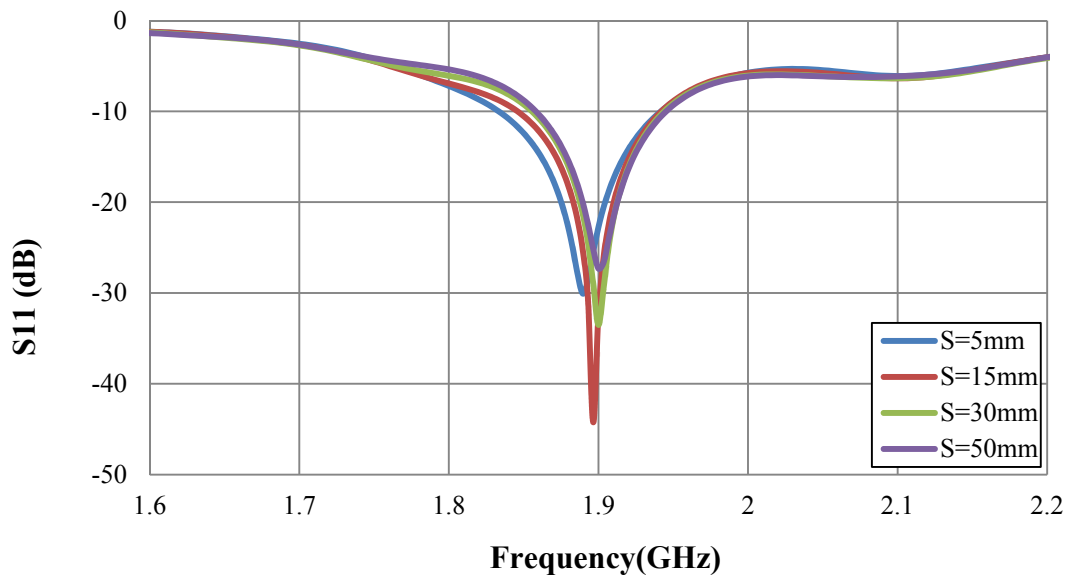
(a)



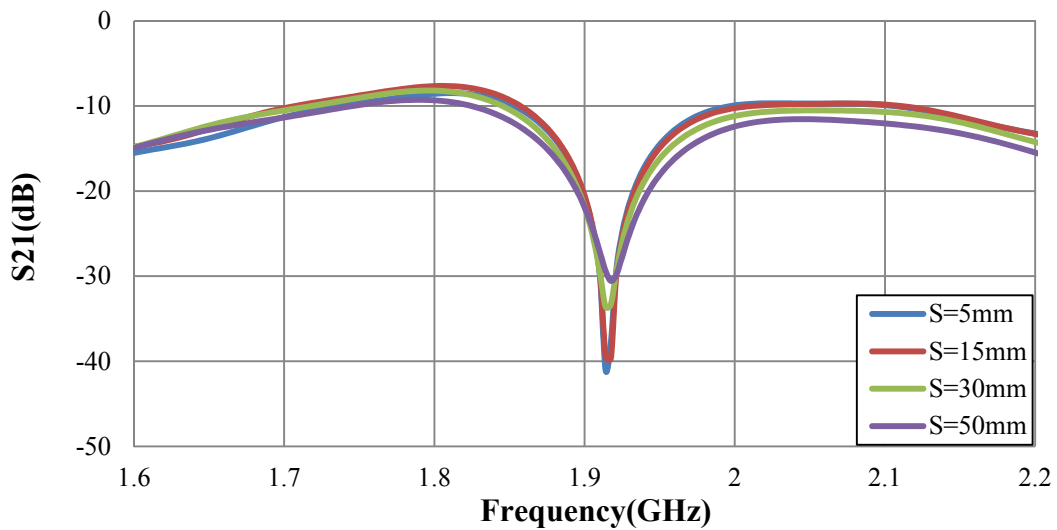
(b)

Figure 3.47 (a) Return loss (S11) of antenna 1 (b) Mutual coupling (S21) of the antenna system with a conventional ground plane in the presence of the head at different of the antenna system distances S from the ground plane

After the miniaturised convoluted slits are inserted in the ground plane, with the PIFA array held by a human hand close to the head, the simulated return loss and mutual coupling of the antenna system for different distances between the head and the ground plane are presented in Figure 3.48. In comparison to the case without the convoluted slits in Figure 3.47, the resonant frequencies of the PIFA are constantly around the desired frequency 1.9GHz. Meanwhile, the mutual coupling between antenna elements reduces to below -25dB for all distances.



(a)



(b)

Figure 3.48 (a) Return loss of antenna 1 (b) Mutual coupling of the antenna system with two convoluted slits in the presence of the head at different distances S from the ground plane

When any high permittivity objects (hand or head) are close to the antenna array, they will reflect the energy transmitted from antennas back to ground plane and produce additional current between antenna elements. The additional current increases the mutual coupling and affects antenna performance. After the proposed slits are employed, they suppress the current flowing on the ground plane between antennas. These results demonstrate that miniaturized convoluted slits produce a significant reduction of the mutual coupling and have the potential to isolate between the antennas and the human body, whether the mobile handset is in free space or close to the human body.

3.5 Single Convoluted Slit between Closely-Packed PIFAs

The preceding simulated and measured results have presented the miniaturized convoluted slits producing a significant reduction of the mutual coupling within the operating band of the antennas. However, for very close placed PIFA array elements, the reduction of mutual coupling becomes even more challenging. This section proposes one miniaturised slit etched on the common ground plane between two closely packed PIFAs for mutual coupling reduction.

3.5.1 A Single Slit on Ground Plane

Two PIFAs are placed on a compact common ground plane with dimensions $100 \times 40 \text{mm}^2$, printed on a 1.2mm-thick FR-4 dielectric substrate ($\epsilon_r=4.5$). Each of the two single-band PIFAs is designed to operate from 1.7-2.1GHz. The antenna configuration is depicted in Figure 3.49 (a) and the two-PIFA array without the slit is present in Figure 3.49 (b). The mutual coupling between the two PIFAs is calculated using 3D full-wave simulation software and is found to have a maximum value of $S_{21} = -7.6 \text{dB}$ at approximately the central operating frequency of the antennas as shown in Figure 3.50 (a).

The proposed convoluted slit is inserted in the ground plane. It is etched between the two PIFAs and close to the short edge of the ground plane as shown in Figure 3.49 (c). Even in the presence of the slit, the mutual coupling between the PIFAs can still be over -10dB, unless the slit dimensions are optimised carefully. The proposed slit has two important parameters: the width and total length of the slit.

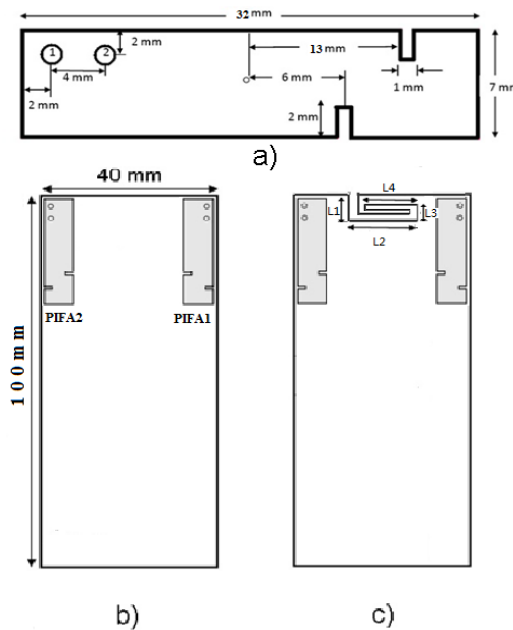
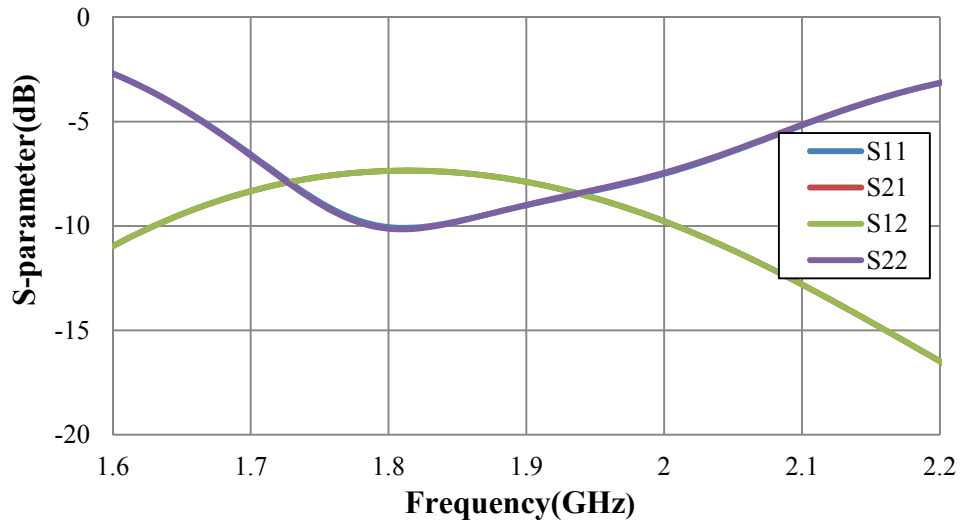


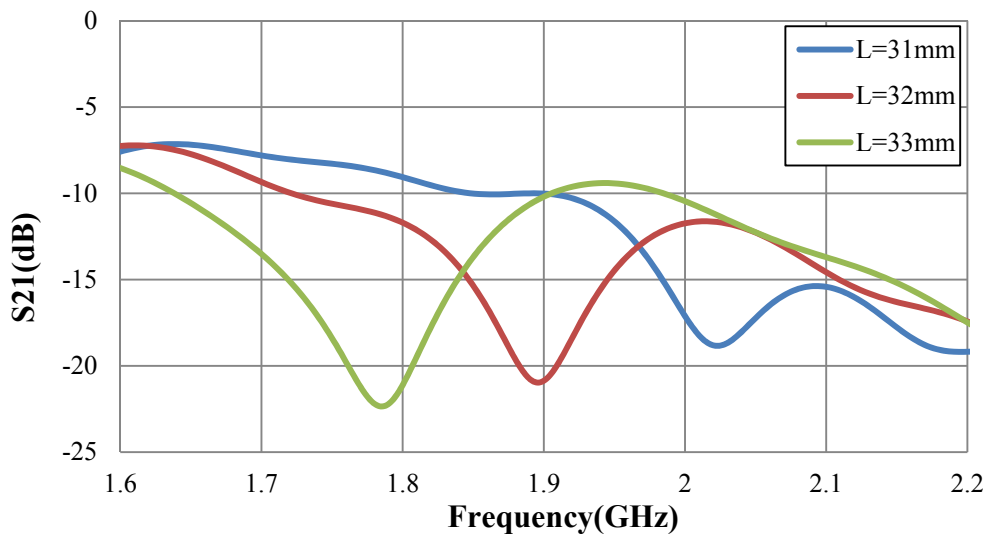
Figure 3.49 Array of closely-packed PIFAs positioned on a 100x40mm ground plane.
 (a) PIFA geometry (b) Array without slit (c) Array with proposed optimized convoluted slit

To observe the effect of the two parameters, the total length of the slit is simulated from 31mm to 33mm. As the length increases, the S21 minimum, which corresponds to the resonance of the slit, shifts from a higher frequency to a lower frequency, as shown in Figure 3.50 (b). An optimised total length of 32mm is found for the resonant frequency of the slit of about 1.9GHz. The effect of the width dimension has also been studied in simulations and shown in Figure 3.50(c). With the width of the slit decreasing from 2mm to 0.5mm, the resonant frequency of S21 decreases from a higher frequency to about 1.9GHz when the width is 1.6mm. Then the resonant frequency increases again with the slit width decreasing. So the width is optimised at 1.6mm in order to resonate within the operating frequency range of the PIFAs. The

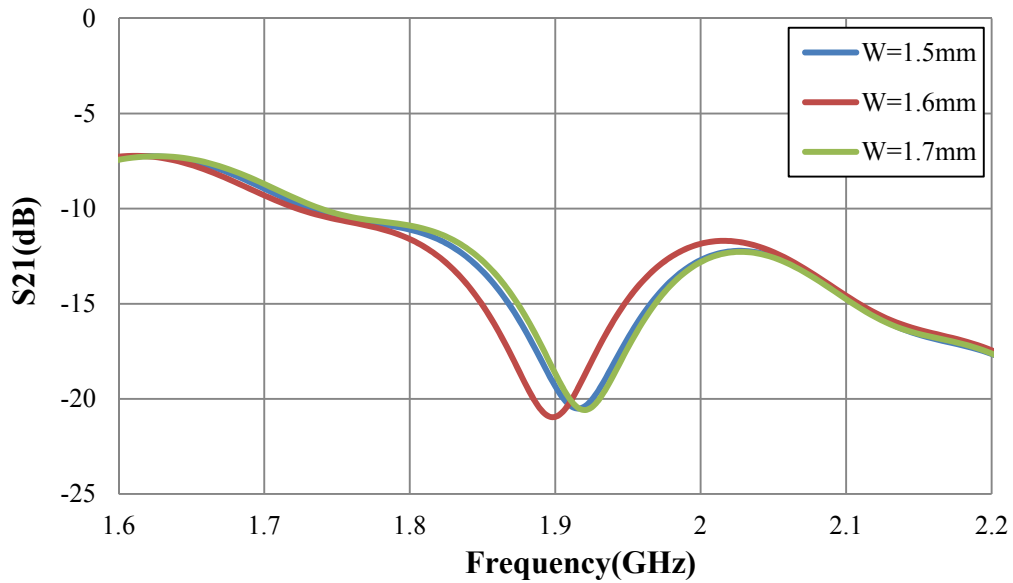
optimised geometry structure as shown in Figure 3.49(c) is: $L_1=6\text{mm}$, $L_2=14\text{mm}$, $L_3=4\text{mm}$ and $L_4=8\text{mm}$. The total length is 32mm , which is approximately a quarter of the guided wavelength. By optimising the geometry of the slit, the S-parameters results are shown in Figure 3.50(d). The mutual coupling was reduced from -7.6dB without the slit to -17.6dB with the slit, at 1.895GHz . This frequency is well within the operating frequency bands of the PIFAs. The optimized convoluted slit slightly affects the input reflection coefficient of the two PIFAs due to its close proximity, and the resonant frequencies of the antennas exhibit a slight shift. However, both antennas remain well matched at the frequency where the slit resonates (1.895GHz).



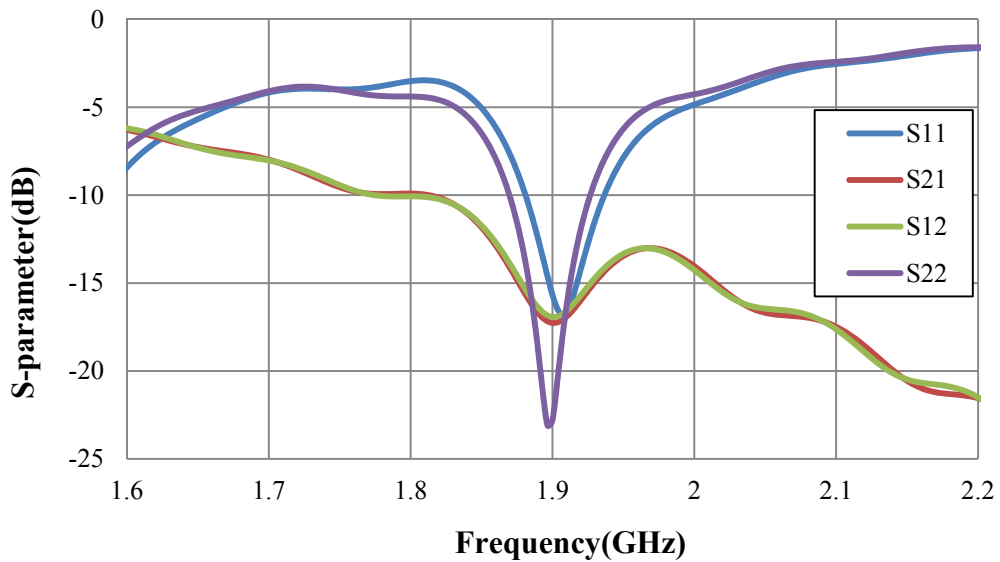
(a)



(b)



(c)



(d)

Figure 3.50 Simulated (using CST MWS) S-parameters of the two-element PIFA array with (a) no slits, (b) S21 with slit of different total length, (c) S21 with slit of different width , (d) optimised slit inserted on the common ground plane

After the parametric studies and optimisation of the slit, the current distribution is studied. The plot of current distribution on the surface of the ground plane is shown in Figure 3.51, at the resonant frequency of the slit (1.895GHz). The current appears at a maximum around the slit, which is due to its resonance and it traps most of the energy.

Less current is propagating across the slitted pattern from one antenna to the other, resulting in the reduction of mutual coupling between the two PIFAs.

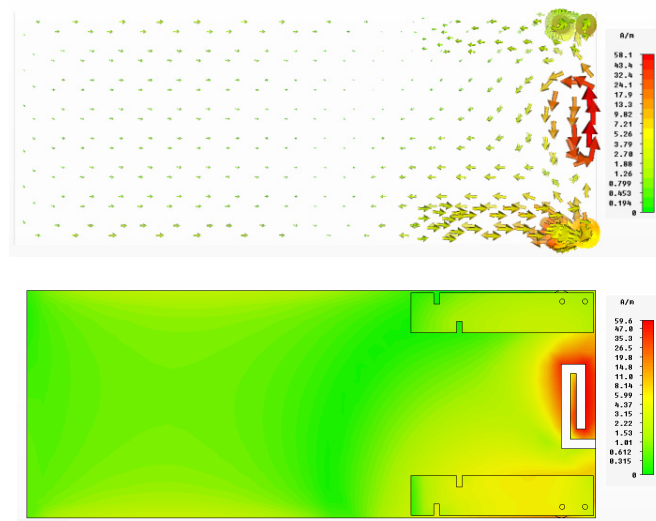


Figure 3.51 Current flow and distribution and current on ground plane

The correlation coefficient between the two antennas in the presence of the slit has also been calculated using equation (2.9) [19]. Both cases, namely the PIFA array with an optimised convoluted slit and without slit, are shown in Figure 3.52. In comparison to the original design of a dual-element PIFA array on a conventional ground plane, the correlation coefficient is significantly reduced around the resonant frequency of PIFAs, with a minimum value of less than 0.071, after the proposed convoluted slit is inserted in the ground plane.

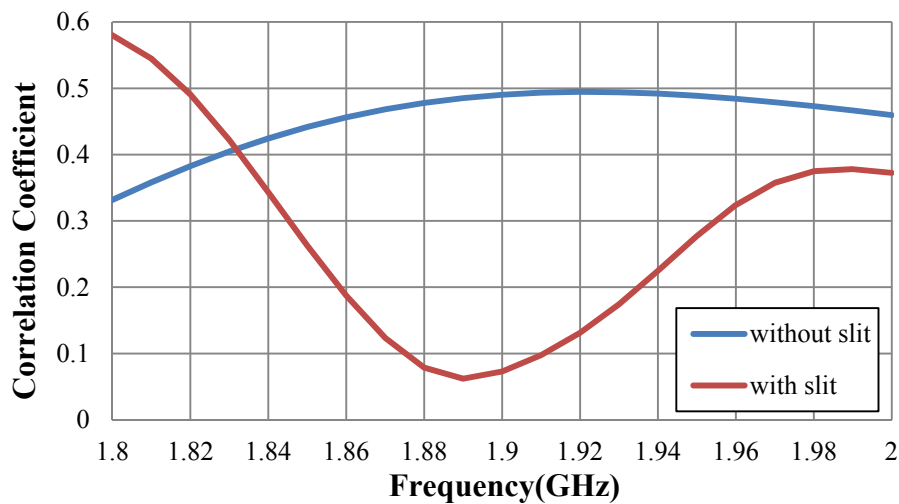


Figure 3.52 Correlation coefficient between two PIFAs on different ground planes

The radiation patterns of the proposed structure at the resonant frequency are presented in Figure 3.53. The radiation patterns in the presence of the proposed convoluted slit are only slightly different than for the array system without the slit. Moreover, the patterns produced by PIFA1 and PIFA2 are slightly different due to the asymmetrical shape and positioning of the slit with respect to the antennas. The losses introduced by the resonance of the slit have also been studied. The radiation efficiency of the original array structure is 98.37% and reduces to 92.05% in the presence of the slit. It is evident that although the radiation efficiency slightly reduces in the presence of the slits, the total efficiency calculated from equation (3.2) is higher, due to the reduced S21 and hence there is reduction of the power which is coupled from one PIFA to the other. At 1.9GHz the total efficiencies are approximately 86.4% and 88.2% with the slits and 68% without the slits.

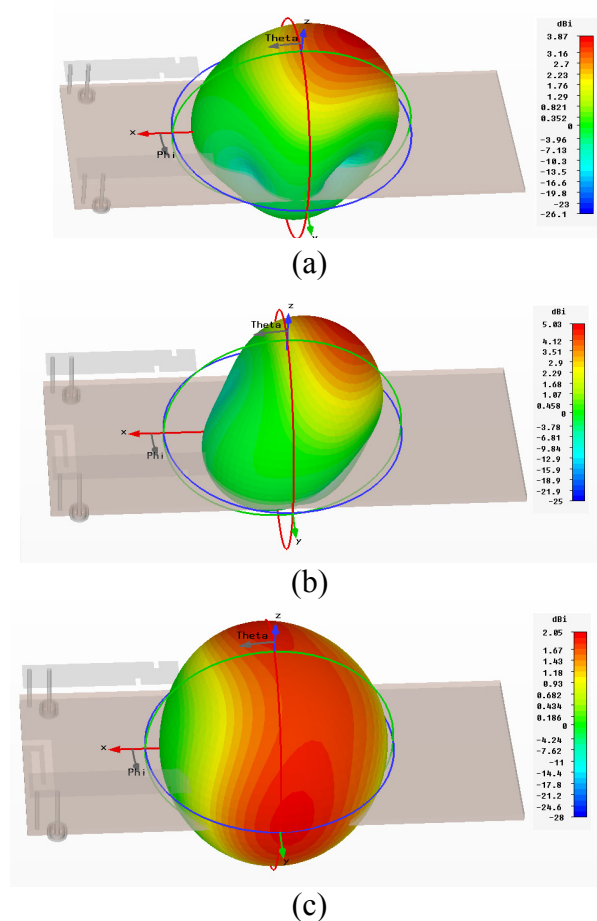


Figure 3.53 Simulated radiation patterns of a) the original array configuration when PIFA1 is excited and b) the array with the slits, when PIFA1 is excited, c) the array with the slits, when PIFA2 is excited

3.5.2 Fabrication and Measurement of Proposed Structures

Two prototypes of the proposed configuration (the original array and one with the convoluted slit) have been fabricated and measured in order to experimentally validate the proposed scheme, as shown in Figure 3.54. The measured S-parameters in the two cases are depicted in Figure 3.55.

In the original structure, the measured maximum mutual coupling (S_{21}) is -9dB. By employing the proposed optimised slit, the mutual coupling between the two antennas drops to -44dB at 1.925GHz instead of the simulation frequency 1.9GHz. The antenna resonances are also slightly shifted with respect to the simulations. The accuracy of the measurements is dependent on multiple factors, such as the cable connection, the bending of materials, and the construction technique of the prototype (in this case it was handmade). However, at the resonance of the slits (1.925 GHz) both antennas are matched. The mutual coupling drops below -40 dBs at 1.925GHz, and assumes values well below -15dBs over the PIFAs operating bandwidth. The measurement results validate the simulation predictions and the operation of the proposed optimised convoluted slit.

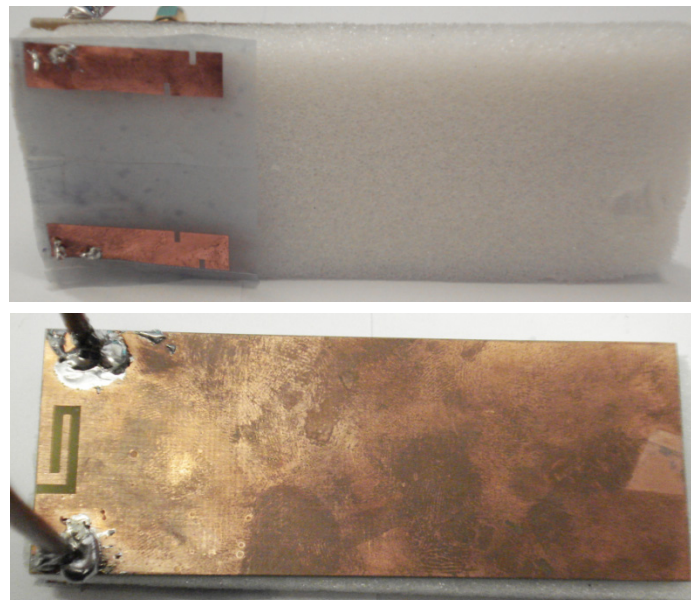
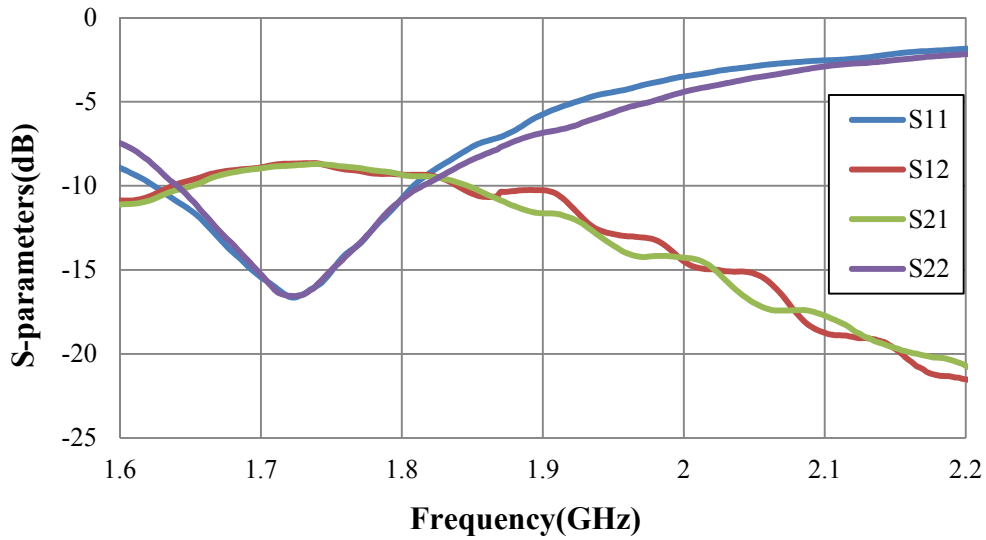
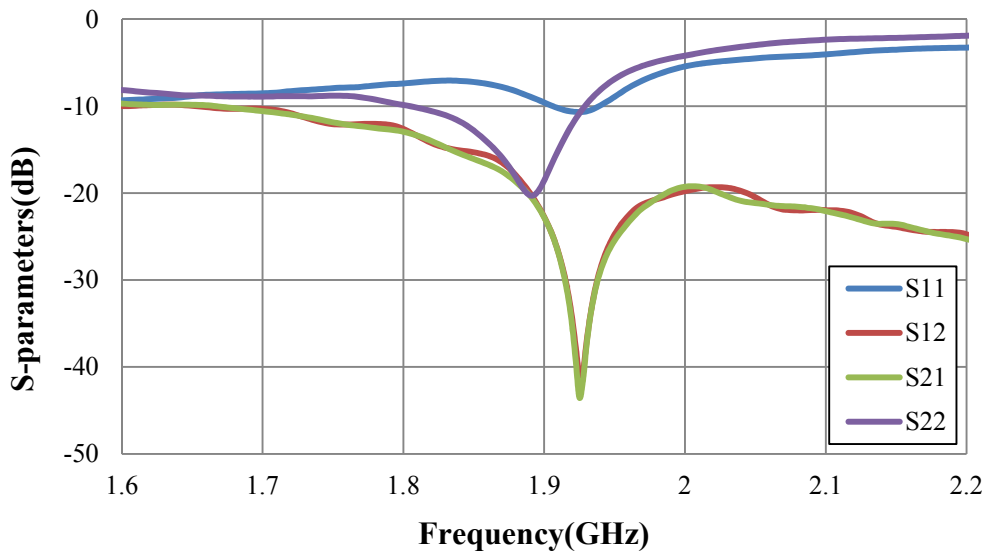


Figure 3.54 Prototype system using the proposed slitted ground plane



(a)



(b)

Figure 3.55 Measured S-parameters for the two-element PIFA array
(a) without slit (b) with optimised slit

3.5 Summary

A novel approach for reducing the electromagnetic coupling between two close spaced PIFAs, which are built in a ground plane for a compact handheld device, has been presented. The proposed technique is based on the insertion of two quarter-wavelength linear slits on the ground plane between the antennas. The slit length and

the distance between two slits have been optimised using full-wave simulations, resulting in a magnetic type resonance of the two slits. The fields and currents on the ground plane were studied, validating the nature of the slits resonance. A transmission zero was inserted in the coupling path of the two PIFAs, resulting in significant reduction of the mutual coupling to values well below -20 dB across the operating bandwidth of the antennas. Finally, the effect of the slits on the radiation performance of the antenna array was studied and presented.

In order to take up less space on the ground plane, novel miniaturized convoluted slits are presented. Although the proposed slits have a small footprint and are positioned close to the edges of the ground plane thereby occupying very little space, there is very little current flowing across the space between the two convoluted slits. A transmission minimum was obtained by virtue of the resonance of the slits resulting in significant reduction of the mutual coupling across the operating frequency of the antennas. The miniaturized convoluted slit structure etched on the ground plane is also employed to reduce coupling of the human body (head and hand) to the antennas while achieving low mutual coupling between antenna array elements when the mobile phone is being held by a user's hand.

The miniaturized convoluted slit is presented to reduce the mutual coupling between two closely packed PIFAs on a compact ground plane in handheld devices. The shape and width of the slit have been optimised. Although occupying very little space on the ground plane, the single convoluted slit traps most of the surface current excited from the PIFAs and reduces the mutual coupling significantly across the operating frequency of the antennas. Surface currents plots have been presented in order to establish the nature of the slit resonance. A fabricated prototype has been experimentally measured and the results confirmed the simulation predictions and the operation of the proposed slit.

References

- [1] S. Haridas, and J. K. Lee, "Quad-band pifa for mobile phones," Department of Electrical Engineering, Syracuse University, Fall 2004
- [2] K. Fujimoto and J. R. James, Eds., "Mobile Antenna Systems Handbook," Norwood, MA, USA: Artech House, 2nd Edition, 2001.
- [3] H. Morishita, Y. Kim, and K. Fujimoto, "Design concept of antennas for small mobile terminals and the future perspective," *IEEE Antennas and Propagation Magazine*, vol. 44, no. 5, pp. 30-43, October 2002.
- [4] Z. Ying, "Some important antenna innovations in the mobile terminal industry in the last decade," *Antenna 06 Nordic antenna symposium*, Sweden, June 2006.
- [5] S. SEKINE, H. SHOKI, and H. MORISHITA, "Antennas for wireless terminals," *Institute of Electronics, Information and Communication Engineers (IEICE) Tran.*, vol. E86-B, no. 3, pp. 1005-1015, March 2003.
- [6] Z. Ying, "Multi-band non-uniform helical antennas," Telefonaktiebolaget L M Ericsson, US006122102 and WO-9815028, October 1996.
- [7] Z. Wu, "Application studies of dielectric resonator antennas," *IEEE International Symposium on Microwave, Antenna, Propagation and EMC Technologies for Wireless Communications*, vol. 2, August 2005, pp. 1435-1438.
- [8] K.-L. Wong, Ed., "Planar Antennas for Wireless Communications," Hoboken, New Jersey: John Wiley & Sons, Inc., 2003.
- [9] K. Hirasawa and M. Haneishi, Eds., "Analysis, Design, and Measurement of Small and Low-Profile Antennas". Artech House Antenna Library, 1992.
- [10] W. L. Stutzman and G. A. Thiele, Eds., "Antenna Theory and Design". A John Wiley & Sons, Inc., Publication. Wiley, 2nd Edition, 2005. pp. 433-494.

- [11] C.-Y. Chiu, C.-H Cheng, R.D. Murch, and C. R. Rowell “Reduction of mutual coupling between closely packed antenna elements”, *IEEE Trans. Antennas and Propag.*, 2007, 55, (6), pp. 1732–1738
- [12] I. Kim, C. W. Jung, Y. J. Kim, and Y. E. Kim “Low-profile wideband MIMO antenna with suppressing mutual coupling between two antennas,” *Microw. Opt. Technol. Lett.*, 2008, 50, (5), pp. 1336–1339.
- [13] R.G. Vaughan and J.B. Andersen, “Antenna diversity in mobile communications,” *IEEE Trans. Vehicular Technology*, vol. 36, pp. 147-172, Nov 1987.
- [14] O. Litschke, M. Geissler, M. Martinez, D. Heberling, “Adaption of the Wheeler-Cap method for measuring the efficiency of mobile handset antennas, ” *Itg Fachbericht (2003) Publisher: VDE; 1999, Pages: 387–390.*
- [15] M. Okoniewski, and M. A. Stuchly, “A study of the handset antenna and human body interaction,” *IEEE Trans. Microwave Theory Tech.*, 44(10), 1855–1864. 1996.
- [16] M. A. Jensen, and Y. Rahmat-Samii, “EM interaction of handset antennas and a human in personal communications,” *Proc. IEEE*, vol. 83, 7–17, 1995.
- [17] H. R. Chuang, “Human operator coupling effects on radiation characteristics of a portable communication dipole antenna,” *IEEE Trans. Antennas Propagat.*, vol. 42, pp. 556-560, 1994.
- [18] G. Goussetis, A. P. Feresidis, G. K. Palikaras, M. Kitra, and J. C. Vardaxoglou “Miniaturization of electromagnetic band gap structures for mobile applications,” *RADIO SCIENCE*, VOL. 40, 2005.
- [19] S. Blanch, J. Romeu and I. Corbella, “Exact representation of antenna system diversity performance from input parameter description,” *Electronics letters*, 2003 Vol. 39 No. 9.

Chapter 4

Slit-Patch EBG Structures on compact wireless terminals

4.1 Introduction

The design of miniaturized convoluted slit structure, built on a compact ground plane for typical handheld devices, has been presented in Chapter three. The convoluted slit structures have succeeded in producing a significant reduction of the mutual coupling across the operating frequency band of the PIFAs. Although the proposed convoluted slits are much smaller than the linear slits, their dimensions still need to be further miniaturized to economise the valuable area on PCB in practical applications such as space-limited wireless terminals [1]. Recently, a novel miniaturized Complementary Metallodielectric Electromagnetic Band Gap (CMEBG) structure was presented to suppress surface wave propagation and to offer a small structural footprint thereby occupying very little space on a compact ground plane [2]. In this chapter, double

layer EBG structures, consisting of conducting elements and apertures placed on either side of a very thin supporting dielectric substrate, are proposed to reduce the mutual coupling, produce maximum miniaturization of the antenna module and widen the bandwidth for the band gap region [3-5].

In comparison to the conventional single layer aperture structures presented in Chapter three, the significant difference is that the new coupled EBG structures place one layer of the conducting patches in close proximity to the existing aperture layer etched on the ground plane [6, 7, 8]. Due to the high coupling between the elements, the effective electrical size of the complementary structure increases. As a result, the band gap shifts towards lower frequencies [3, 9]. The linear slit structures based on two coupled quarter-wavelength slits has been presented to reduce the mutual coupling between two PIFAs on a typical handheld device ground plane in Chapter three. However, due to their length, they occupied a relatively large area of the ground plane between the two antennas, which is impractical in many realistic designs of handheld devices. Therefore, the novel double-layer slit-patch EBG structures are proposed for producing maximum miniaturization of the linear slits on ground plane.

In this chapter, the concept of Coupled Electromagnetic Band Gap is introduced. A 50Ω microstrip line is printed on a thin polyester dielectric sheet and placed at the top of a rectangular grounded substrate. Some slits are etched on ground plane. Another thin dielectric sheet underneath the ground plane supports the conducting patches. The transmission response of the microstrip line is obtained from 3D electromagnetic simulation software. Subsequently, after the slit-patch structures are optimized, a dual-element CPW-fed printed monopole antenna array operating at 2.44GHz is studied to further evaluate the electromagnetic properties of the proposed double-layer EBG structure. Moreover, the double-layer structure reduce mutual coupling between two UWB planar monopoles array and significantly reduce the size of antenna array. The prototypes of different structures were fabricated and measured. The good

agreement between simulations and measurements demonstrates that the application of the proposed slit-patch EBG structures significantly reduces the mutual coupling between closely spaced antennas. Based on this, the separation between MIMO antenna elements is dramatically reduced to miniaturise the dimension of the whole antenna module.

4.2 Theory and Geometry of Double Layer EBG

As discussed in Chapter two and Chapter three, the mutual coupling between the two antennas, which degrades the performance of the antenna array, is mainly caused by the current flow on the ground plane. Although the conventional EBG structures are able to suppress surface current, they are unsuitable for the design of compact wireless terminal devices because of their relative large volume [10, 11]. The proposed novel double-layer slit-patch EBG structure is proposed to reduce the size of the structure on ground plane. It consists of a two-layer structure with conducting patches and aperture slits placed on either side of a very thin dielectric layer, as shown in Figure 4.1(a). The aperture is rotated 90° with respect to the conducting patch shown in Figure 4.1(b). All the elements are polarized with the electric field [6]. Due to the strong electromagnetic coupling between the two layers elements, the effective electrical length of the double layer structure increases, resulting in the resonant frequency of the slit-patch structure decreasing [7].

The proposed double-layer structure can be described as a parallel circuit consisting of capacitive and inductive loads to better understand its mechanism shown in Figure 4.1(c). The parallel LC circuit can be used to be described as a unit cell (single

resonator) of the structure and will produce a stop-band effect in the resonant frequency range. The resonant frequency is derived as [4]:

$$f = \frac{\omega}{2\pi} = \frac{1}{2\pi\sqrt{LC}} \quad (4.1)$$

where L is the inductance and C is the capacitance predominantly formed by two closely spaced parallel conducting plates (conducting patches and ground plane). The estimate of capacitance is made according to [1]:

$$C = \epsilon_r \epsilon_0 \frac{A}{d} \quad (4.2)$$

where A is the overlap area of the double layer slit-patch structure, ϵ_r is the relative static permittivity, ϵ_0 is the free space permittivity and d is the separation between the two parallel plates (conducting patch and ground plane). In order to further reduce the resonant frequency of the slit-patch structure, the capacitance of the slit-patch structure is increased through using two methods: reducing the separation between the two layers, or increasing the overlapping area. The separation (d) between the two layers retains a very small value (0.055mm) for all geometries in this thesis. Also, when the width of the conductor patches increases, the overlap area A will increase, and the capacitance will assume higher values. As a result, the resonance is expected to move towards lower frequency. So the band gap could be shifted by enlarging the width of the conductor patches. The bandwidth can be calculated from the formula given below:

$$BW = \frac{1}{Q} = \frac{\sqrt{\frac{L}{C}}}{\sqrt{\frac{\mu_0}{\epsilon_0}}} \quad (4.3)$$

When the overlapping area between the conducting patches and the ground plane is increased, the bandwidth is decreased because the capacitance increases. Therefore, the stop-band bandwidth is expected to decrease by increasing the overlap area. The equivalent circuit description gives a good qualitative insight but does not model the response of the proposed structures accurately. This is largely due to the compact size

of the ground plane and the complicated geometries and strong coupling of the slit-patch structures.

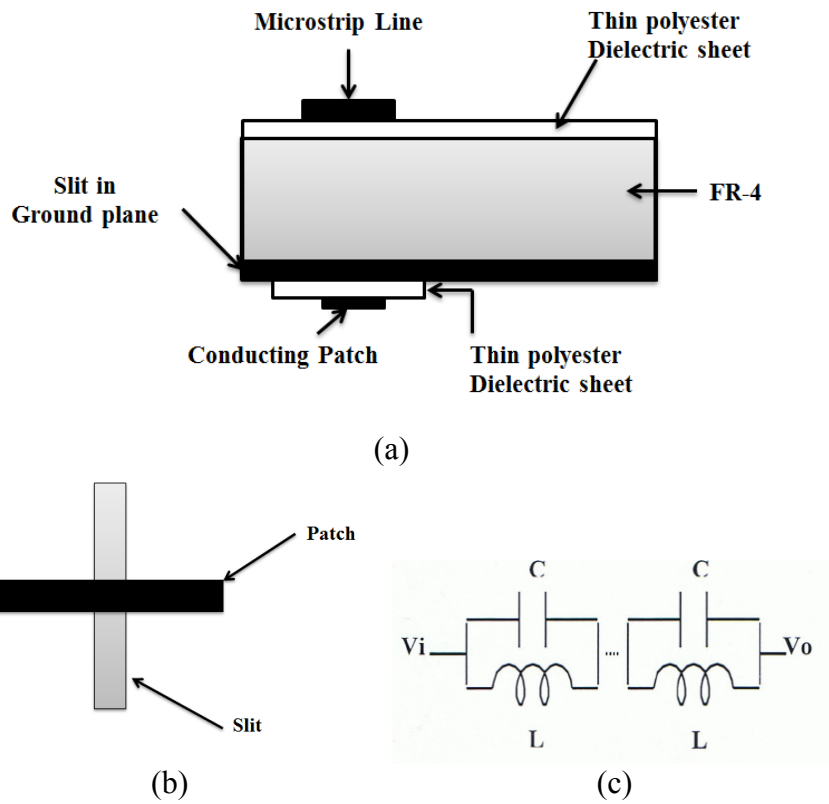


Figure 4.1(a) The slit-patch EBG structure, (b) Complementary dipoles schematic and (c) Equivalent circuit of slit-patch EBG structure

4.3 Microstrip Line Excitation

The configuration of the double layer slit-patch EBG structure is depicted in Figure 4.1. The resonant frequency of the double layer slit-patch structures is very sensitive because of the strong coupling in the small separation region. In this section, we initially use a microstrip line excitation as an efficient way, compared to any complex antenna array, for analysing the stop-band/band gap properties of the proposed slit-patch structure and hence optimise their geometries.

The microstrip line is printed on a $100 \times 40 \text{ mm}^2$, 1.55 mm thick, FR-4 dielectric substrate ($\epsilon_r=4.5$) backed by a copper ground plane. One linear shaped slit is inserted in the common ground plane. The dimensions of the slit (15mm length and 1.6mm width) are optimised to resonate around 3.3GHz. The configuration of this structure is depicted in Figure 4.2.

In order to investigate the specifications of the proposed double-layer slit-patch structure, a series of studies are presented. The first parametric study is to validate the effect of the proposed structure. The simulated transmission response (S_{21}) is shown in Figure 4.3. The cut-off frequency (-10dB) emerges at 2.85GHz and extends up to 4.55GHz when a single linear slit is etched on the ground plane. After one thin conducting patch (4mm length and 0.4mm width) is printed on a very thin substrate ($\epsilon_r=3$) of 0.055 mm which positioned in the middle of the linear slit and close to the ground plane, the band-gap of S_{21} shifts towards to lower frequency. And the absolute bandwidth (-10dB) of S_{21} decreases from 1.7GHz to 0.8GHz. These simulated results are perfectly in agreement with the trends predicated on the circuits analysis presented in last section.

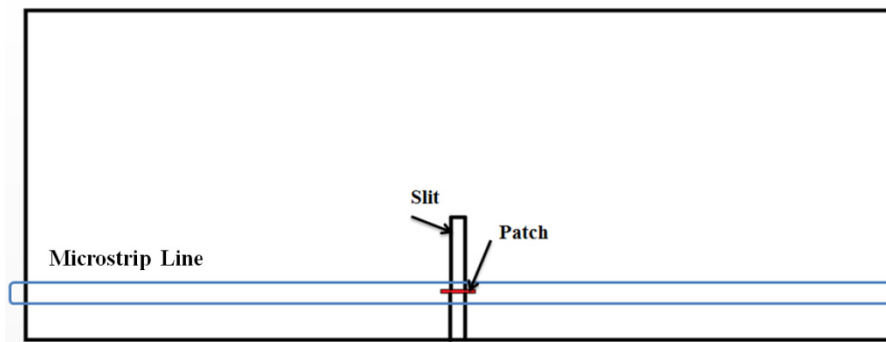


Figure 4.2 Geometry of one slit-patch EBG structure excited by microstrip line

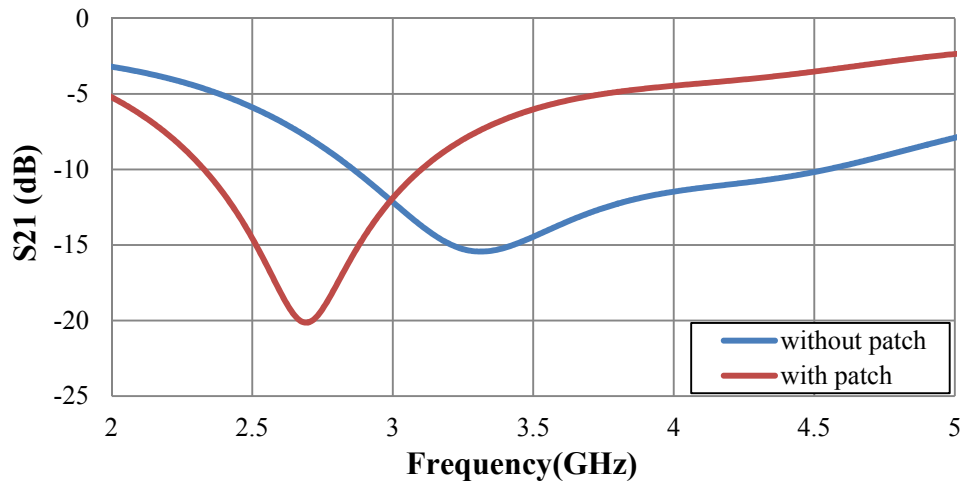


Figure 4.3 S21 of slit-patch EBG structure with and without the conducting patch

As mentioned above, the effective electrical size of the slit-patch EBG structure increases as the overlapping area increases. It causes the band gap to shift towards a lower frequency. On the basis of keeping the resonant frequency of the proposed structure around the desired operating frequency of the antenna, the dimension of the slit etched on the ground plane could be miniaturised by increasing the area of the conducting patch. It will take up less valuable area on the PCB and avoid affecting the other electronic components installed on ground plane. So, the second parametric study is the alteration of the conducting patch width for enlarging the overlapping area. It will directly increase the capacitance of the slit-patch EBG structure. The reduction of band-gap frequency and bandwidth ensues. The simulated transmission response (S21) of the proposed structure accompanied by the alteration of the conducting patch width was illustrated Figure 4.4.

The length of the conducting patch is defined as 4mm. The cut-off frequency of the band-gap is defined at -10dB in this thesis. The cut-off frequency emerges from 2.05GHz to 2.68GHz when the width of the conducting patch is 0.5mm. It produces an absolute bandwidth of 0.63GHz. When the width increase to 1mm, the band gap shifts towards a lower frequency and emerges from 1.73 GHz to 2.17GHz. When the width of the patch is 1.5mm, the band gap emerges from 1.53GHz to 1.87GHz. Finally,

when the width of the patch increases to 2mm, the absolute bandwidth is just 0.29GHz from 1.42GHz to 1.71GHz. The presented results are in agreement with the conclusion from the theoretical analysis.

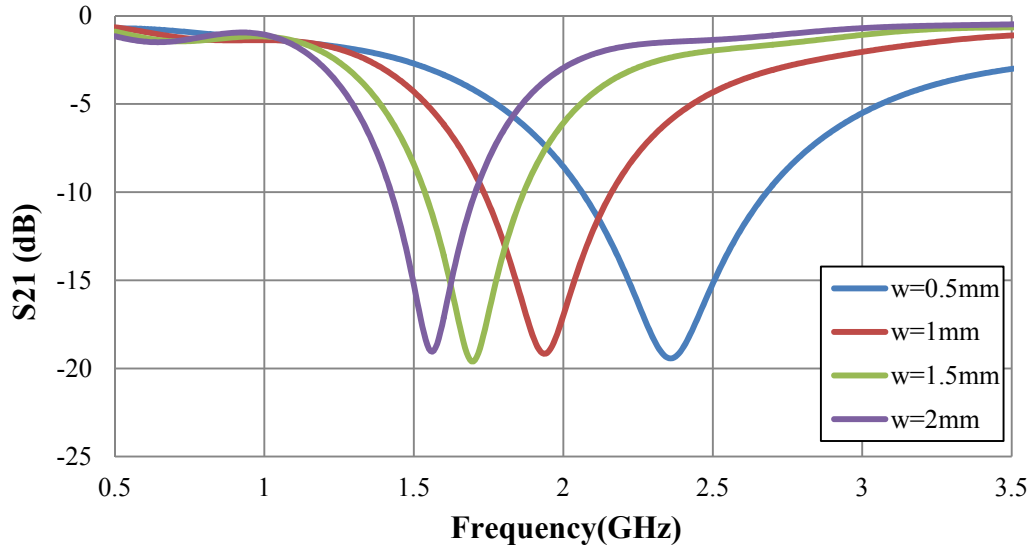


Figure 4.4 S21 of slit-patch EBG structure with different width of conducting patch

Although the band gap shifts towards a lower frequency with increasing the overlapping area of the slit-patch structure, the absolute bandwidth also decreases too. In order to overcome this limitation, multiple double-layer slit-patch EBG structures are proposed to obtain the desirable bandwidth from the relatively small structures, as shown in Figure 4.5. Two or three identical proposed slit-patch structures are placed on the ground plane. The periodicity of the resulting EBG structure D is 5mm, and the geometry of each unit cell is the same as before.

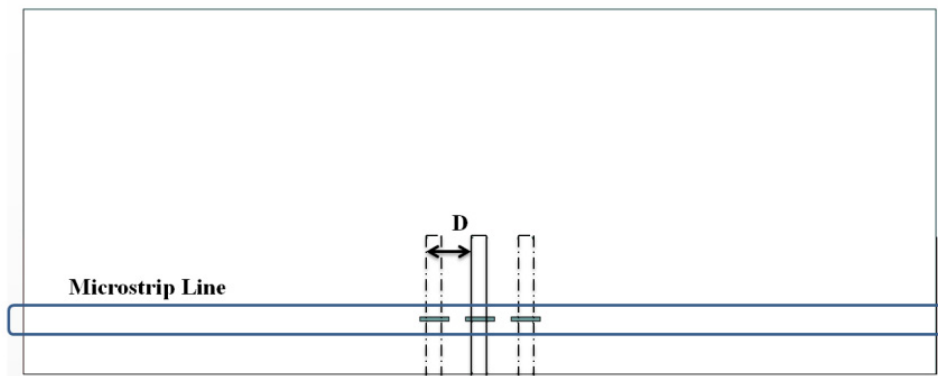


Figure 4.5 Multiple double-layer slit-patch structures with periodicity ($D=5\text{mm}$)

Figure 4.6 illustrates a comparison of simulated data (S21) for one, two and three slit-patch structures respectively. When the number of the slit-patch EBG structures increases, the lower cut-off frequency of the band gap slightly decreased, and the upper band gap extended to a higher frequency as the number of slit-patch structures increased. It is evident that the absolute bandwidth increases considerably with increasing numbers of slit-patch unit cells. The bandwidth (-10dB) of three slit-patch structures is about three times wider compared to the one slit-patch unit cell. These simulated results are encouraging since the slit-patch EBG structures are able to support an expected broadband with an increase their number.

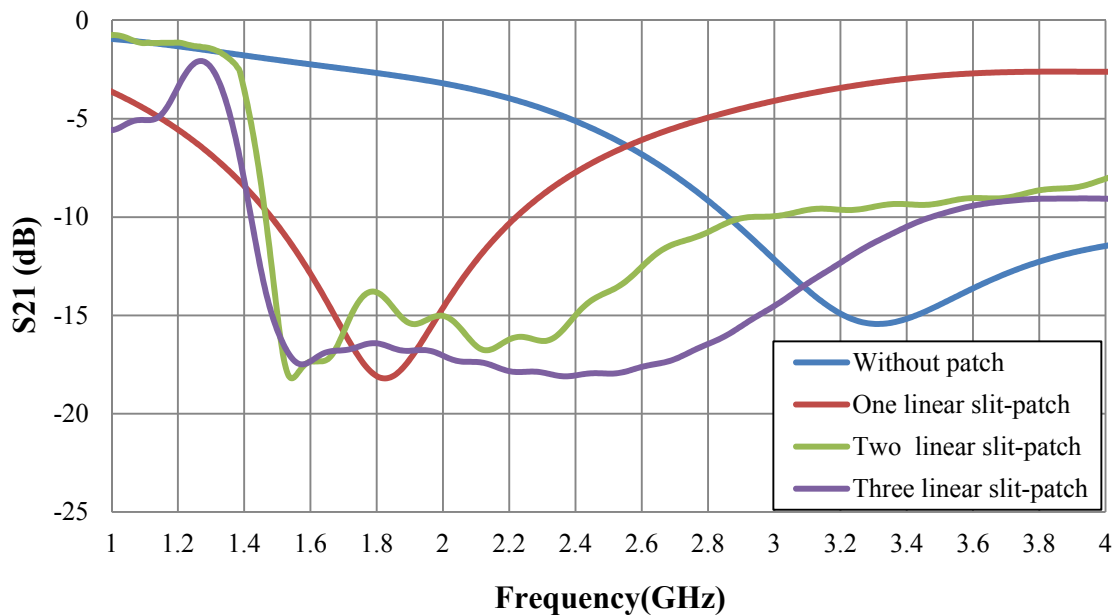


Figure 4.6 S21 of multiple double-layer slit-patch structures

4.4 Printed CPW Monopoles with Slit-Patch Structure

In the previous section, the proposed slit-patch EBG structures have been presented to shift the band gap towards low frequency with increasing the width of the conducting patch. Multiple identical slit-patch EBG structures were employed to extend the bandwidth of the transmission response. In order to illustrate the versatility

of the double-layer slit-patch EBG structure, this structure is employed for the reduction of mutual coupling of modern, compact and widely used antenna configurations.

Printed CPW (coplanar waveguide) fed monopoles have been widely used for many mobile communication standards such as GSM (900 MHz), DCS (1800 or 1900MHz), UMTS, etc [12, 13]. In this section, the proposed slit-patch EBG structures are implemented with a dual-element printed CPW-fed monopole array operating at 2.44GHz. In order to reduce the size of the printed CPW monopole and obtain broader bandwidth, a U-shape slot is etched on the radiating element of the proposed antenna as shown in Figure 4.7. The radiating element is fed by a 50 Ω coplanar waveguide line of 1mm width. Both of them are printed on a 60x50mm², 1.5 mm thick, FR-4 dielectric substrate ($\epsilon_r=4.5$).

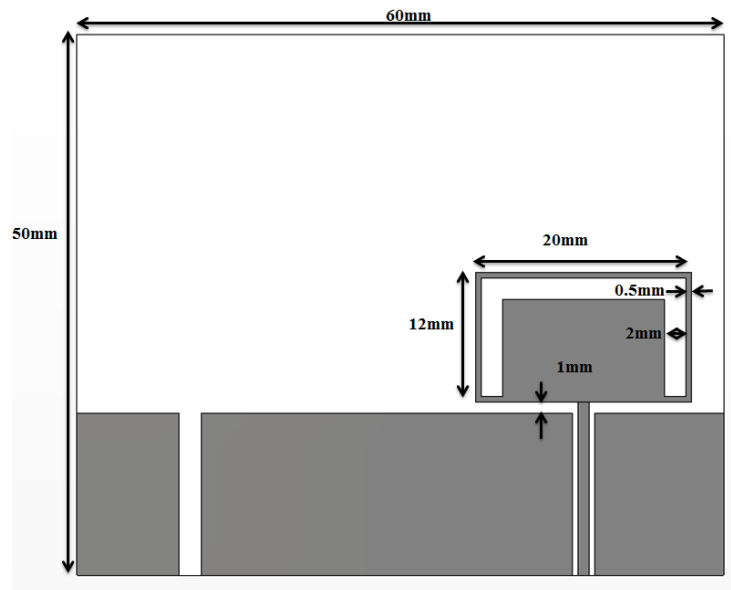


Figure 4.7 Geometry of one U-shape slot printed monopole

After the simulations, the dimensions of the printed monopole are optimized as 20 mm length and 12mm width, thus making the antenna operate within the desirable frequency range. The width of the U-shaped arm is 2mm. The gap between the radiating element and the ground plane remains constant at 1mm for all geometries.

The simulated S11 of the proposed printed monopole is shown in Figure 4.8. The resonance of the printed monopole is at 2.44GHz. The simulated bandwidth (-10dB) is 140MHz from 2.36GHz to 2.5GHz. And, two identical printed CPW-fed monopoles will be implemented on the ground plane to form part of a MIMO system.

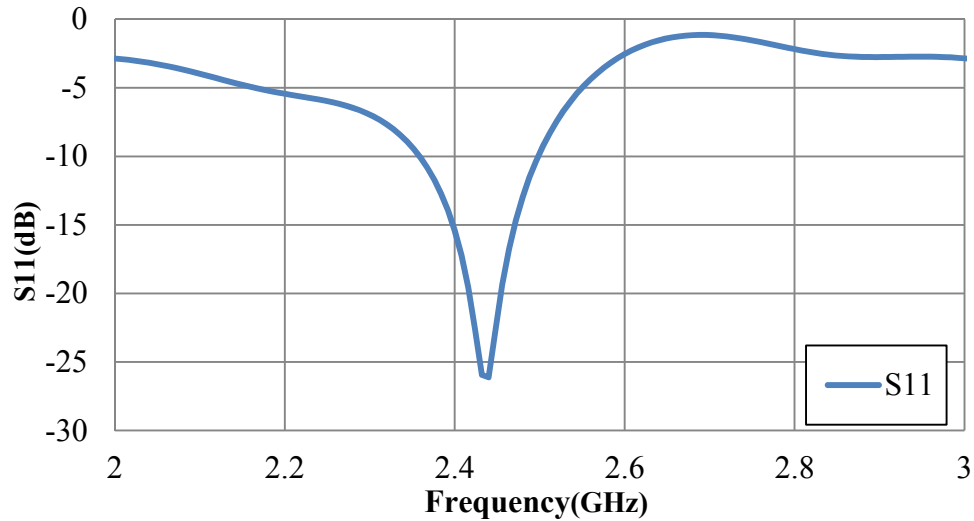


Figure 4.8 Simulated S11 of proposed printed monopole

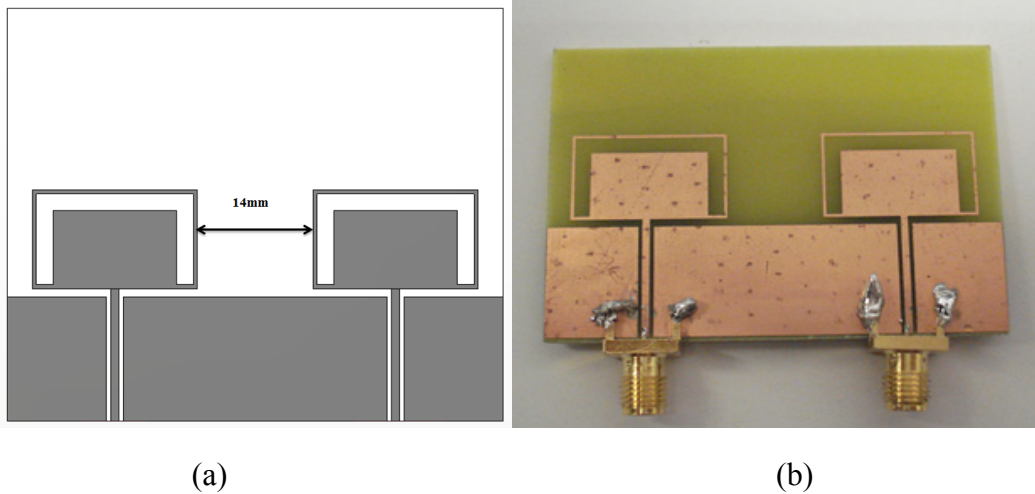


Figure 4.9 (a) The configuration and (b) Experimental model of the dual element printed monopole antenna array

Based on the configuration and dimension of the single antenna element, a dual-element printed monopole array was simulated and fabricated. The antenna array is placed on a substrate with size of $60 \times 50 \text{mm}^2$, as shown in Figure 4.9. The two antennas are placed only 14mm (0.11λ , $\lambda=127\text{mm}$) apart on the substrate. The

dimensions and other relevant positions of the printed monopoles are the same as the single antenna shown in Figure 4.7. A prototype of the simulated dual-elements antenna system has been fabricated and measured in the laboratory at Loughborough University.

The simulated and measured S-parameters of the dual-element antenna array are shown in Figure 4.10. It is noted that the reflection coefficients (S11 and S22) of two printed monopoles are very similar due to the two antennas being completely symmetrical on the substrate. The resonance frequencies of S11 and S22 have a slight shifting (less than 20MHz) between measured and simulated results. The reason for the difference between simulations and measurements will be explained below. The mutual coupling (S21) between printed monopole array elements is about -14dB in both simulation and measurement at the resonant frequency of the antenna, due to the small separation between the two monopoles.

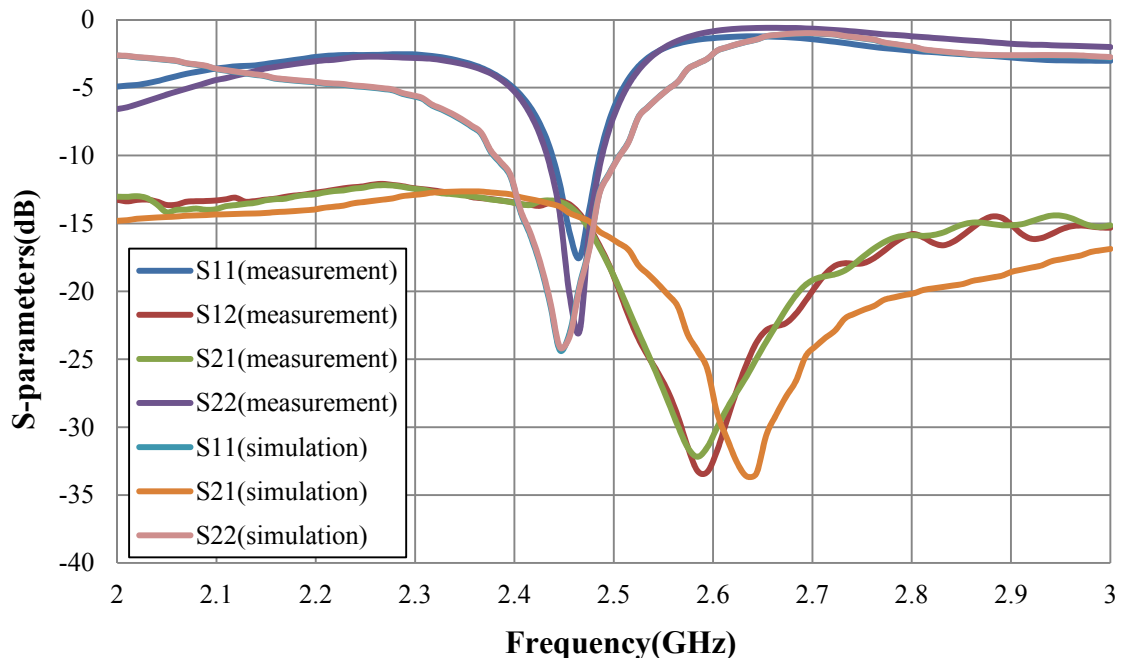


Figure 4.10 Simulated and measured S-parameters of the dual-elements antenna array with a conventional ground plane

The current flow and distribution on the ground plane at the resonant frequency 2.44GHz was obtained from the simulation software, as shown in Figure 4.11. It is evident that strong currents propagate along the top edge of the ground plane between the two monopoles. This is the main factor that produces high mutual coupling between closely spaced printed monopoles.

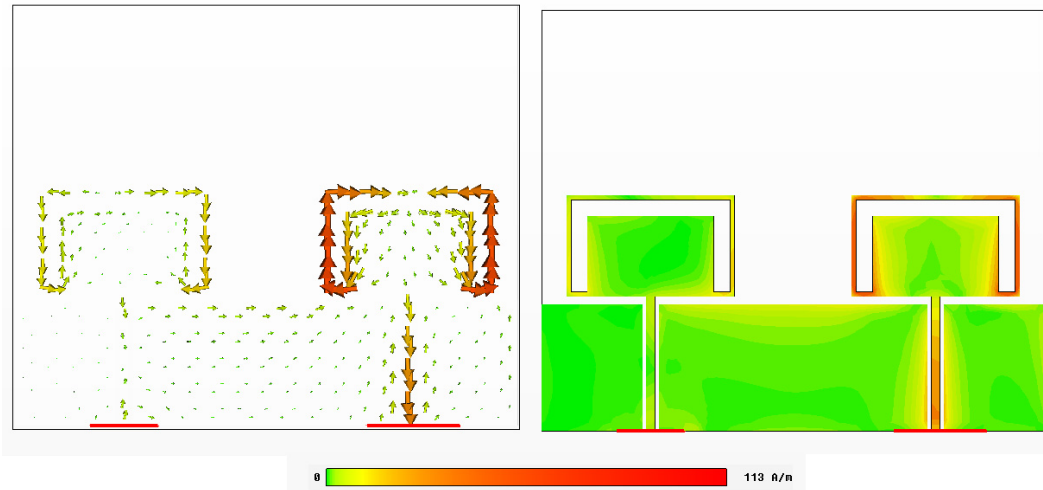


Figure 4.11 Current flow and distribution on the ground plane induced at 2.44GHz

The small, low-profile printed monopoles have been widely studied and implemented for cellular communication and PCS such as tablet PC, laptop, etc. When the manufacturers build one MIMO antenna array into compact portable devices, they want the antennas intergraded into a compact module while having low mutual coupling and correlation between the antenna elements for obtaining good diversity performance and high channel capacity. Due to the small separation between antenna elements, high mutual coupling will seriously degrade the performance of antenna system. In order to produce a significant reduction of the mutual coupling between antennas and miniaturise the antenna array, the proposed slit-patch EBG structure will be mounted on the ground plane between two printed CWP-fed monopoles. The dimensions of the antenna elements are exactly the same as before. The configuration of the antenna array with one slit-patch EBG structure and the

corresponding experimental model is presented in Figure 4.12. The slit-patch structure consists of conducting patches and linear slits placed on either side of a very thin ($55\mu\text{m}$) dielectric layer. The optimized dimensions of the linear slit etched on the ground plane are 9.65mm length and 1mm width. The conducting patch has dimensions 6mm length and 3mm width. A prototype based on the simulated dual-element antenna array with one slit-patch EBG structure has been fabricated.

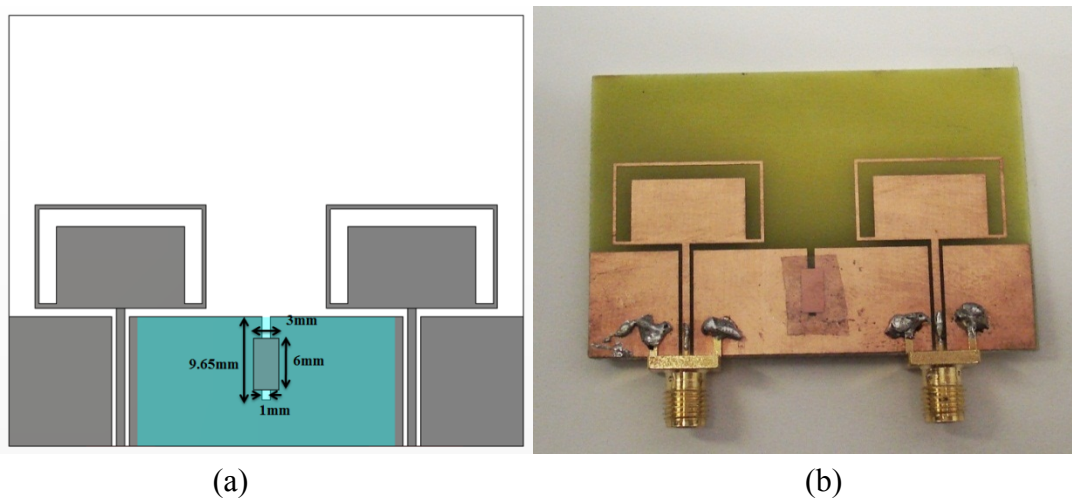


Figure 4.12 (a) The configuration and (b) Experiment model of the dual element antenna array with one slit-patch EBG structure

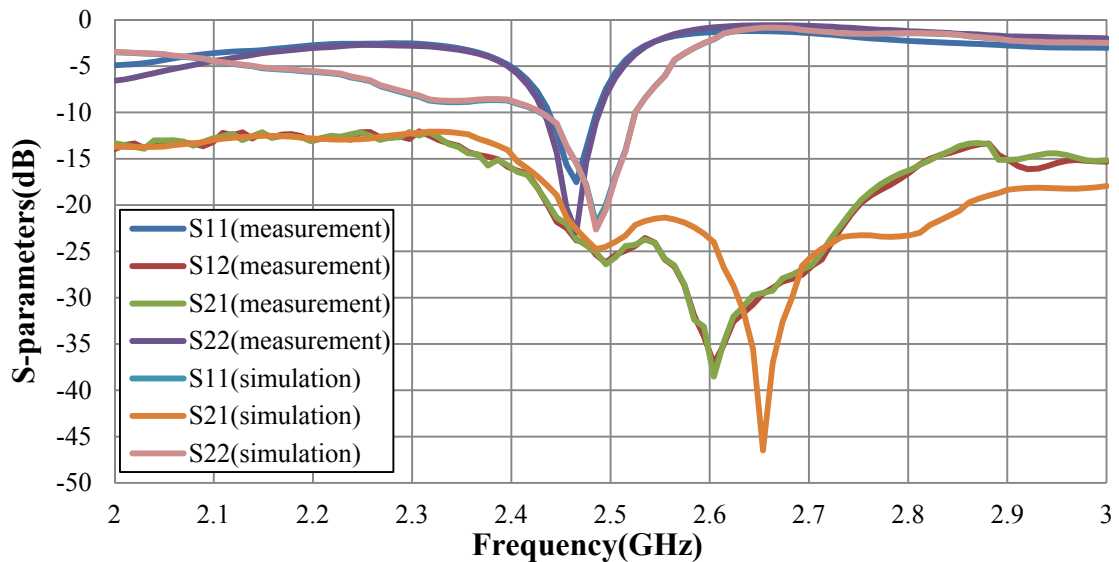


Figure 4.13 Simulated and measured S-parameters of the dual-element antenna array with one slit-patch EBG structure

The simulated and measured S-parameters are depicted in Figure 4.13. The measured resonant frequencies of antennas (S11 and S22) are at 2.465GHz, which are slightly lower (20MHz) than the simulated results. These minor discrepancies are due to the fabrication imperfections in the manual soldering of the feeding ports. The measured bandwidth (-10dB) of S11 and S22 are less than the simulation results. After one slit-patch EBG structure is implemented between two printed monopoles, a minimum is obtained in the mutual coupling (S21) between the two antenna elements, at exactly 2.485GHz corresponding to the resonance of the proposed slit-patch structure. The modified slit-patch structure produces isolation better than -24dB in both simulation and measurement. The reason for achieving the low mutual coupling will be investigated in the following text by inspecting the surface currents.

The simulated current flow and distribution at the resonant frequency is presented. Figure 4.14 depicts the close proximity slit-patch EBG structure effectively traps surface current around the end of slit-patch structure. The proposed slit-patch EBG structure improves the isolation between antennas and results in the sharp minimum in the S21 response. Furthermore, due to the simple geometry and the small footprint, this slit-patch EBG structure is advantageous for use in compact devices with a large number of electronic components installed on the ground plane.

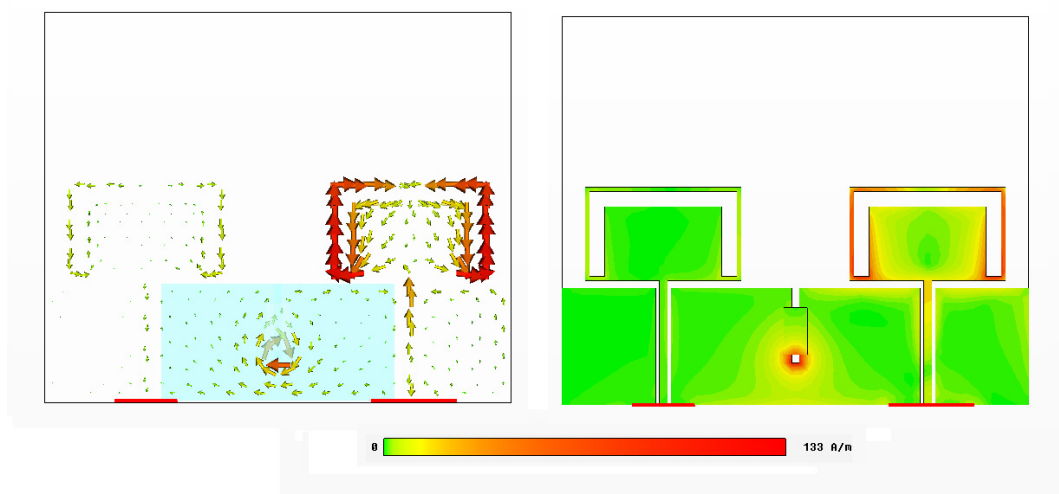
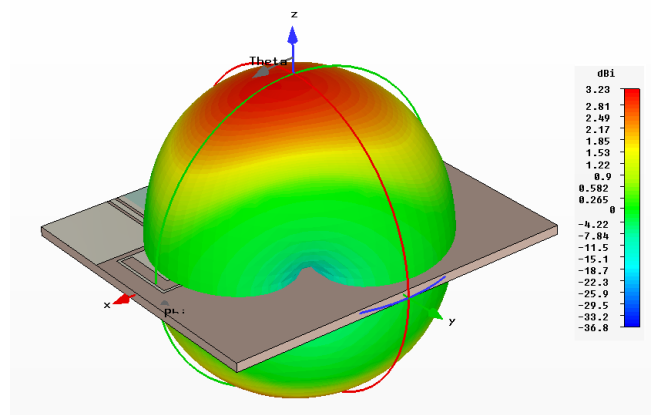
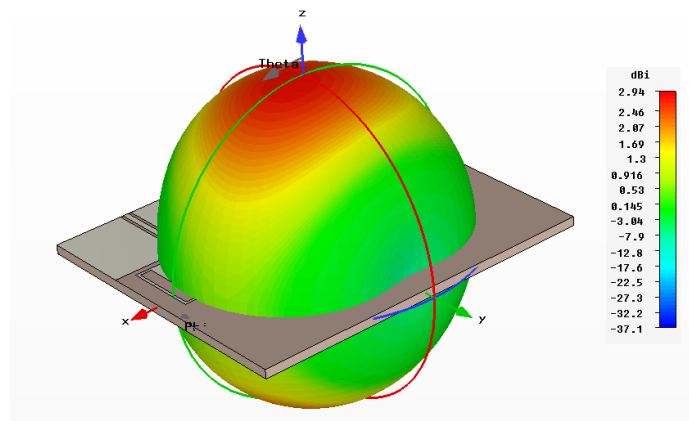


Figure 4.14 Current flow and distribution on the ground plane with one slit-patch EBG structure

The radiation patterns of the antenna system at the resonant frequency were obtained from the simulation software. The radiation patterns in the presence of the slit-patch structure (Figure 4.15(b)) have been found to be only slightly different to the antenna system with a conventional ground plane (Figure 4.15(a)). The radiation pattern in the presence of the slit-patch structure is slightly more omni-directional (directivity of 2.94dBi compared to 3.23dBi). The total efficiency of the original array structure at 2.45GHz is about 65.4% and increases to 72.6% in the presence of the slit-patch structure.



(a)



(b)

Figure 4.15 Simulated radiation patterns of (a) the original array configuration when printed monopole1 (the left element) is excited at 2.45GHz and (b) the antenna array in the presence of one slit-patch structure, when the same element is excited

As presented in last section, by employing multiple double-layer slit-patch EBG structures, the bandwidth of S21 increases considerably as the number of slit-patch unit cells increase. Here, two identical proposed EBG structures are mounted on the ground plane. The separation between the two slits is 5mm. The distance between the two patch edges is 2mm. The other dimensions of the printed monopoles and slit-patch EBG structure are exactly the same as before. The configuration and experimental prototype of the proposed antenna system are shown in Figure 4.16

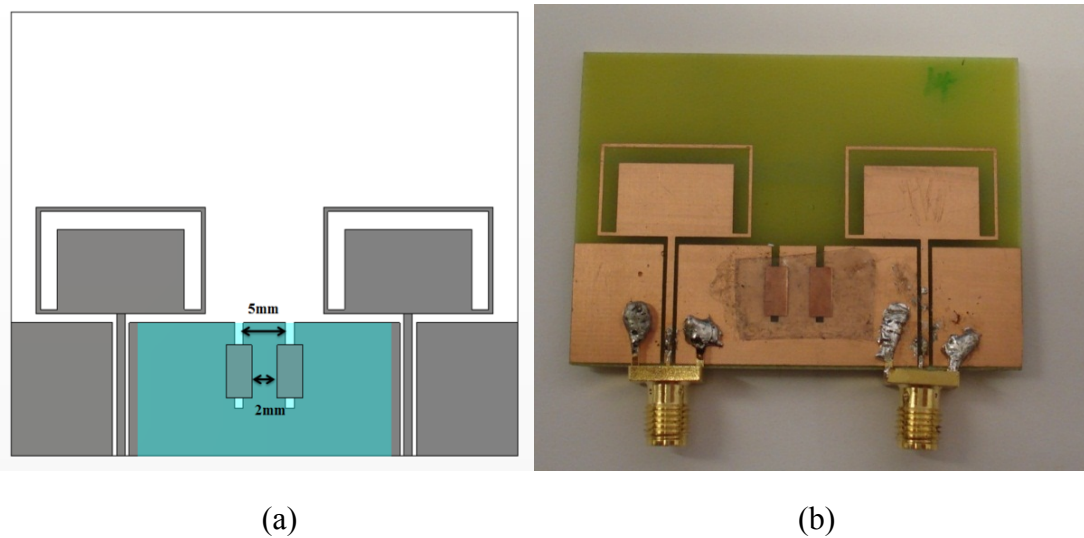


Figure 4.16 (a) The configuration and (b) Experimental model of the dual element antenna array with the two slit-patch EBG structure

The simulated and measured S-parameters of the two antenna array with two slit-patch EBG structures are shown in Figure 4.17. As the entire antenna system is fully symmetric on the ground plane, the simulated antenna characteristics (S11 and S22) are basically same. The measured return loss of Antenna 1 is slightly different from Antenna 2. These minor discrepancies are due to fabrication imperfections in the manual soldering of the feeding ports. Nevertheless, at the resonance of the slit-patch (2.485GHz) both antennas are well matched ($S_{11} < -15$ dB and $S_{22} < -15$ dB) and the mutual coupling drops to -30dB. The measured S21 between the antennas in the presence of two slit-patch structures is significantly reduced in comparison to the

initial structure. The bandwidth of antenna 1 and 2 (S11, S22) in both simulation and measurement are much better than the antenna array with one slit-patch EBG structure after employing one additional double-layer slit-patch unit cell on the ground plane.

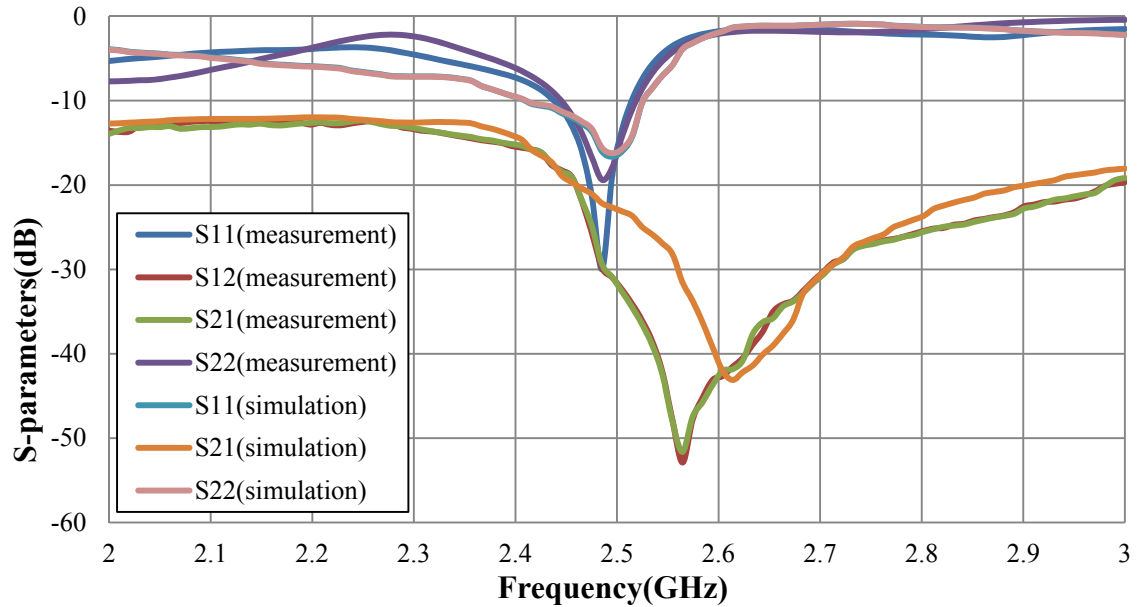
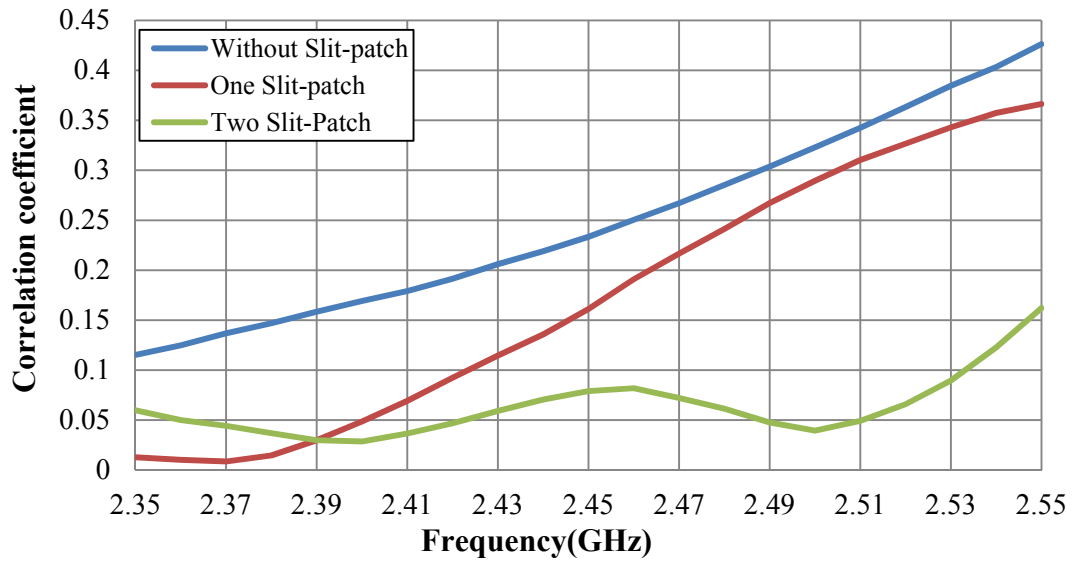
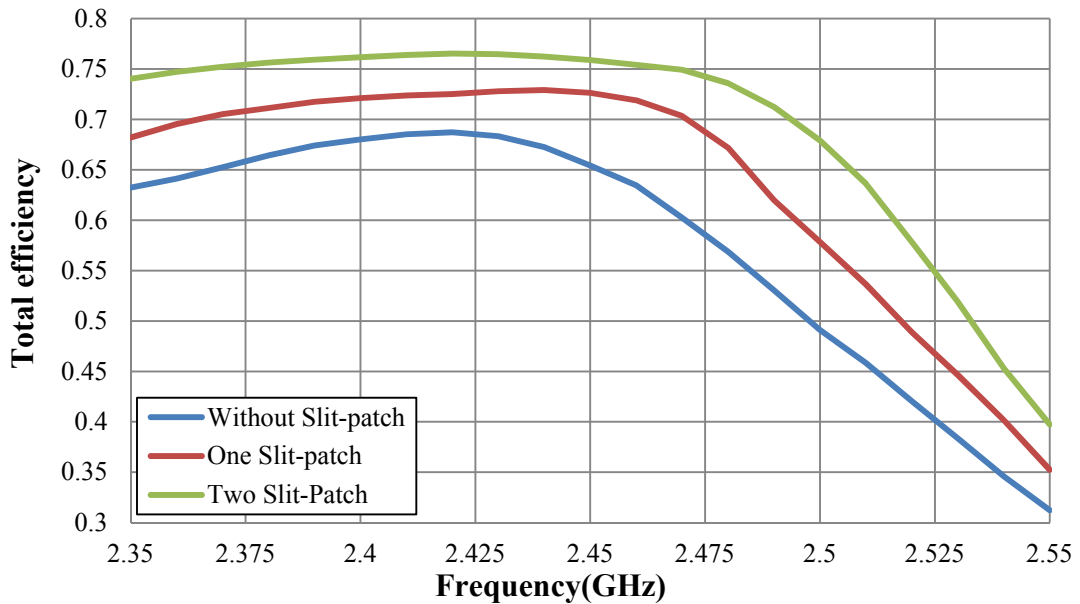


Figure 4.17 Simulated and measured S-parameters of printed monopole array with two slit-patch EBG structure

The correlation coefficient between the two antennas in the presence of the slit-patch EBG structures has also been calculated by using equation (2.9) [13]. All cases, namely the antenna array with one, two optimised slit-patch structures, and without the proposed structure are shown in Figure 4.18(a). The correlation coefficient is significantly reduced, after the proposed slit-patch EBG structures are placed on the ground plane. The total efficiency of the antenna increases when the number of the slit-patch structures increase, as shown in Figure 4.18(b). Furthermore, based on the equation (3.2), the increased efficiency in the presence of the slit-patch EBG structure is due to the fact that the mutual coupling between two antennas is reduced, compared to the original array.



(a)



(b)

Figure 4.18 (a) Correlation coefficient between the two antennas (b) Total efficiency of the whole antenna system in the presence of multiple slit-patch structures

In the previous simulation experiments, the separation between the two antennas is only 14mm (0.11λ). This is a small spacing between two printed CPW-fed monopoles. In order to investigate the effect of the optimized slit-patch structures and produce maximum miniaturization of the antenna array, thereby occupying less space in a mobile terminal, the two-element printed monopoles are shifted with variable

interelement distance denoted by D (12mm, 8mm, and 6mm respectively) on the ground plane as shown in Figure 4.19. The simulated results (S_{11} and S_{21}) corresponding to their locations have been displayed in Figure 4.20. With two antennas close to each other, the resonant frequency of the antenna (S_{11}) has slightly shifted towards a lower frequency. All S_{21} are below -19dB around the desired frequency (2.49GHz) regardless of the alteration of interelement distance between the two printed monopoles. This result is encouraging since the proposed slit-patch EBG structure can significantly reduce the mutual coupling even if the two printed monopoles are very close to each other.

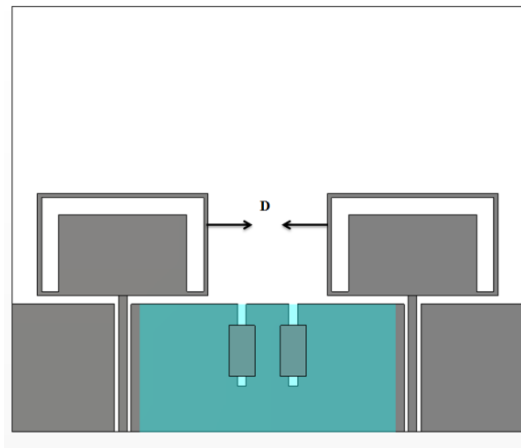
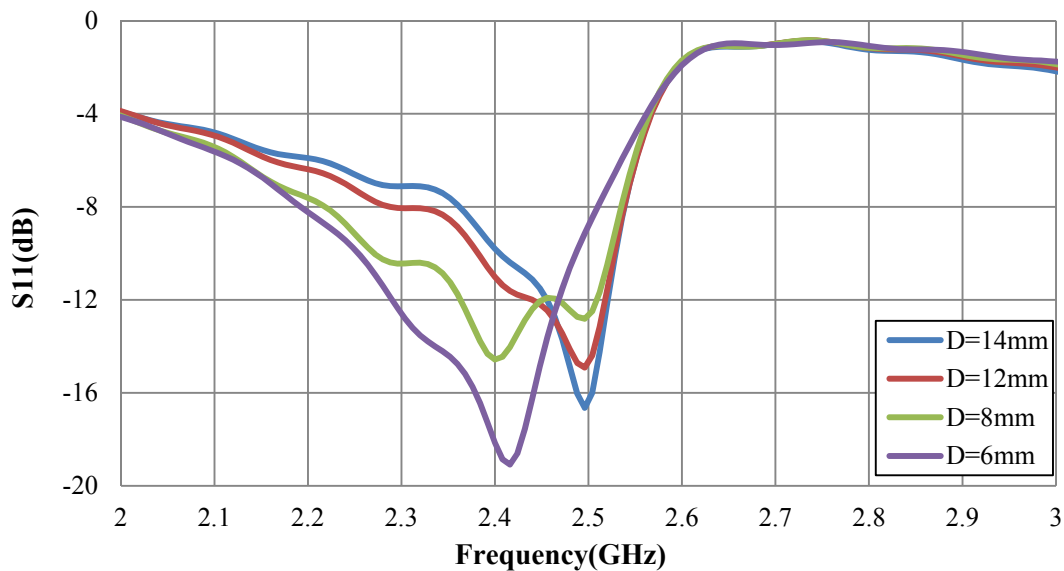
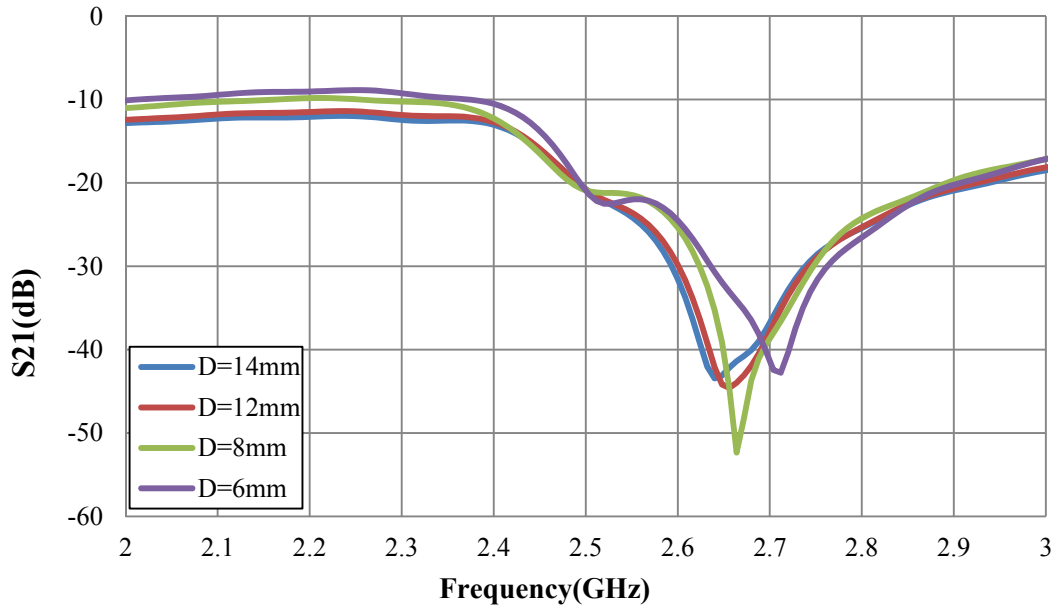


Figure 4.19 The variable interelement separations (D) between two monopoles



(a)



(b)

Figure 4.20 (a) S11 and (b) S21 of antenna array with various separations (D)

The prototype of the closely spaced antenna array (interelement distance $D=8\text{mm}$) with the two slit-patch structures was fabricated and measured. The prototype and configuration of the proposed antenna system are shown in Figure 4.21. The simulated and measured S-parameters are shown in Figure 4.22. The measured bandwidth (-10dB) of antenna 1 and 2 are still much less than the simulation result. These minor discrepancies will be discussed below. Nevertheless, at the resonance of the slit-patch (2.4556GHz) both antennas are well matched ($S_{11} < -10\text{ dB}$ and $S_{22} < -10\text{ dB}$). In comparison with the original position in Figure 4.17, the measured S21 slightly increases to -23dB when the interelement distance (D) between the two antennas is 8mm . But it is noted that the area of antenna array has been miniaturized by employing the proposed slit-patch EBG structures, as compared to the original design.

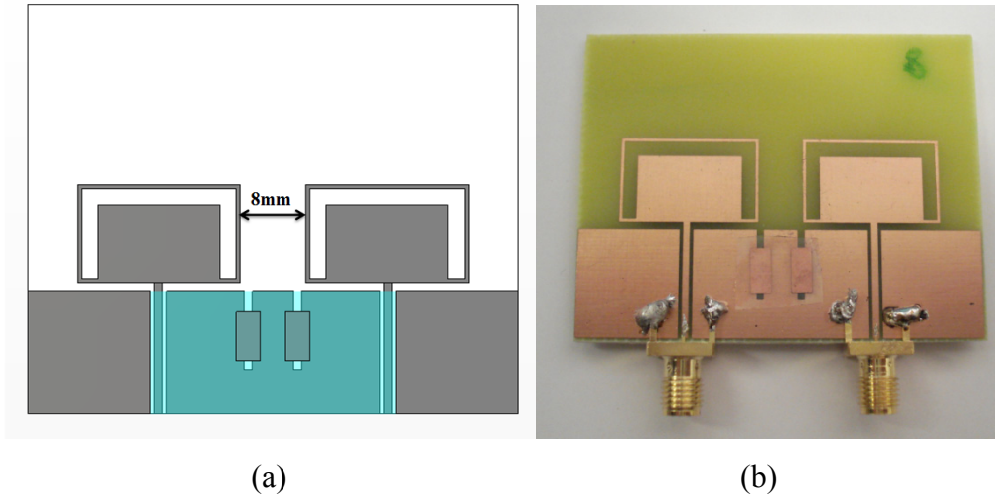


Figure 4.21 (a) The configuration and (b) Experiment model of the dual element antenna array with the two slit-patch structure when D is 8mm

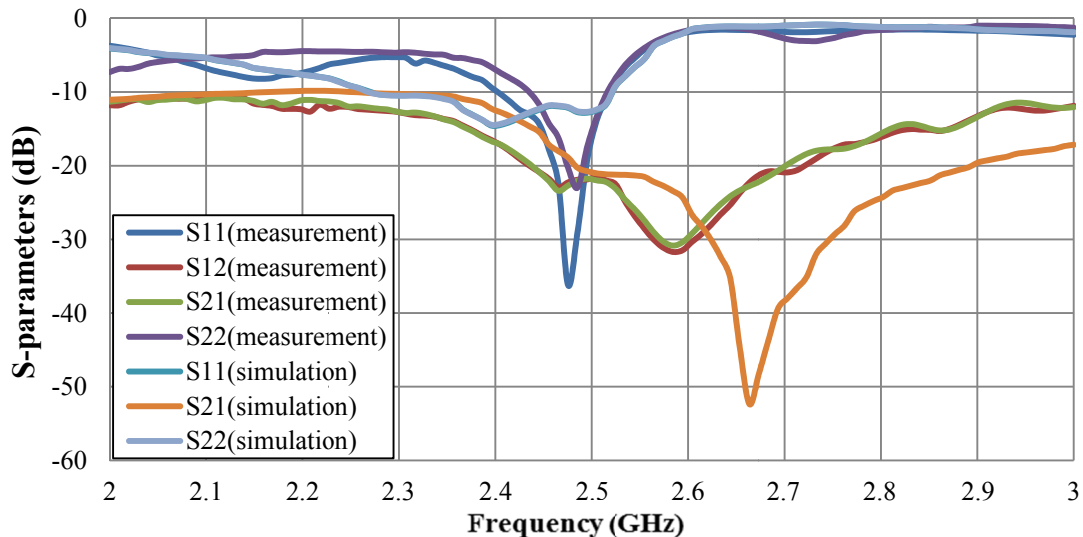
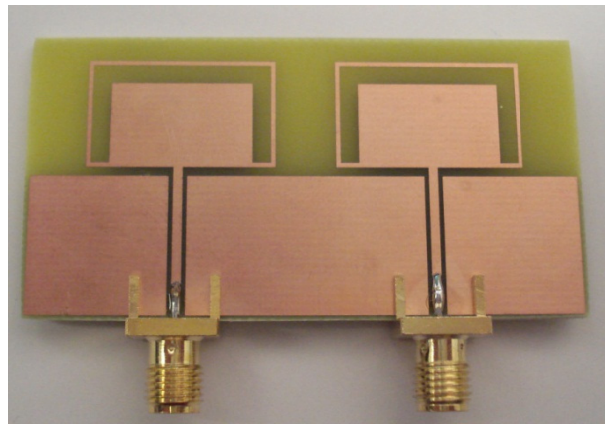


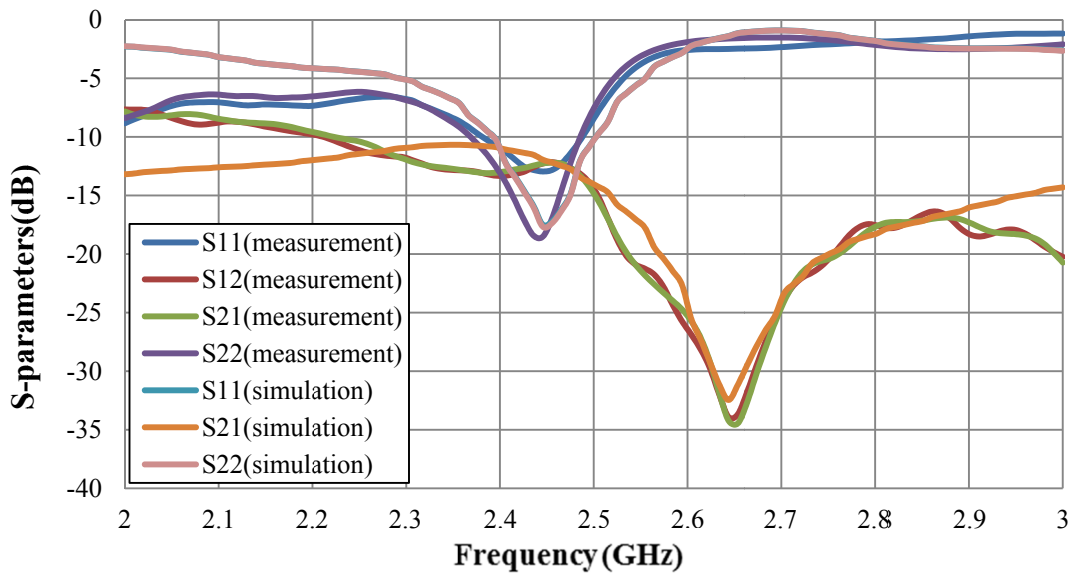
Figure 4.22 Simulated and measured S-parameters of printed monopole array with two slit-patch EBG structure when D is 8mm

As presented above, the measured bandwidth of S_{11} and S_{22} are much less than the simulated results in Figures 4.10, 4.13 and 4.17. However, the measured graph curves for the return loss (S_{11} and S_{22}) and mutual coupling (S_{12} and S_{21}) seem to retain their shape in the simulations. One prototype of two printed monopoles on a conventional ground plane without the slit-patch EBG structure was fabricated and measured to verify the factor that produces the difference between simulated and measured results. The dimensions of the printed monopoles are exactly the same as

before. And the interelement distance(D) is 8mm. The fabricated prototype of the antenna module is shown in Figure 4.22(a).



(a)



(b)

Figure 4.23 (a) Prototype and (b) Simulated and measured S-parameters of the printed monopole array with a conventional ground plane when D is 8mm

The simulated and measured S-parameters of the dual-elements antenna array with a conventional ground plane are shown in Figure 4.23(b). The measured results are in agreement with the results obtained from the simulation. The mutual coupling is about -13dB across the operating frequency band. The bandwidth of S11 and S22(-10dB) is more than 100MHz in both simulation and measurement. These discrepancies between simulated and measured results are due to the limitation of the CST software

and computer performance. The proposed complementary structure employs conducting patches in close proximity to the linear slit etched on the ground plane. The interelement distance between the two element layers is 0.055mm which requires a very small mesh to match the structure in simulation software, thus a lot of computer memory is necessary for the simulation. However, in the department laboratory, the computer cannot support such large amounts of data operation whilst maintaining accuracy. This situation causes the discrepancies whereby the measured antenna bandwidth is much less than the simulation result.

4.5 UWB Planar Monopole with Slit-Patch Structure

As discussed in chapters three, the separation between the antenna elements should be more than a half wavelength to achieve a low mutual coupling between antennas. Either the PIFAs or the printed CPW monopoles which are presented in previous sections operate within a narrow frequency band. In order to demonstrate the electromagnetic properties of the proposed slit-patch EBG structure in a broader frequency band, a dual-element UWB (Ultra WideBand) planar monopole array has been proposed and studied in this section. The UWB technology has attracted much attention since the Federal Communications Commission (FCC) allowed the free license of the frequency spectrum 3.1-10.6GHz to UWB system at low power usage in 2002 [14]. The UWB technology requires the bandwidth of antenna more than 500 MHz or 20% of the center frequency. Planar UWB monopoles have been used for many applications for their attractive characteristics [15-17]. Nevertheless, they will produce significant surface current on the PCB which is particularly problematic in the case of UWB antennas printed on a compact ground plane [18]. The surface

current on the PCB will produce high mutual coupling between the antenna elements when multiple planar UWB monopoles are employed to form MIMO system.

In this section, the slit-patch EBG structure is proposed to suppress the surface currents on the ground plane and reduce the mutual coupling between two UWB planar monopole elements operating from 3GHz to 6GHz.

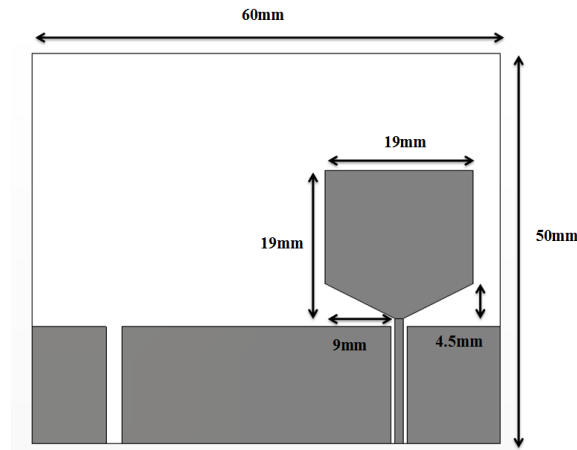


Figure 4.24 One UWB monopole planar geometry

A UWB planar monopole is printed on a FR-4 substrate (1.5mm thickness) with a size of $60 \times 50 \text{mm}^2$. The relative permittivity of the FR-4 dielectric substrate is 4.5. The radiating element is fed by a coplanar waveguide (CPW) line of 1.3mm width. In order to facilitate fabrication, the UWB antenna and the coplanar waveguide line are printed on the same side of the substrate. In order to enhance bandwidth of square monopole antenna, a simple method is to remove the square sides close to the ground plane as shown in Figure 4.24 [19-20]. After the simulations, the dimensions of the antenna are optimized as 19mm length with two bevels ($9 \text{mm} \times 4.5 \text{mm}$) for all cases in this section. The simulated S11 of the UWB planar monopole is depicted in Figure 4.25. The simulated bandwidth (-10dB) of antenna emerges at 2.238 GHz and extends up to 7GHz. This antenna, which agrees with the requirement of the UWB system, has 136% fractional bandwidth and 4.762GHz absolute bandwidth.

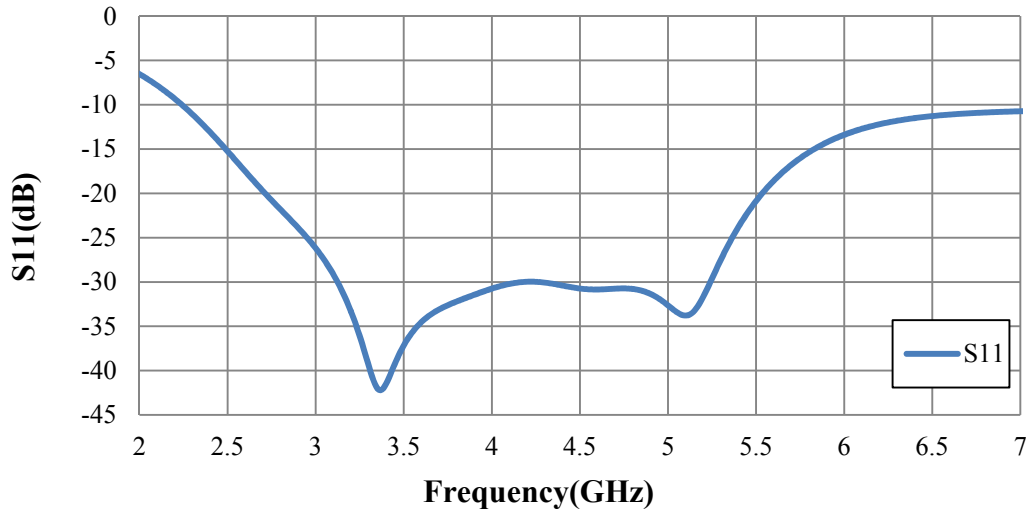


Figure 4.25 Simulated S11 of the UWB planar monopole

Based on the configuration and dimensions of the single antenna element, a dual-element UWB monopole planar array is also studied. The two antennas are placed on the proposed substrate with size of $60 \times 50 \text{ mm}^2$. The separation between the two radiating elements is only 15mm. The dimensions and other relevant positions are the same as the single antenna element. A configuration and an experimental prototype of the proposed antenna system are shown in Figure 4.26.

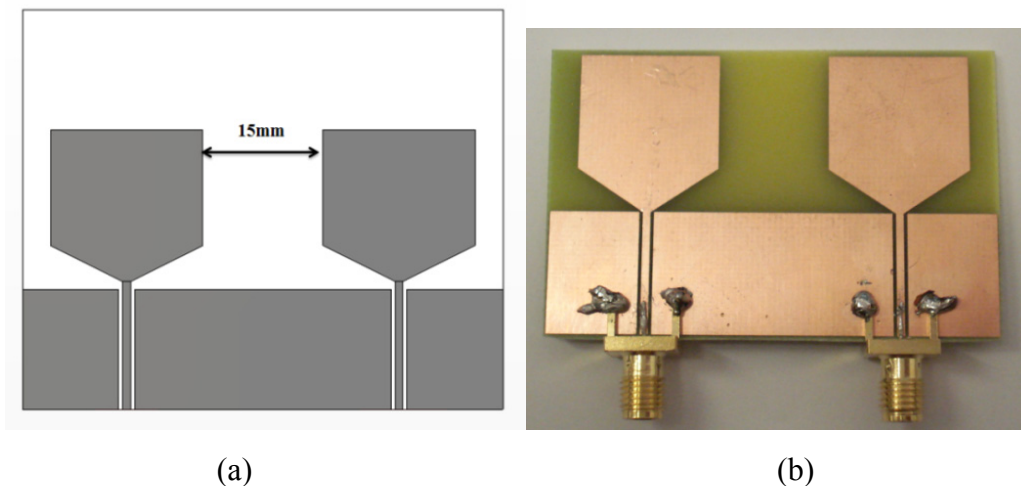


Figure 4.26 (a) The configuration and (b) Experimental model of the dual element antenna array

The simulated and measured S-parameters of the dual-elements antenna array are shown in Figure 4.27. Due to the two antennas being completely symmetrical on the substrate, the simulated S11 and S22 are identical in operating frequency. In comparison to the single planar monopole, the simulated S11 and S22 slightly shift towards a higher frequency from 2.235GHz to 2.39GHz at the lower frequency range. It is caused by the high mutual coupling when two planar UWB antennas are closely packed on the compact substrate. The UWB monopoles have been fabricated as shown in Figure 4.26(b). The measured mutual coupling (S21) curves seem to retain their shape compared to the simulation results across the operating frequency band. However, the measured return loss of the antennas (S11 and S22) are different to the simulated results in some frequency bands. Nevertheless, both antennas are well matched ($S_{11} < -10$ dB and $S_{22} < -10$ dB) across the operating frequency band from 3 GHz to 6 GHz in both the simulated result and measured result. These discrepancies between simulated and measured results are caused by a large amount of surface current flowing back from the radiation elements to the coaxial cable and producing the secondary radiation when the two planar monopoles were placed close to each other [18].

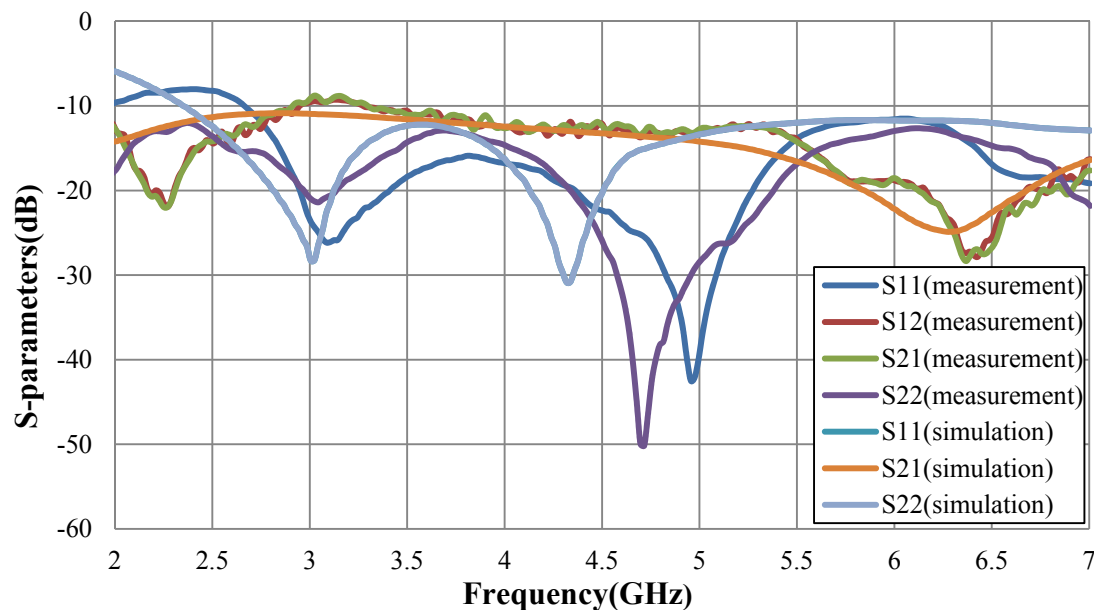


Figure 4.27 Simulated and measured S-parameters of the dual-elements antenna array

The mutual coupling between two antenna array elements is more than -13dB across the whole operating frequency when the two antennas are 15mm apart on the substrate. In order to produce a significant reduction of the mutual coupling within the operating band, the relevant slit-patch EBG structure is proposed as a miniaturized element and inserted in the compact ground plane between the two planar monopoles. The dimensions of the antenna elements are exactly same as before. This slit-patch EBG structure is positioned at the middle of top edge of the ground plane. Figure 4.28 shows the configuration and prototype of the proposed antenna system. After a series of simulations, the slit is optimized as 9.65 mm length and 1mm width. The conducting patch is of 3mm length and 1mm width. A prototype of the antenna array with one slit-patch EBG structure has been fabricated and measured. Figure 4.29 depicts the simulated and measured S-parameters. After the double-layer slit-patch EBG structure was inserted in the ground plane, a minimum is obtained in the mutual coupling between the two antennas, at exactly 3.25GHz corresponding to the resonance of the slit-patch EBG structure. However, there is no any obvious reduction in the remaining operating frequency band. This is because one single slit-patch EBG structure is just able to reduce mutual coupling in a relatively narrow band not supporting a wide band. As next step, multiple slit-patch unit cells are proposed to increase the S21 bandwidth to cover the whole operation frequency band.

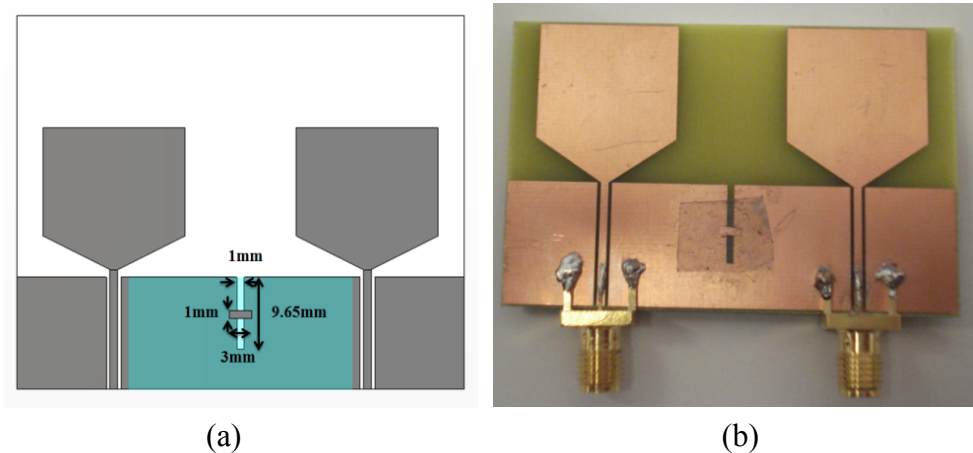


Figure 4.28(a) The configuration and (b) Experiment model of dual element antenna array and with one slit-patch structure

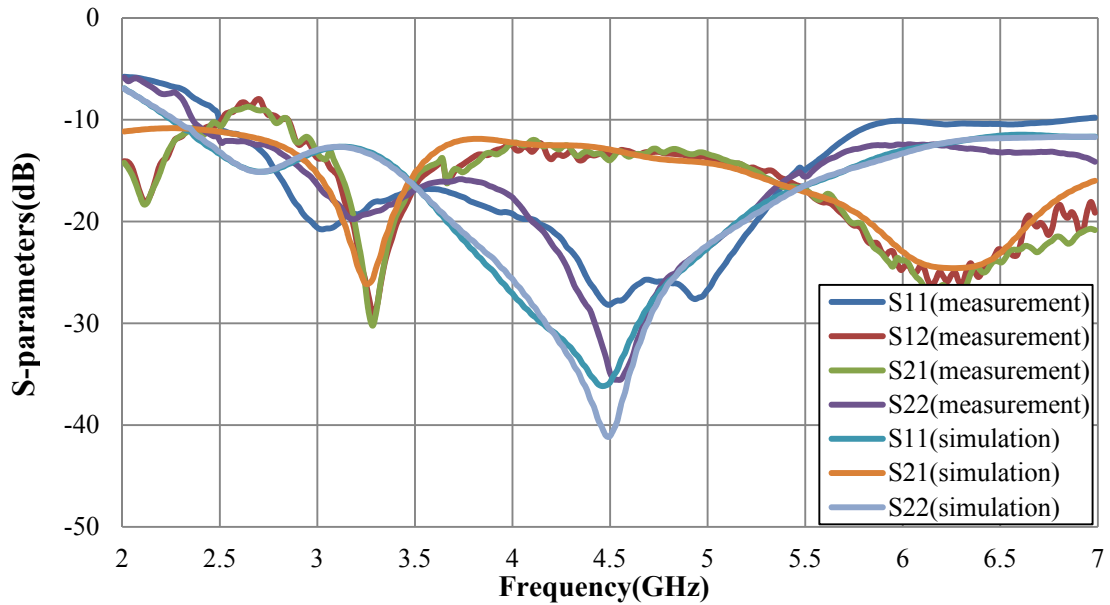


Figure 4.29 Simulated and measured S-parameters of the UWB planar monopole array with one slit-patch structure

The multiple double-layer slit-patch EBG structures have been shown to obtain a good isolation within a wider bandwidth in section 4.3. The mutual coupling is affected by the operating frequency because the electrical separation expressed as the number of wavelength between the antenna array elements changes significantly over the ultra-wide frequency band. The desired operating frequency band of the proposed UWB planar monopole is from 3GHz to 6 GHz not a narrow band. Therefore, it is a challenge to reduce the mutual coupling across the ultra-wide frequency band. Initially, two identical proposed slit-patch EBG structures are mounted on ground plane shown in Figure 4.30. The separation between the two slits is 6mm. The distance between the two patch edges is 3mm. The other dimensions of antenna system are same as before. A configuration and an experimental prototype of the proposed antenna system are shown in Figure 4.30.

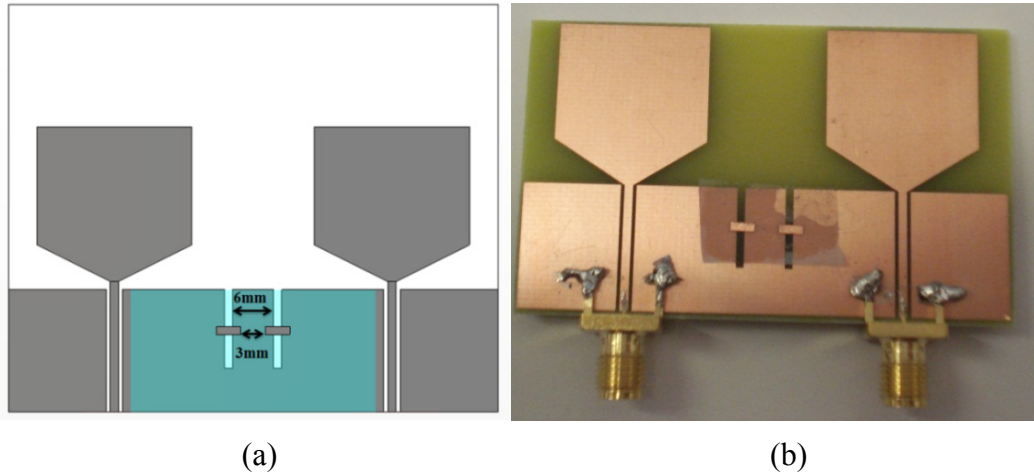


Figure 4.30 (a) The configuration and (b) Experimental model of the dual element antenna array with two slit-patch structure

The simulated and measured S-parameters of the two antenna array with the two slit-patch structure are shown in Figure 4.31. As the entire antenna system is fully symmetric, the simulated antenna characteristics (S_{11} and S_{22}) are basically same. The measured return loss of Antenna 1 is slightly different to Antenna 2 in some frequency ranges. These minor discrepancies are due to fabrication imperfections in the manual soldering of the feeding ports. Nevertheless, both antennas are well matched ($S_{11} < -10$ dB and $S_{22} < -10$ dB) across the whole operating frequency band from 3 to 6GHz. The measured S_{21} between the two antennas in the presence of the two slit-patch structures is significantly reduced in comparison to the initial structure in the low frequency range. Both simulated and measured bandwidths of S_{21} are much more than the antenna array with the one slit-patch structure as a result of employing an additional slit-patch EBG structures. However, there is no obvious reduction in the remaining operating frequency band. It cannot cover the whole operating frequency of the planar UWB monopoles.

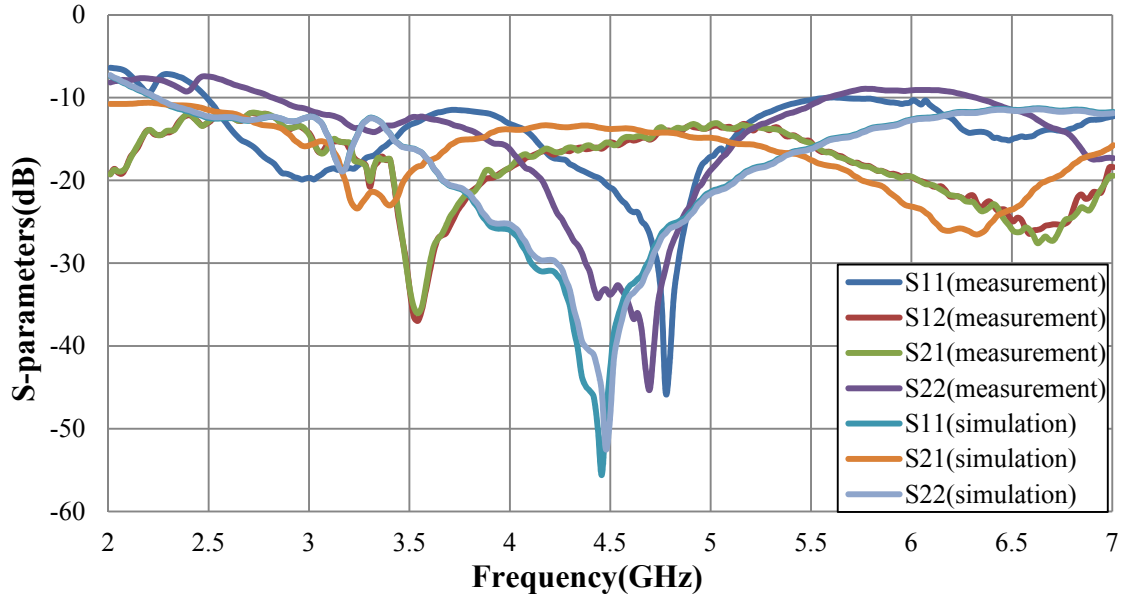


Figure 4.31 Simulated and measured S-parameters of UWB planar monopole array with two slit-patch structure

Finally, three identical slit-patch EBG structures are mounted on the ground plane to improve the isolation between antenna elements across the entire operating frequency range of UWB monopole. The three slit-patch structures are arranged much closer, as shown in Figure 4.32(a). The spacing between the two slits is 2.1mm. The distance between the two conducting patch edges is 0.1mm. The other dimensions of the planar monopole are the same as before. A configuration and an experimental prototype of the antenna system are shown in Figure 4.32.

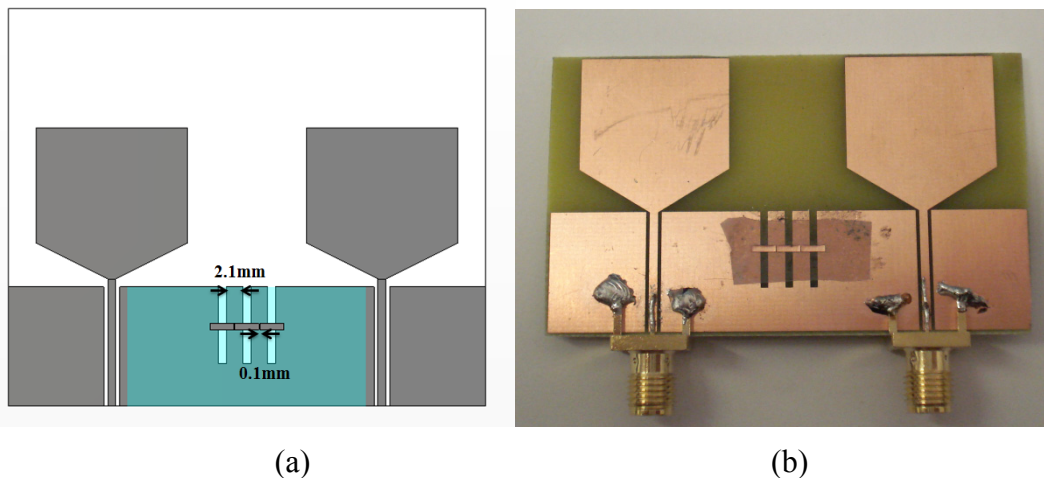


Figure 4.32 (a) The configuration and (b) Experiment model of the dual element antenna array with three slit-patch structure

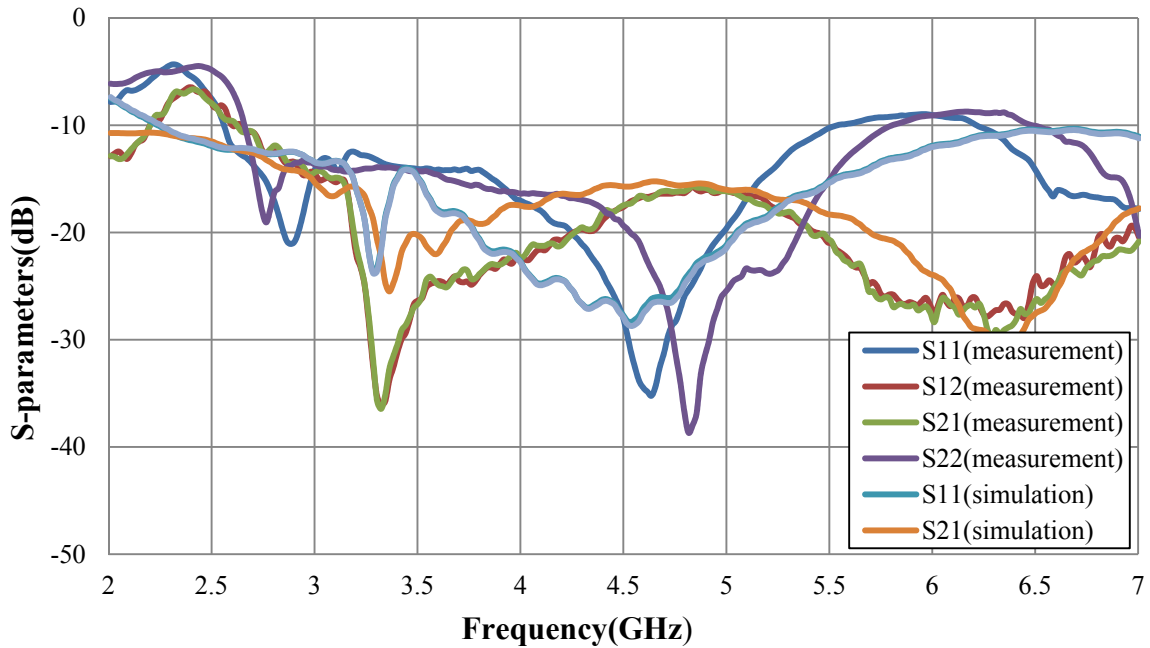


Figure 4.33 Simulated and measured S-parameters of UWB planar monopole array with three slit-patch structure

Figure 4.33 shows the simulated and measured S-parameters of the two UWB planar monopoles array with the three slit-path structures. The S21 of the new antenna system has an obvious reduction in the higher operation frequency band. The mutual coupling in both simulation and measurement are less than -15dB across the entirety of the operating frequency range. It is also worth gaining a better understanding of its mechanism by investigating the surface current density. As shown in Figure 4.34, a large portion of surface current is being trapped by the first slit next to the excited UWB monopole. When the current flows across the slit-patch structures, they are gradually weakening. Finally, less current succeeds in flowing across the slitted pattern from one antenna element to the other one. It makes less energy propagate between two UWB planar monopoles.

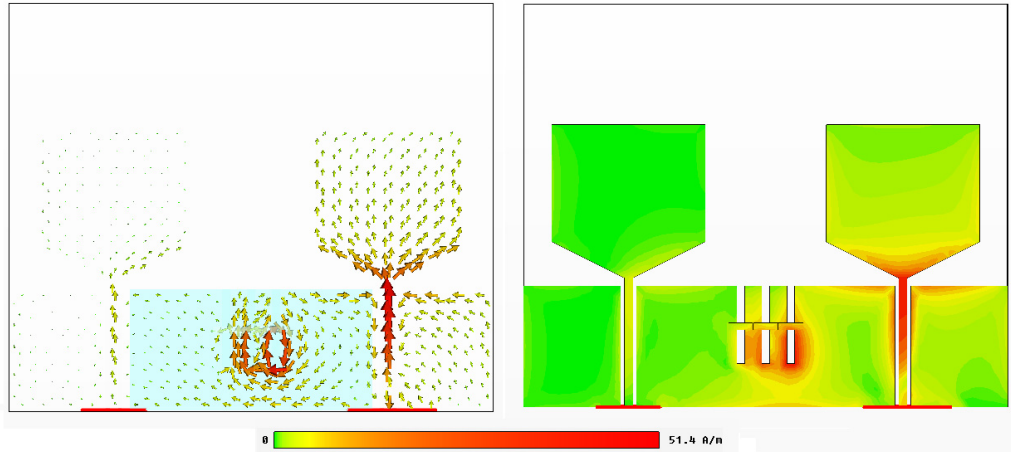
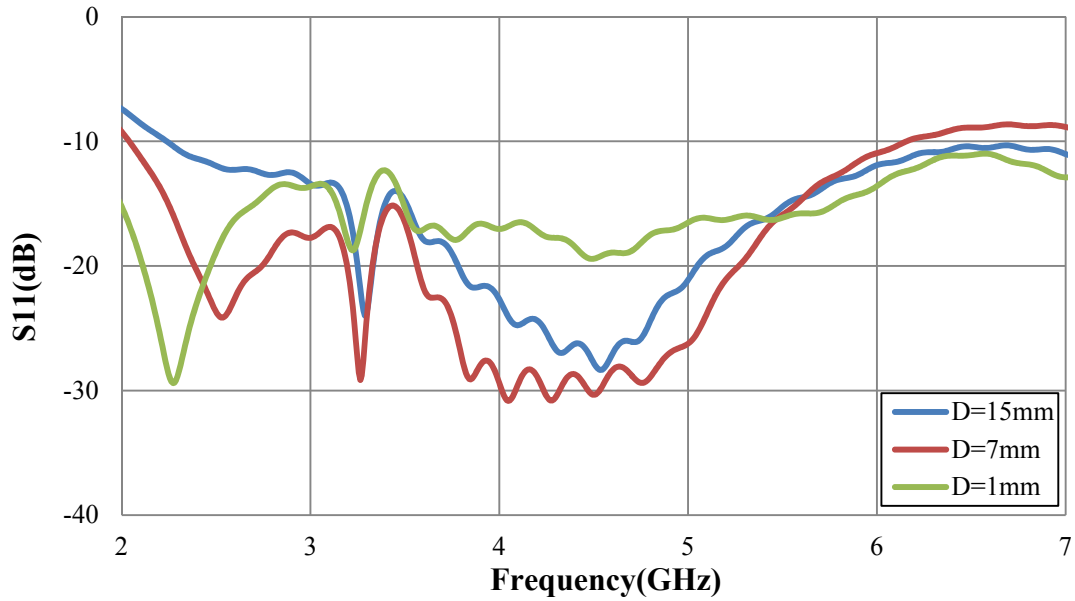
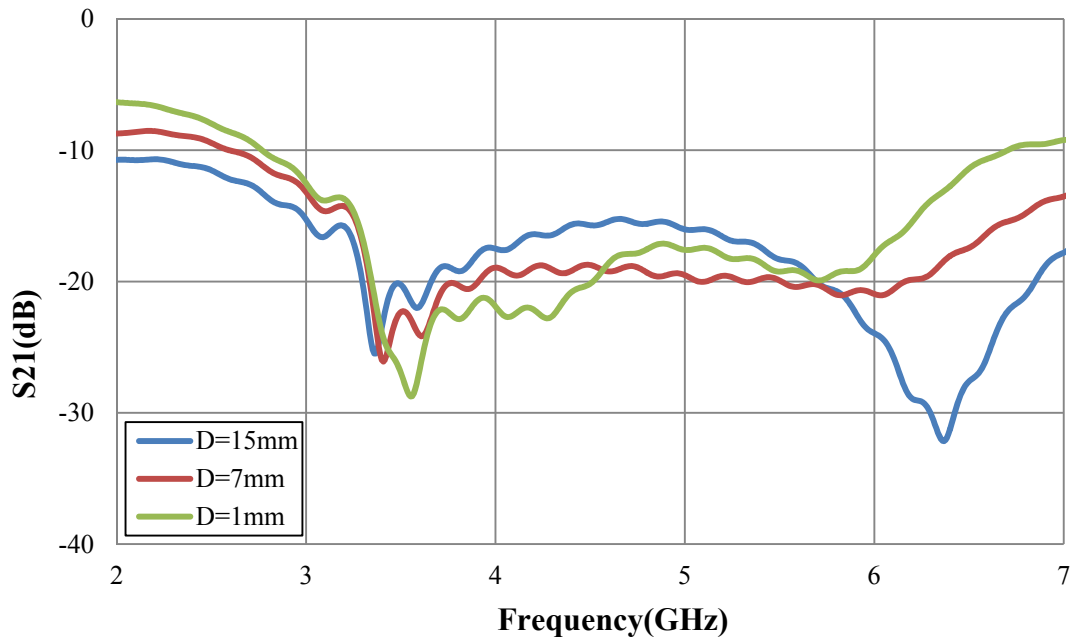


Figure 4.34 Current flow and distribution on the ground plane with three slit-patch structure at 3.5GHz

In the previous simulation experiments, the separation between the two radiating elements is 15mm. This is a small spacing between two planar monopoles. In order to investigate the effect of the slit-patch EBG structures and to produce the maximum reduction of the area of antenna array, thereby occupying very little space in a mobile terminal, the two-element UWB planar monopoles are shifted with variable interelement distance (D) (15mm, 7mm, and 1mm respectively) on the substrate. The simulated results (S_{11} and S_{21}) corresponding to their locations have been displayed in Figure 4.35. With the separation between two antennas decreasing, the value of $|S_{11}|$ slightly decreases. However, the S_{11} is still below -10dB across the whole operation frequency range from 3GHz to 6GHz. Moreover, there is good isolation (less than -15dB) between the two antennas within the operating frequency, regardless of the alteration of the interelement distance between the two antennas. These results are encouraging since the slit-patch EBG structure can significantly reduce the mutual coupling even if the two printed monopoles are very close to each other.



(a)



(b)

Figure 4.35 (a) S11 and (b) S21 of the antenna array with various separations (D)

The design of a closely spaced antenna array with three slit-patch structures was fabricated and measured when the interelement distance (D) between two planar monopoles is 1mm. The configuration and prototype of the proposed antenna array are shown in Figure 4.36.

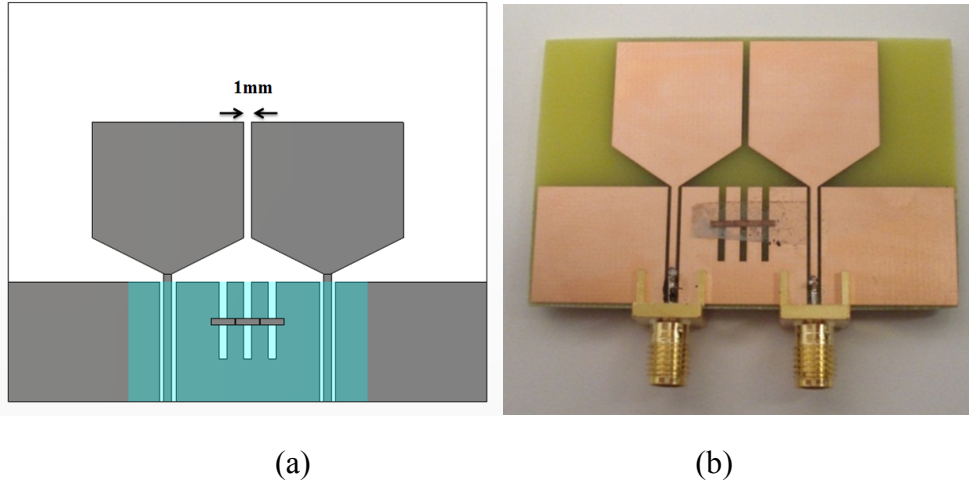


Figure 4.36 (a) The configuration and (b) Experimental model of the dual element antenna array with three slit-patch structure when D is 1mm

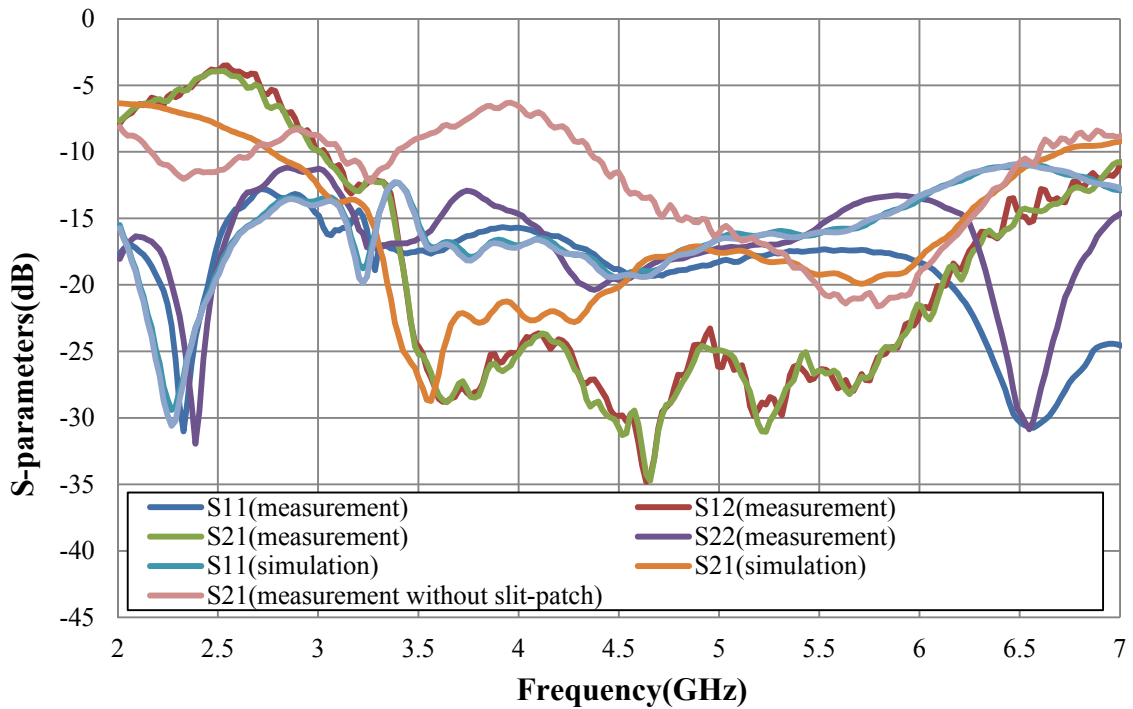


Figure 4.37 The simulated and measured S-parameters of the dual-element UWB monopole array with three slit-patch structure when D is 1mm

When the separation between the two antenna decreases to 1mm, the simulated and measured S-parameters are shown in Figure 4.37. The measured S11 and S22 are similar to the simulation result. Some minor discrepancies have been discussed above. Nevertheless, both antennas are well matched ($S_{11} < -10$ dB and $S_{22} < -10$ dB) across

the whole operation frequency band. When the two UWB monopole array are very close to each other, the mutual coupling between antenna elements is over -10dB from 3.37GHz to 4.35 GHz when the antenna system is employed with a conventional ground plane. The insertion of the three slit-patch EBG structures adds a transmission zero in the coupling coefficient between the antennas, reducing the S21 to values lower than -20dB across most of the operating frequency band of the UWB monopoles from 3.44GHz to 6.13GHz. Finally, the measured mutual coupling between the antennas in the proposed design is significantly reduced, as compared to the original design without slit-patch EBG structure. By employing the proposed slit-patch EBG structures, the area of antenna array has gained significant reduction whilst maintaining the performance of the antenna system. The simulated surface current on the ground plane at the 3.5GHz is presented. In Figure 4.38, the three slit-patch EBG structure are able to trap most of current on the ground plane, even if the two planar monopoles are very close to each other. This is a clear indication the proposed slit-patch EBG structure reduce the mutual coupling between two close spaced UWB antennas.

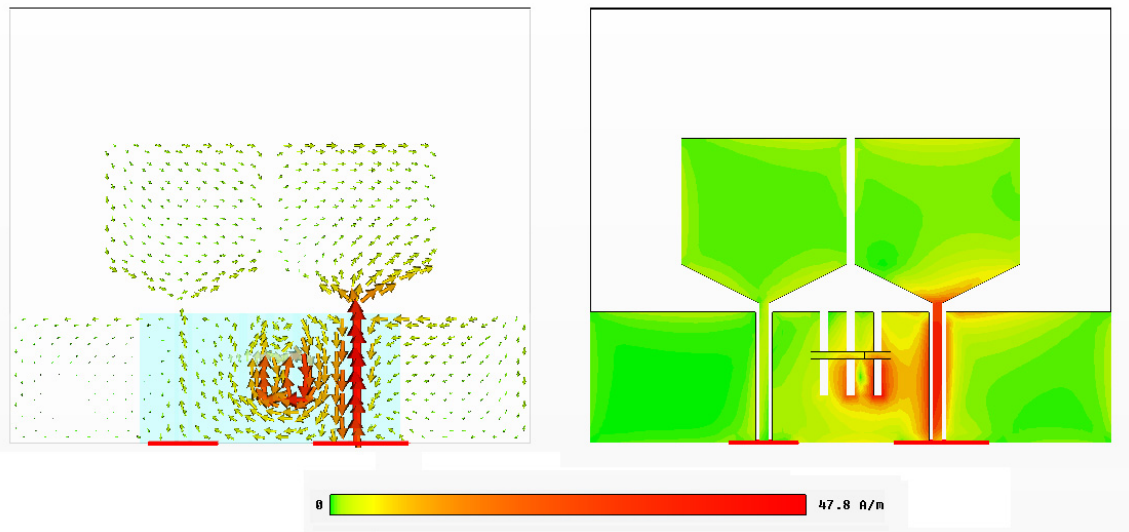


Figure 4.38 Current flow and distribution on the ground with three slit-patch structure when D is 1mm

The total efficiency has also been calculated from the simulated results by using equation (3.2). Figure 4.39 illustrates the simulated total efficiency with different numbers of slit-patch EBG structures. It is noted that the total efficiency is improved as the number of the slit-patch structures increase. It also clearly shows the characteristics of the slit-patch structures. The total efficiency of the antenna array with one slit-patch structure has an obvious improvement at the lower frequency band in comparison to the antenna system with a common ground plane. The total efficiency of the antenna array increases as the number of slit-patch structures increase. Meanwhile, the maximum of the total efficiency shifts to high frequency. After the separation between two planar monopoles reduce to 1mm, the total efficiency of antenna with a conventional ground plane has a significant reduction due to higher mutual coupling between antenna elements. The total efficiency has an obvious improvement across the operating frequency of antennas in the presence of the slit-patch EBG structures.

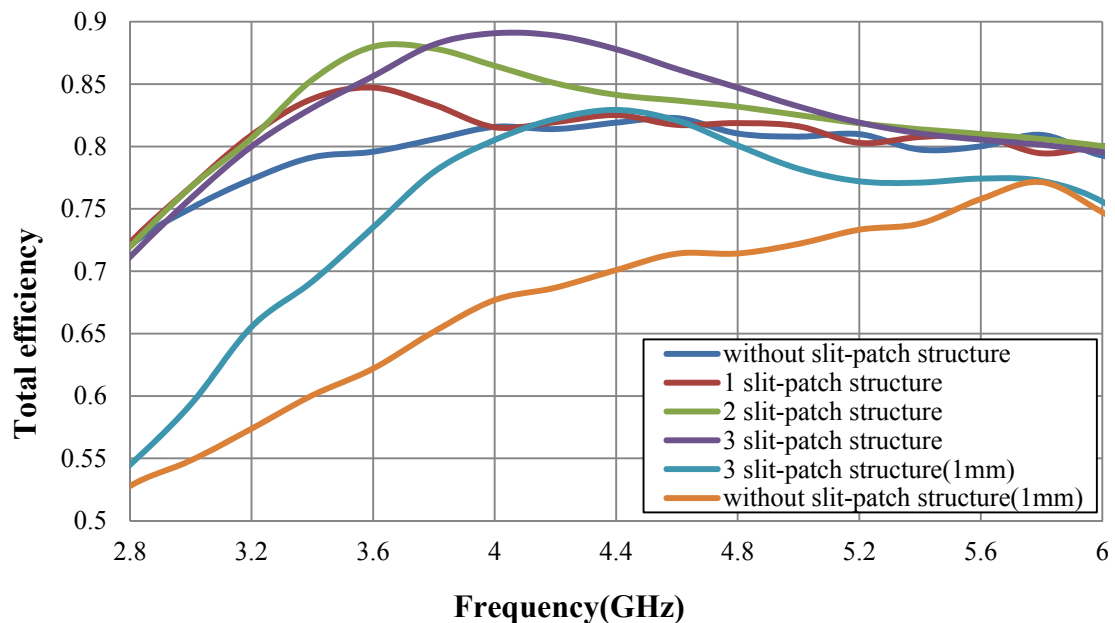


Figure 4.39 the total efficiency of the whole antenna system in the presence of multiple slit-patch structures

4.6 Summary

This chapter presents the introduction of the slit-patch EBG structures and their transmission characteristics. The proposed structures are comprised of the simple geometry conducting elements. A parallel LC circuit description was used to provide a qualitative explanation for the performance of the proposed slit-patch EBG structure. The dimensions of the proposed structures are optimized to produce maximum miniaturization thereby occupying very little space on ground plane. A microstrip line excitation is initially employed for the analysis and design of the proposed double-layer EBG structures. Simulated transmission response with different widths of conducting patch was presented. Multiple slit-patch EBG structures were studied to extend the bandwidth of the transmission response (S21).

A modified printed monopole and its dual-element antenna array are mounted on a compact substrate for wireless terminal devices operating around 2.44GHz. The proposed slit-patch EBG structures significantly reduce the mutual coupling between two antennas from -14dB to less than -30dB. Two identical slit-patch structures are presented to significantly reduce the correlation coefficient between the two antennas and improve the total efficiency of antenna. Although the proposed double-layer EBG structures have small footprint on the ground plane, they produce the transmission minimum around the antenna operating frequency regardless of the alteration of the interelement distance between the two monopoles (distance $\geq 8\text{mm}$).

A dual-element UWB planar monopole array operating from 3GHz to 6GHz has been investigated with the slit-patch EBG structures. An isolation of better than 15dB between the two antenna array elements has been obtained across the entirety of the operation frequency range by employing three slit-patch EBG structures. When the separation of two UWB planar monopole array reduces to 1mm, a significant

reduction of mutual coupling between the antenna elements was achieved by employing the proposed slit-patch EBG structures. This further confirms that the design of the miniaturized double-layer slit-patch EBG structures can produce a reduction of the mutual coupling between antenna elements and also lead to the maximum reduction of the area of antenna array.

References

- [1] Q. Li, A. P. Feresidis, “Miniaturised Slit-Patch EBG Structures For Decoupling PIFAs on Handheld Devices,” *Loughborough Antennas & Propagation Conference*, 14-15 November 2011, Loughborough, UK
- [2] G. Goussetis, A. P. Feresidis, G. Apostolopoulos, J. C. Vardaxoglou, “Miniaturisation of Defected Ground Plane Using Complementary Metallodielectric Electromagnetic Band Gap Structures,” *IEEE international Workshop on Antenna Technology: small Antennas and Novel Metamaterials*, Wat 2006, New York, U.S.A, march 2006
- [3] J. C. Vardaxoglou and D. Lockyer, “Modified FSS response from two sided and closely coupled arrays.” *Electron. Lett.*, vol. 30, no. 22, pp.1818–1819, 1994.
- [4] D. S. Lockyer and J. C. Vardaxoglou, “Reconfigurable FSS response from two layers of slotted dipole arrays,” *Electron. Lett*, vol. 32, no. 6, pp. 512–513, 1996.
- [5] D. S. Lockyer, J. C. Vardaxoglou, and R. A. Simpkin, “Complementary frequency selective surfaces,” *IEE Proceedings Microwaves, Antennas and*

Propagation . vol.147, pp. 501-507, Dec 2000.

- [6] G. Apostolopoulos, A. P. Feresidis, G. Goussetis, J. C. Vardaxoglou
“Complementary metallo-dielectric electromagnetic band gap structures,”
Microwave Conference, 2005 European, Vol. 2, Oct 2005.
- [7] A. P. Feresidis,, G. Apostolopoulos., N. Serfas and J.C. Vardaxoglou,
“Closely Coupled Metallodielectric Electromagnetic Band Gap (CCMEBG)
Structures formed by double layer Dipole and Tripole arrays,” *IEEE
Transaction Antennas and propagation*, Vol. 52, pp 1149-1158, May 2004.
- [8] G. Apostolopoulos, A. Feresidis, J.C. Vardaxoglou “Miniaturised EBG
structures based on complementary geometries,” *IEEE Antennas and
Propagation Society International Symposium*, pp 2253 - 2256 9-14 July
2006
- [9] D. S. Lockyer and J. C. Vardaxoglou, “Reconfigurable FSS response from
two layers of slotted dipole arrays,” *Electron. Lett.*, vol. 32, no. 6, pp. 512–
513, 1996.
- [10] F. M. Yan “The application of EBG in antennas,” Telecom market March,
2003, QingHua University.
- [11] B. A. Munk, “Frequency Selective Surface theory and design,” John
Wiles&Sons, pp. 5-37, Aug 2000
- [12] C. A. Balanis, “Antenna Theory: Analysis and Design,” A John Wiley &
Sons, Inc., Publication, pp. 433-494.
- [13] J. Liang, L. Guo, C.C.Chiau, X. Chen, and C.G.Parini, “Study of CPW fed
circular disc monopole antenna for ultra-wideband applications,” *IEE
Proceedings on Microwaves, Antennas & Propagation*, vol. 152, no. 6, pp.
520-526, Dec 2005.
- [14] Federal Communications Commission (FCC), “Revision of Part 15 of the
Commission’ s Rules Regarding Ultra Wideband Transmission Systems,”
First Rep. and Order, ET Docket 98-153, FCC 02-48, Adopted: Feb. 2002;
Released: Apr. 2002.

- [15] J. Liang, C Chiau, X. Chen and C.G. Parini, "Study of a Printed Circular Disc Monopole Antenna for UWB Systems," *IEEE Trans. On Ant. and Prop.*, vol. 53, no. 11, pp.3500-3504, Nov. 2005.
- [16] K. L. Wong; C. H. Wu; S. W. Su, "Ultrawide-band square planar metal-plate monopole antenna with a trident-shaped feeding strip," *IEEE Transaction. on Antenna. and Propagation.*, vol. 53 , no. 4, pp.1262 - 1269, 2005.
- [17] C.-C. Lin, Y.-C. Kan, L.-C. Kuo, and H.-R. Chuang, "A planar triangular monopole antenna for UWB communication," *IEEE Microwave and Wireless Components Letters*, vol. 15, no. 10, pp. 624-626, Oct. 2005.
- [18] L. Liu, Y.F. Weng, S. W. Cheung, T. I. Yuk, and L. J. Foged, "Modeling of cable for measurements of small monopole antennas," *Loughborough Antennas & Propagation Conference*, 14-15 November 2011, Loughborough, UK
- [19] M. J. Ammann, "Control of the impedance bandwidth of wideband planar monopole antennas using a beveling technique," *Microwave Opt. Technol. Lett.*, vol.30, no. 4, pp.229-232, Aug. 2001
- [20] J. Qui, Z. Du, J. Lu, and K. Gong, "A case study to improve the impedance bandwidth of a planar monopole," *Microwave Opt. Technol. Lett.*, vol. 45, no. 2, pp. 124-126, Apr. 2004.

Chapter 5

Convolute Slit and Conducting Patch on Mobile Terminals

5.1 Introduction

The novel miniaturized Complementary Metallodielectric Electromagnetic Band Gap (CMEBG) structure has been presented to suppress surface wave propagation and to offer a small structural footprint thereby occupying very little space on a compact ground plane [1-5]. The simulated and measured results demonstrated that the design of the novel miniaturised double-layer slit-patch EBG structures efficiently reduce the mutual coupling between antenna elements in Chapter 4. The proposed slit-patch EBG structure comprised of linear slits and conducting patches has been investigated with a dual-element CPW-fed printed monopole array and a dual-element UWB planar monopole array. These two kinds of antennas have been widely used as separate antenna modules for compact wireless devices. However, when the slit-patch

EBG structure is employed for a handheld device, it can still be viewed as impractical for many realistic designs because the linear slits will occupy a large part of the ground plane. Therefore, a new structure which employs miniaturized convoluted slits (instead of the linear slits) in conjunction with closely coupled patches is proposed for compact mobile phones. The proposed structure places one layer of conducting patches in close proximity to the existing convoluted slits etched on the ground plane for producing maximum electric fields and coupling between them. As discussed in Chapter 4, the effective electrical length of the slit-patch EBG structure increases, due to the strong coupling between two layers elements, resulting in the resonant frequency of the slit-patch structure decreasing [3, 6].

In order to further miniaturise the dimension of the convoluted slits, the conducting patches are placed in close proximity to the convoluted slits. As discussed in Chapter four, the resonant frequency of the double layer slit-patch structures is very sensitive because of the strong coupling in the separation region between two layers. Therefore, we initially use a microstrip line excitation as a more efficient way, compared to any complex antenna array, for analysing the stop-band/band gap properties of the proposed slit-patch structures and hence optimise their geometries. Due to the conducting patch being in close proximity to the convoluted slits, resulting in the high capacitance of the slit-patch structure [7], the cut-off frequency and the absolute bandwidth decrease, as presented in Chapter four. In order to overcome this limitation and obtain much more bandwidth, multiple identical double-layer slit-patch EBG structures are employed to enhance the bandwidth. A dual-element PIFA antenna array operating at 1.9GHz is subsequently employed to investigate the property of the slit-patch EBG structure comprising convoluted slits and conducting patches. Two prototypes of the dual-element antenna array with the proposed slit-patch structures were fabricated. Measurements are in good agreement with simulated results, and verify that the optimised slit-patch EBG structures significantly reduce the mutual coupling between closely spaced PIFAs.

5.2 Double Layer Convoluted Slit-Patch Design

The proposed slit-patch EBG structure is shown in Figure 5.1. As discussed in Chapter four, the key design parameter of the proposed structures is the coupling of the evanescent fields within the dielectric region separating the two arrays of slits and patches respectively. The conducting patches and aperture slits are placed on either side of a very thin ($55\mu\text{m}$) dielectric layer. In Chapter four, the slit-patch EBG structures comprising linear slits and conducting patches have succeeded in shifting the band gap towards lower frequency. For applications relevant to handset device, new slit-patch EBG structure which consists of convoluted slits and conducting patches will be studied in this chapter.

In Figure 5.1, a 50Ω microstrip line is printed on a thin polyester dielectric sheet ($\epsilon_r=3$) and placed at the top of a rectangular grounded substrate. A convoluted slit is etched on the ground plane. Another thin dielectric sheet (0.055 mm thickness, $\epsilon_r=3$) underneath the ground plane supports the conducting patches.

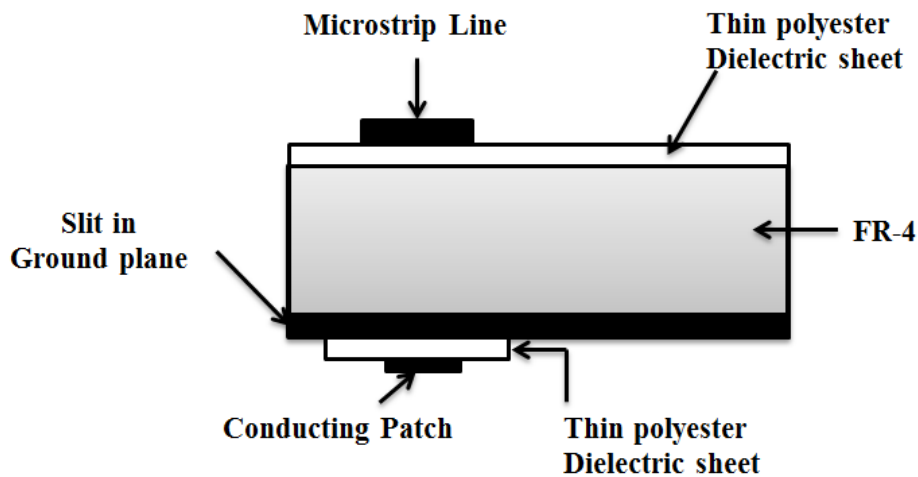


Figure 5.1 Configuration of the slit-patch EBG structure

The new slit-patch EBG structure is depicted in Figure 5.2. The microstrip line is mounted on a 100mm×40mm, 1.55mm thick, FR-4 dielectric substrate ($\epsilon_r=4.5$) backed by a copper ground plane. The convoluted shaped slit is etched close to the bottom edge of the ground plane. The dimensions of the slit were optimised in order to resonate around 1.65GHz. The final geometry of the slit is defined as $L_1=6\text{mm}$, $L_2=14\text{mm}$, $L_3=5\text{mm}$, $L_4=10\text{mm}$, and the slit width is 1.61mm. A double-layer slit-patch EBG structure is implemented, as shown in Figure 5.3. In order to evaluate the specifications of the double layer convoluted slit-patch structure, a series of studies are performed. The first parametric study is to observe the effect of the proposed structures. The simulated transmission response (S_{21}) was shown in Figure 5.4. After one thin conducting patch (15.5mm length and 0.5mm width) is printed on the convoluted slit, the centre of band gap shifts to a lower frequency (from 1.65GHz to 1.375GHz). And the absolute bandwidth (-10dB) of S_{21} decreased from 110 MHz to 60MHz. These simulated results are in agreement with the predicated on the circuits analysis presented in section 4.2.

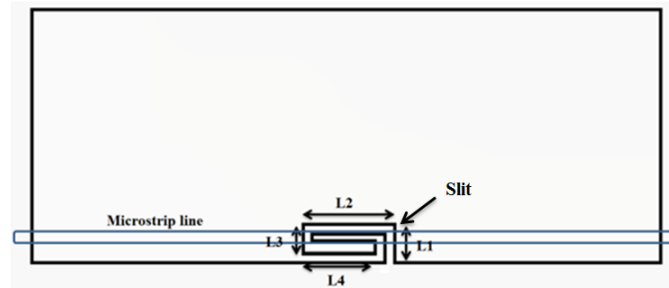


Figure 5.2 Single convoluted slit excited by a microstrip line

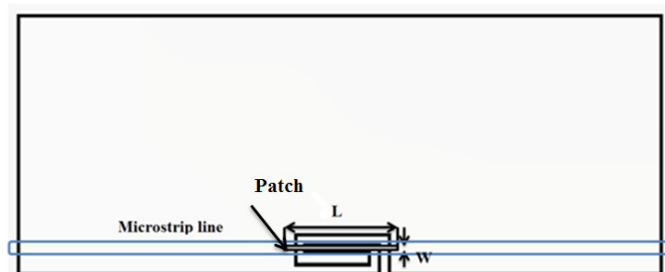


Figure 5.3 Geometry of one convoluted slit-patch EBG structure

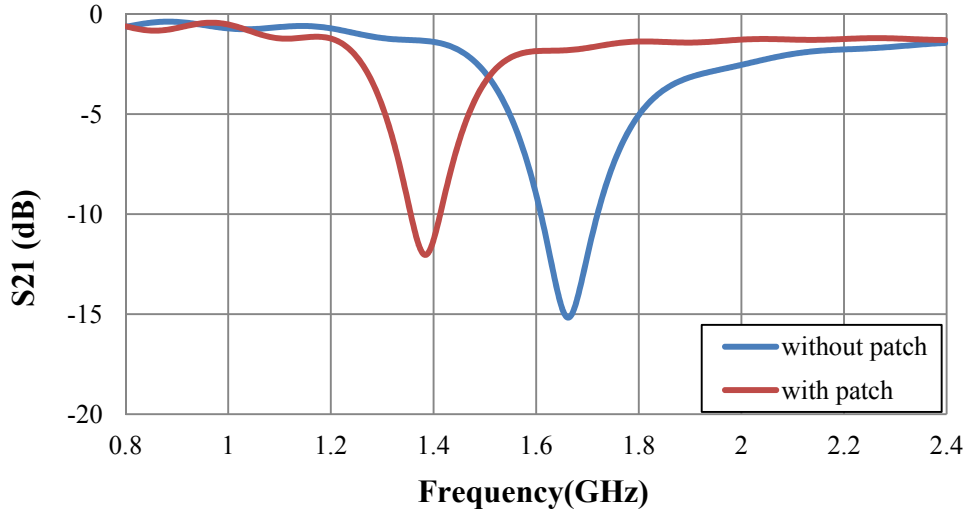


Figure 5.4 Simulated S21 with and without a conducting patch

As discussed in chapter 4, with the overlapping area enlarging, the capacitance of the slit-patch EBG structure increases. The reduction of band-gap frequency and bandwidth ensues. On the basis of keeping the resonant frequency of the slit-patch EBG structure around the desired operating frequency of the antenna, the area of the convoluted slit on ground plane could be reduced by increasing the width of the conducting patch. It will take up less valuable area on the PCB and avoid affecting the other electronic components installed on ground plane. The second study is the alteration of the conducting patch width for enlarging the overlapping area. It will directly increase the capacitance of the slit-patch structure. Figure 5.5 presents the simulated transmission response (S21) of the proposed structure accompanied by the alteration of the conducting patch width. The length of the conducting patch is defined as 15.5mm which is slightly longer than the convoluted slit for all geometries. When the width of the conducting patch increases from 0.25mm to 1mm, the center of the band gap shifts from 1.43GHz to 1.25GHz shown in Figure 5.5. In this way, the size of the convoluted slit could be reduced by increasing the width of the conducting patch. As a result, the slit-patch EBG structure will occupy a small footprint near the edge of the ground plane which is advantageous for utilisation in of compact handset devices with a large number of electronic components installed on the ground plane.

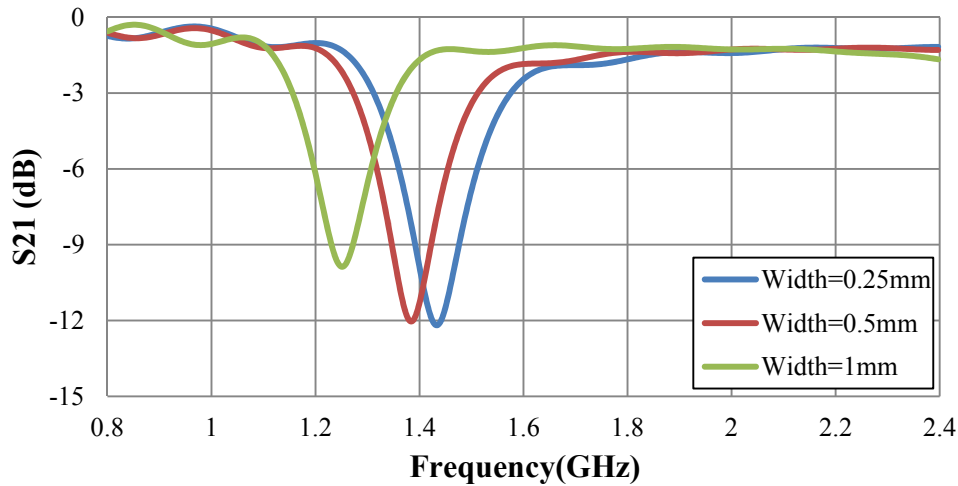


Figure 5.5 Simulated S21 with different width of conducting patch

Although the band gap shifts towards a lower frequency with increasing the overlap area of the slit-patch structure, the absolute bandwidth also decreases too. In order to overcome this limitation, two identical slit-patch structures are employed to obtain the desirable bandwidth, as shown in Figure 5.6. The actual size of the slit-patch EBG structure is the same as the single one. Figure 5.7 illustrates a comparison of simulated data (S21) for one and two slit-patch EBG structures respectively. When the number of the proposed EBG structures increased, the cut-off frequency of the band gap slightly decreased. However it is evident that the bandwidth increases considerably after employing two slit-patch unit cells. The bandwidth (-10dB) of two slit-patch structures is about double when compared to one slit-patch EBG structure. These simulated results are encouraging since the proposed slit-patch EBG structure supports an expected broader band with increasing the number of slit-patch structures.

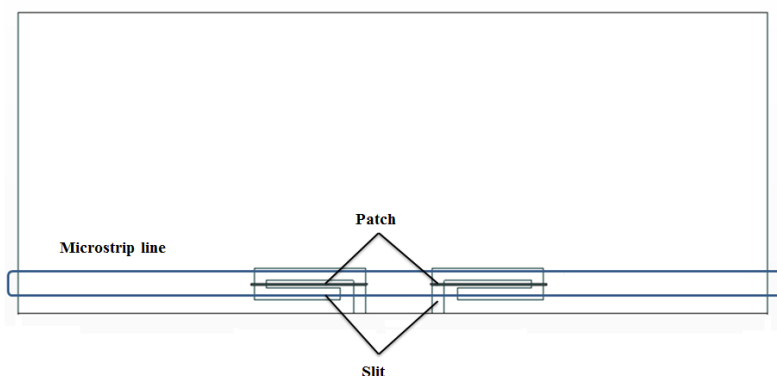


Figure 5.6 Two identical slit-patch EBG structures on the ground plane

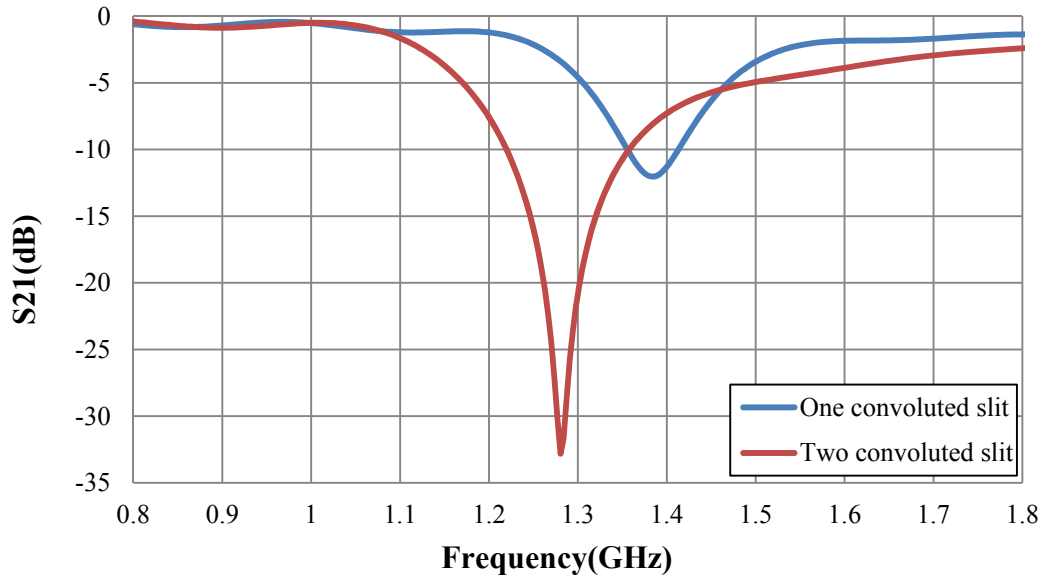


Figure 5.7 Simulated S21 with multiple double-layer slit-patch structures

5.3 Decoupling PIFAs on Compact Ground Plane

In the previous section, the proposed slit-patch structures have succeeded in shifting the band gap towards lower frequency with increasing the width of the conducting patch. Multiple identical slit-patch EBG structures were employed to extend the bandwidth of the transmission response. In order to evaluate the adaptability of the proposed slit-patch EBG structures, this structure is further studied for application with a PIFA array. A dual-element PIFA array is mounted on a $100 \times 40 \text{ mm}^2$, 1.2 mm thick, FR-4 dielectric substrate ($\epsilon_r=4.5$) backed by a common ground plane. The two PIFA elements are designed to operate at approximately 1.9GHz. The mutual coupling between two PIFA elements which are approximately a half-wavelength apart is about -10dB at the resonant frequency. The two-element PIFA array configuration with two convoluted slits is shown in Figure 5.8(a). The slit dimensions are $L_1=6\text{mm}$, $L_2=14\text{mm}$, $L_3=5\text{mm}$, $L_4=10\text{mm}$, and the slit width is 1.62mm. The coupling between the two array elements was simulated to be $S_{21} = -27 \text{ dB}$ at 1.92GHz in Figure. 5.9.

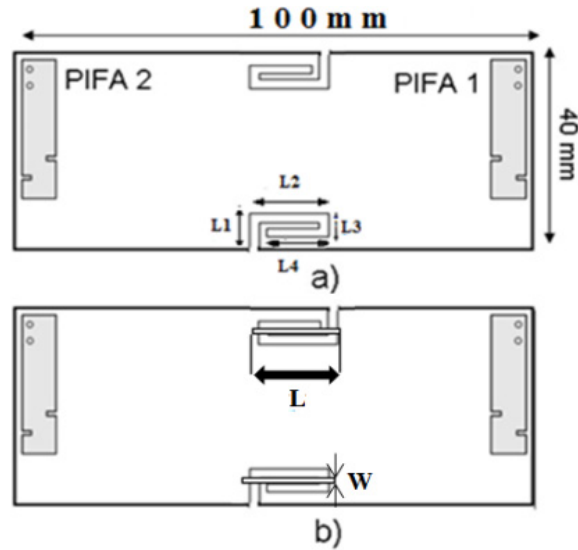


Figure 5.8 Two-element PIFA array with (a) two convoluted slits (b) two convoluted slit-patch structures

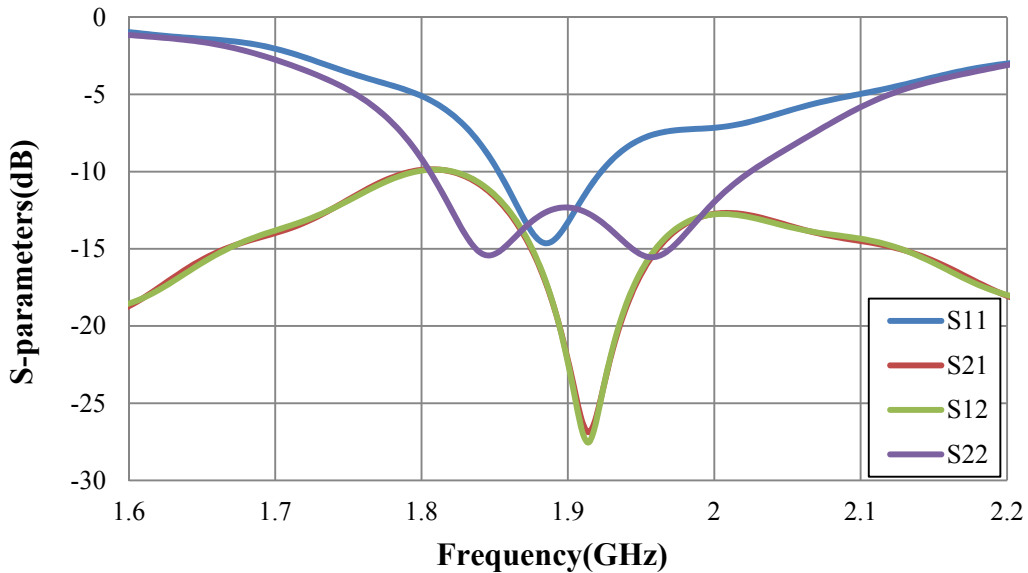
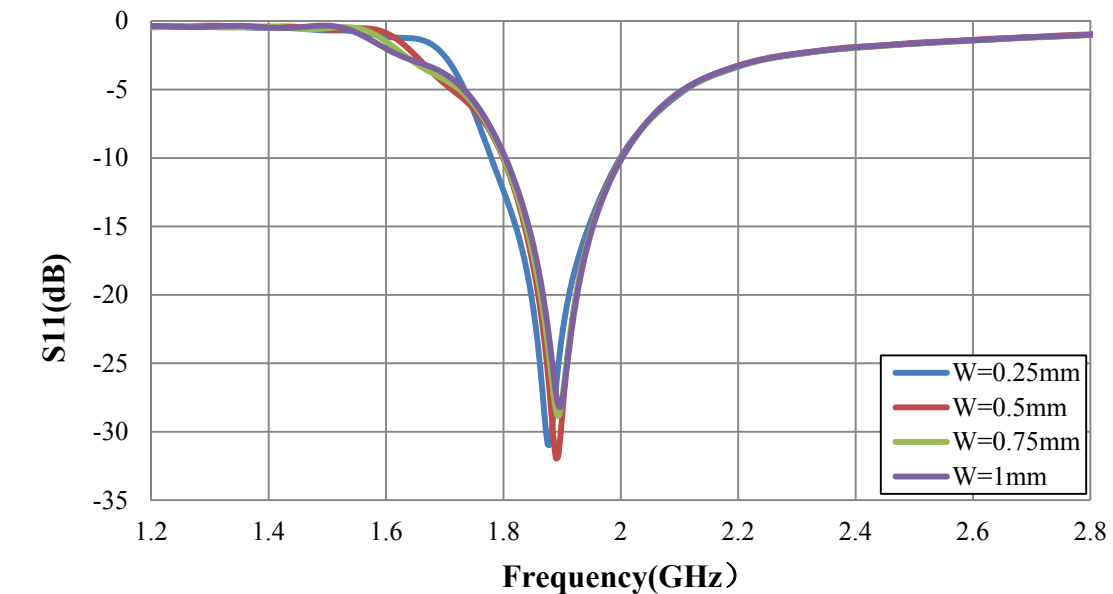


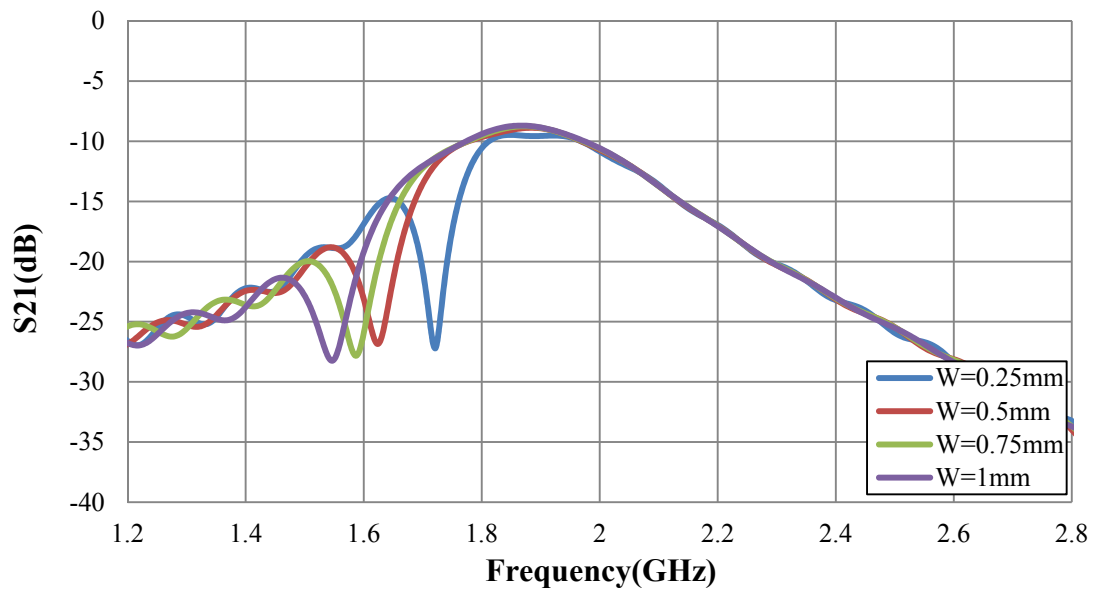
Figure 5.9 Simulated S-parameters of the PIFA array with two convoluted slits on ground plane

By placing the layer of conducting patches in close proximity to the convoluted slits, when the width (W) of the conducting patch increases from 0.25mm to 1mm, the minimum of S_{21} shifts to lower frequency region (from 1.72GHz to 1.54GHz), as in Figure 5.10(b). But the simulated S_{11} remains around 1.9GHz as shown in Figure 5.10(a). In order to make the resonance of the slit-patch structure match the antenna's operating frequency, the dimension of the convoluted slit is decreased. After a series of simulations, the width of the slits was optimized as 1mm, with $L_1=4$ mm,

$L_2=10.7\text{mm}$, $L_3=3\text{mm}$, $L_4=8.5\text{mm}$ as shown in Figure 5.8(b). This new structure occupies just half the area of the convoluted slits on their own (no patch). The conducting patch is optimized as 15.5mm length and 0.5mm width. A sharp transmission minimum is obtained at 1.86GHz with the S_{21} reduced to -27dB , as shown in Figure 5.11. Both antennas remain well matched at the frequency where the slit-patch structure resonates.



(a)



(b)

Figure 5.10 Simulated (a) S_{11} and (b) S_{21} of the PIFA array with the different width of slit-patch

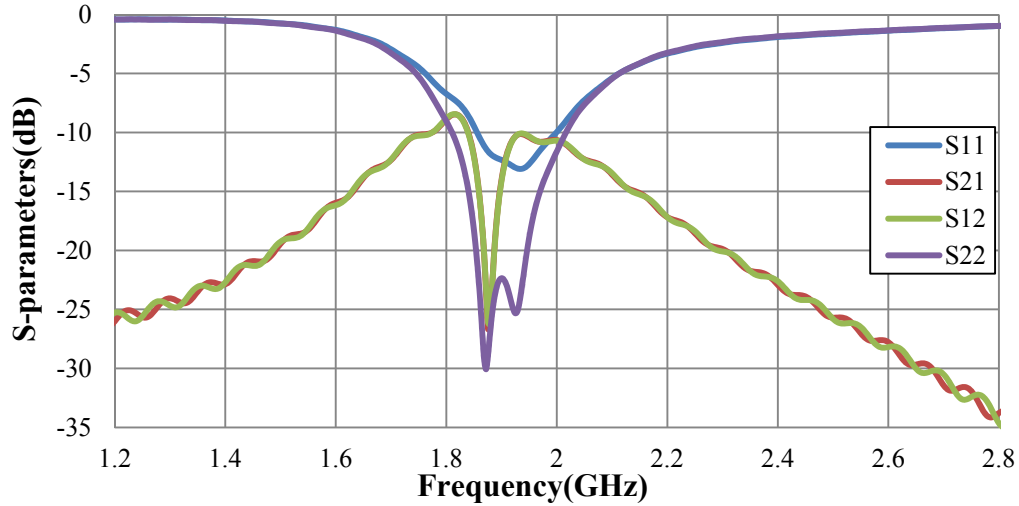


Figure 5.11 Simulated S-parameters of the PIFA array with the slit-patch on the ground plane

As expected, the bandwidth (-15dB) of mutual coupling (S21) between two PIFAs drastically decreases from 0.102GHz to 0.038GHz when placing the conducting patch on the existing convoluted slits. Four identical slit-patch unit cells are mounted on the ground plane to obtain much more bandwidth, as shown in Figure 5.12. The separation between the two slits is 10.25mm. The distance between the two patch edges is 5mm. The other dimensions of the slit-patch EBG structures are exactly the same as before.

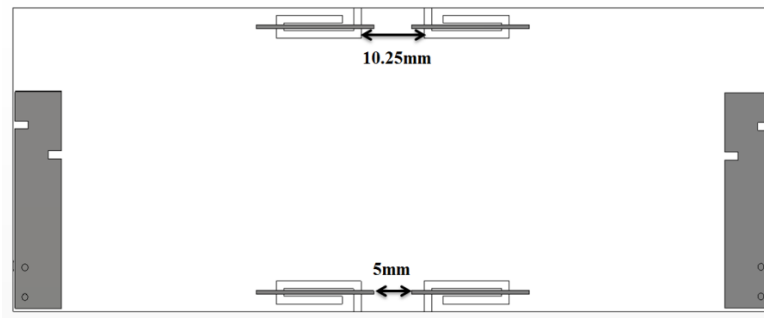


Figure 5.12 Two-element PIFA array with four convoluted slit-patch structures

The simulated S-parameter of the antenna array with four convoluted slit-patch structures is presented in Figure 5.13. The band gap (-15dB) of S21 emerges at 1.88GHz and extends to 1.938GHz. It produces an absolute bandwidth of 0.058GHz. Like the discussions presented in Chapter four, the simulated bandwidth of the

double-layer structure is always different to the measured result, due to the limitation of the CST software and the computer resource. The measured results are presented below.

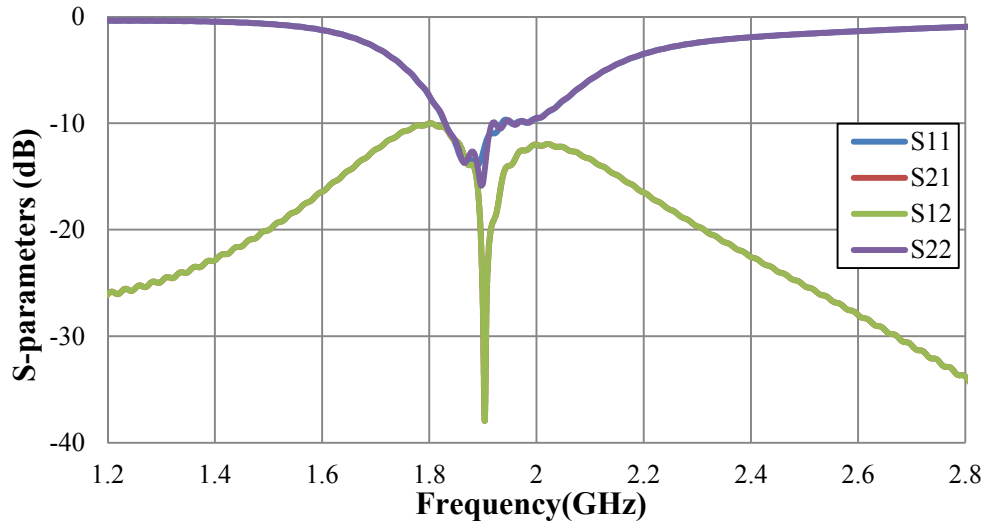


Figure 5.13 Simulated S-parameters of the PIFA array with four slit-patch structures

The correlation coefficient between the two antennas in the presence of the slit-patch structures has also been calculated by using equation (2.9) [8]. The correlation coefficient of all cases, namely the antenna array with two and four optimized slit-patch structures, is presented in Figure 5.14. The correlation coefficient is significantly reduced, after the proposed slit-patch EBG structures are placed on the ground plane.

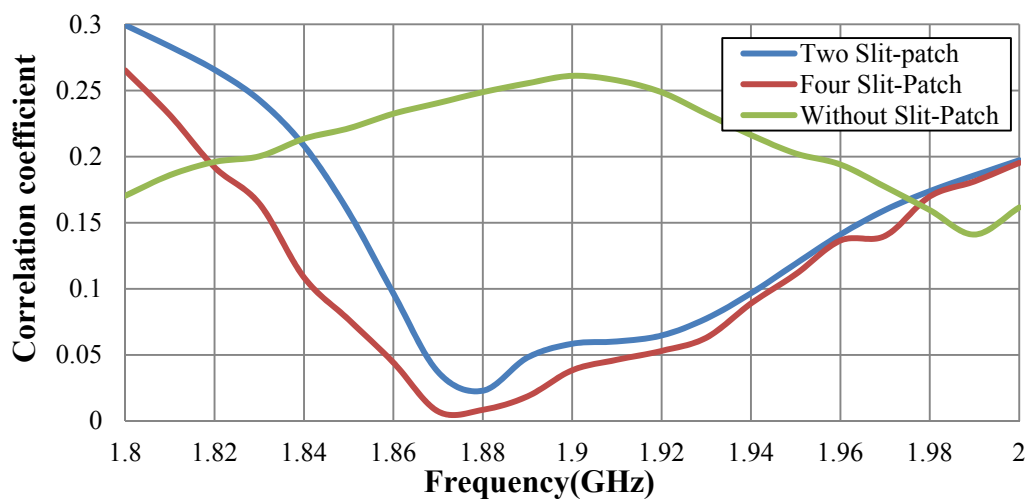
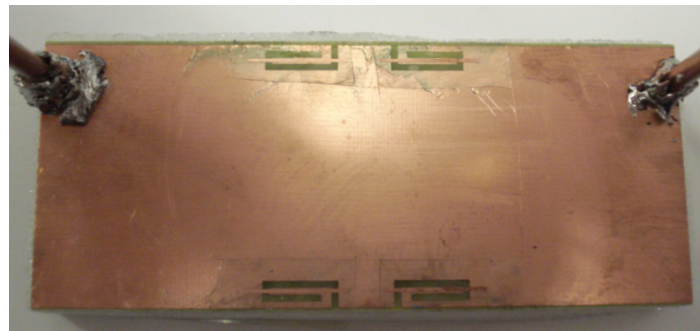


Figure 5.14 Correlation coefficient for two and four Slit-patch EBG structures

Based on the optimised simulated configurations, two prototypes of the dual-element antenna array with the proposed slit-patch structures were fabricated and measured in the laboratory at Loughborough University, as shown in Figure 5.15. An anritsu 37000D vector network analyzer recorded the S-Parameters data from the prototypes.

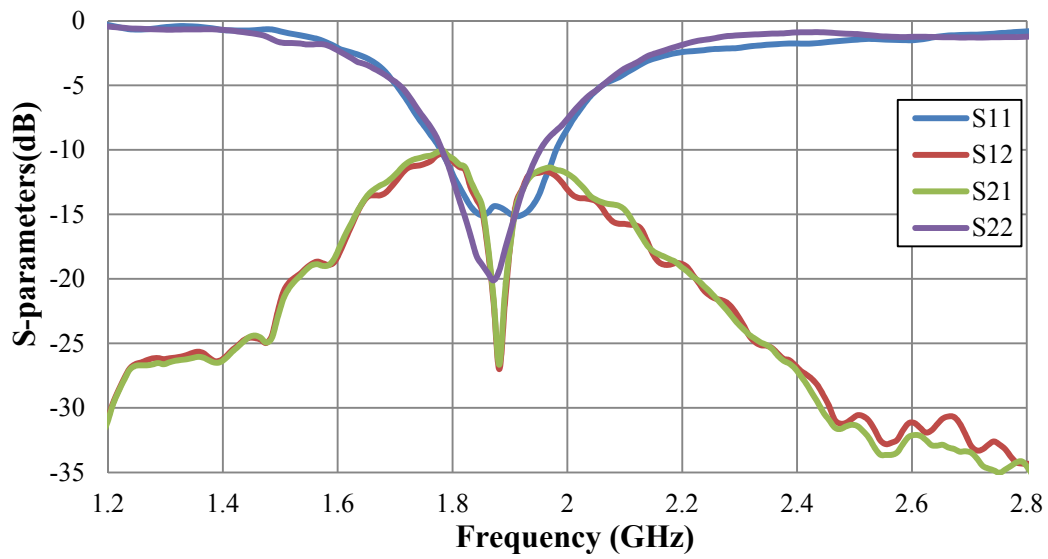


(a)

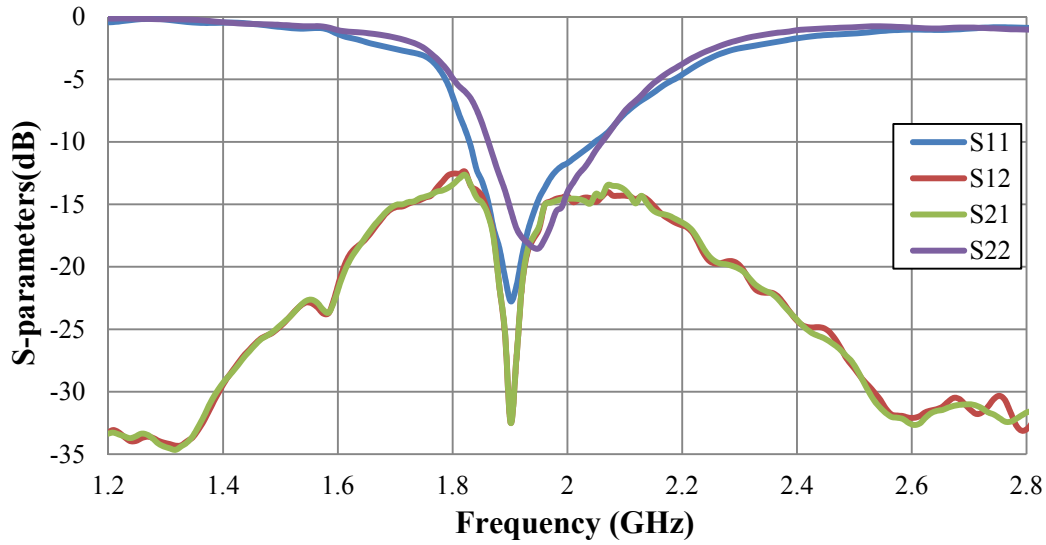


(b)

Figure 5.15 Photograph of the prototype PIFAs with (a) two slit-patch structures (b) four slit-patch structures on the ground plane



(a)



(b)

Figure 5.16 Measured S-parameters for a PIFA array (a) with two slit-patch structures, and (b) with four slit-patch structures

The measured S-parameter with two slit-patch structures on the ground plane is shown in Figure 5.16(a). The centre resonant frequencies of the PIFAs are at 1.88GHz, which is 0.01GHz higher than the simulated one (1.87GHz). These minor discrepancies between simulated and measured results are due to multiple factors, such as the cable connection, the bending of materials, and the construction technique of the prototype. The measured -15dB bandwidth (55MHz) is slightly wider than the simulated result (50MHz). Figure 5.16(b) illustrates the measured S-parameter with four slit-patch structures. The antenna resonances are also slightly shifted with respect to the simulations. Nevertheless, at the resonance of the slit-patch structures (1.9GHz) both antennas are matched ($S_{11} < -10$ dB and $S_{22} < -10$ dB). Furthermore, the value of measured S21 in the presence of four slit-patch structures is reduced in comparison to the initial antenna system which employs two slit-patch EBG structures. And, the measured bandwidth (-15dB) of S21 increases to 140MHz, which is much more than the PIFA array with two slit-patch EBG structures.

5.4 Summary

This chapter presented a new slit-patch EBG structure and its transmission characteristics. The proposed structure consists of two closely coupled layers, one made of conducting patches and the other made of convoluted slits on a common ground plane. Simulations of the transmission response with different conducting patch widths were presented. Multiple slit-patch EBG structures were proposed to extend the bandwidth of the transmission response.

The designs of new slit-patch EBG structures significantly reduced the mutual coupling between two PIFAs operating at 1.9GHz from -10dB to less than -20dB. The dimensions of the proposed structures are optimized to produce maximum miniaturization of the convoluted slits thereby occupying less area on the compact ground plane. Simulations for different widths of conducting patches were presented. Four identical slit-patch structures are employed to reduce the correlation coefficient between the two PIFAs and extend the bandwidth of S21. Two prototypes of antenna array with two and four slit-patch structures have been fabricated and measured to experimentally validate the proposed design. Good agreement was presented between the measurements and simulations.

References

- [1] D.S Lockyer, ; J.C Vardaxoglou, ; R.A Simpkin, "Complementary frequency selective surfaces," *IEE Proceedings: Microwaves, Antennas and Propagation*, Vol: 147, Issue:6 Dec 2000 pp: 501 – 507.

- [2] A. P. Feresidis, G. Apostolopoulos, N. Serfas, J. C. Vardaxoglou, "Closely coupled metallodielectric electromagnetic band-gap structures formed by double-layer dipole and tripole arrays," *IEEE Transactions on Antennas and Propagation*, Vol : 52 , Issue:5 May 2004 pp: 1149 – 1158.
- [3] J. C. Vardaxoglou and D.S Lockyer, "Modified FSS response from two sided and closely coupled arrays," *Electron. Lett.*, vol. 30, no. 22, pp.1818–1819, 1994.
- [4] D. S. Lockyer and J. C. Vardaxoglou, "Reconfigurable FSS response from two layers of slotted dipole arrays," *Electron. Lett.*, vol. 32, no. 6, pp. 512–513, 1996.
- [5] D. S. Lockyer, J. C. Vardaxoglou, and R. A. Simpkin, "Complementary frequency selective surfaces," *IEE Proceedings: Microwaves, Antennas and Propagation*, vol. 147, pp. 501-507, DEC 2000.
- [6] G. Apostolopoulos, A.P. Feresidis, G. Goussetis, J.C. Vardaxoglou, "Complementary metallo-dielectric electromagnetic band gap structures," *Microwave Conference*, 2005 European Oct. 2005.
- [7] Q. Li, A. P. Feresidis, "Miniaturised Slit-Patch EBG Structures For Decoupling PIFAs on Handheld Devices," *Loughborough Antennas & Propagation Conference*, 14-15 November 2011, Loughborough, UK.
- [8] S. Blanch, J. Romeu, I. Corbella, "Exact representation of antenna system diversity performance from input parameter description," *Electronics letters*, 2003 Vol. 39 No. 9, pp. 705-707. May 2003.

Chapter 6

Conclusions and Future Work

6.1 Conclusions

MIMO systems have shown a remarkable performance for increasing the channel capacity without additional radio spectrum. The data transmission rate, reliability and coverage of the MIMO system has been significantly improved by introducing diversity techniques and space-time coding. MIMO technologies have been implemented in the 3G and 4G communication systems. Multiple antenna elements are employed at both transmitters and receivers to form a MIMO system. However, the mutual coupling between antenna array elements is still a daunting challenge when the MIMO system is implemented into compact wireless terminal. The high mutual coupling will degrade the performance of the antenna array and affects the channel capacity. In order to solve this important problem in the design and implementation of multiple antenna terminal, novel structures for reducing the electromagnetic coupling between closely packed antennas have been presented in this thesis.

Initially, a modified PIFA and its dual-element array placed on a common ground plane were proposed and optimized for a small mobile terminal operating at 1.9GHz. Although the distribution of the antenna array had been optimized, the mutual coupling was still over -10dB at the resonance of antennas. The proposed structure was based on the insertion of two coupled linear slits on the ground plane between the antennas. After the length of the slit and the distance between them has been optimized, a transmission zero ($S_{21} < -20\text{dB}$) is introduced in the coupling path between the two antennas, reducing the electromagnetic coupling between them to particularly low values.

In order to take up less space on the ground plane, two miniaturized convoluted slits are presented. Although the proposed slits have a small footprint and are positioned close to the edges of the ground plane thereby occupying very little space, there is very little current flowing across the space between the two convoluted slits. A transmission minimum was obtained by virtue of the resonance of the slits resulting in a significant reduction of the mutual coupling across the operating frequency of the antennas. The miniaturized convoluted slits etched on the ground plane also succeeded in reducing the coupling of the human body (head and hand) to the antennas when the mobile phone was being held by a user's hand. A single miniaturized convoluted slit was etched between the two very close spaced PIFAs and close to the short edge of the ground plane of handheld devices. Although occupying very little space on the ground plane, the single convoluted slit trapped a large portion of the surface current excited from the PIFAs, and significantly reduced the mutual coupling across the operating frequency of the antennas.

To further reduce the area of the slits on the ground plane, a double-layer slit-patch EBG structure was introduced and its transmission characteristics were studied. These structures consisted of two closely coupled layers, one made of conducting patches and another made of linear slits. They were placed in very close proximity to each

other (55 μ m) with a rotation of 90⁰ between the elements to produce maximum coupling. A microstrip line excitation was initially employed for the efficient analysis and design of the proposed double-layer structures. Simulated transmission response with different widths of conducting patch was presented. Multiple slit-patch structures were studied to extend the bandwidth of the transmission response.

A modified printed CPW-fed monopole and its dual-element antenna array were mounted on a compact substrate for a wireless terminal device operating around 2.44GHz. The proposed slit-patch EBG structures significantly reduced the mutual coupling between the two antennas from -14dB to less than -30dB. Two identical slit-patch structures were presented to reduce the correlation coefficient between the two antennas and improve the total efficiency of antenna array. Although the proposed double-layer EBG structures have small footprint on the ground plane, they produce the transmission minimum around the antenna operating frequency regardless of the alteration of the interelement distance between the two monopoles (distance ≥ 8 mm).

A dual-element UWB planar monopole array operating from 3GHz to 6GHz has been investigated with the slit-patch EBG structures. An isolation of better than 15dB between the two antenna array elements has been obtained across the entirety of the operation frequency range by employing three slit-patch EBG structures. When the separation of two UWB planar monopole array reduces to 1mm, a significant reduction of mutual coupling between the antenna elements was achieved by employing the proposed slit-patch EBG structures. This further confirms that the design of the miniaturized double-layer slit-patch EBG structures can produce a reduction of the mutual coupling between antenna elements and also lead to the maximum reduction of the area of antenna array.

Likewise, the new double-layer slit-patch EBG structures applied to the convoluted slits. Simulations of the transmission response (S₂₁) with different widths of

conductor patch were presented. Multiple slit-patch EBG structures were employed to extend the bandwidth of the transmission response. The dimensions of the proposed structures are optimised to produce maximum miniaturization of the convoluted slits thereby occupying less area on a compact ground plane. Two identical slit-patch structures significantly reduced the mutual coupling between two PIFAs operating at 1.9GHz from -10dB to less than -20dB. After that, four identical slit-patch structures are employed to reduce the correlation coefficient between the two PIFAs and extend the bandwidth of S21.

6.2 Future Work

Future research on the topic of this thesis could include the following:

- In this project, all the MIMO systems employed two antenna elements at the wireless terminal end. They are restricted to the tight space available in compact terminal devices. But more antenna elements could be employed for some larger wireless devices such as laptop, pack radio section and PDA. A new antenna array (4 x 4 MIMO system) could be proposed and optimised by using either the simulations and real practice.
- In this project, PIFA, printed monopole and UWB antenna have been implemented to investigate the proposed single-layer and double-layer structures for compact wireless terminals. New types of antennas (dipoles and monopoles) could be studied for wireless routers and base stations.

- As shown in the Chapter three, the effect of the human body to the performance of the antenna array has been presented in simulation. The prototypes of the model of the human body could be fabricated and measured for different positions.
- Designs of multiple multi-band antennas integrated with the proposed slit-patch structures could be carried out to reduce the mutual coupling between antenna array elements.
- A MIMO channel model in indoor environment could be established to evaluate the channel capacities of the different antenna arrays integrated with the different structures such as: the defected ground structures and the double-layer slit-patch EBG structures.

Appendix

Wheeler-Cap Method for measuring antenna efficiency

The antenna radiation efficiency is an important parameter which describes the ratio of the radiated power to the input power. A high efficiency means more power radiated from antenna. A low efficiency shows that a lot of the power was absorbed as losses. The radiation efficiency η_{rad} represents the losses associated within an antenna. It can be calculated as:

$$\eta_{rad} = \frac{P_{rad}}{P_{in}} \quad (a.1)$$

The total efficiency η_{total} could be calculated from the radiation efficiency and the S-parameters:

$$\eta_{tot} = \eta_{rad}(1 - |S_{21}|^2 - |S_{11}|^2) \quad (a.2)$$

One method named as the Wheeler-Cap has become the standard for measuring the antenna efficiency because of its repeatability, simple implementation, accuracy and minimum of data analysis [1, 2]. This method determines the input power as the radiated power P_{rad} and losses power P_{losses} . The powers could be modeled as the radiation resistance R_{rad} and the loss resistance R_{losses} . The Wheeler-Cap method introduces two controlled environments: the proposed antenna in: free space and a closed cap as shown in Figure A.1 below. The equivalent circuits are described using the principle of Wheeler-Cap method. When the antenna is placed in the free space, R_1 is measured as the sum of R_{rad} and R_{losses} [3]. When the antenna is placed in a metallic cap, the R_2 is measured as the R_{losses} . In this way, the antenna efficiency

could be obtained from simple laboratory equipment [4].

$$\eta_{rad} = \frac{P_{rad}}{P_{in}} = \frac{P_{rad}}{P_{rad}+P_{losses}} = \frac{R_{rad}}{R_{rad}+R_{losses}} = \frac{R_1-R_2}{R_1} \quad (a.3)$$

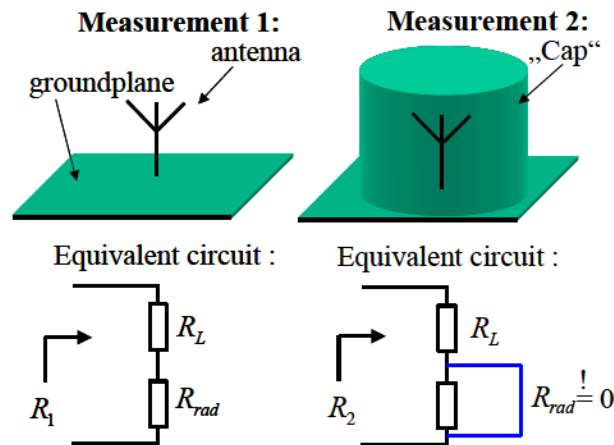


Figure A.1 The Wheeler-Cap method and the equivalent circuit [3]

REFERENCES

- [1] H.A. Wheeler, "Fundamental Limitations of Small Antennas," Proc. IRE, Vol. 35, S. 1479-1484, December 1947
- [2] H. A. Wheeler, "The radiansphere around a small antenna," Proc. IRE, S. 1325-1331, August 1959.
- [3] O. Litschke, M. Geissler, M. Martinez, D. Heberling, "Adaption of the Wheeler-Cap method for measuring the efficiency of mobile handset antennas," Itg Fachbericht (2003) Publisher: VDE; 1999, Pages: 387–390.
- [4] E.H. Newman, P. Bohley, C.H. Walter, "Two Methods for the Measurement of Antenna Efficiency," IEEE Trans On Ant. And Propagation, Vol.AP-23, No. 4, S.457-461, July 1975.